Evaluation of a Helical Diode Array and Planned Dose Perturbation Model for Pretreatment Verification of Volumetric Modulated Arc Therapy

by

Evan David Maynard
B.Sc., University of Victoria, 2010

A Thesis Submitted in Partial Fulfillment of the
Requirements for the Degree of

MASTER OF SCIENCE

in the Department of Physics and Astronomy

Evaluation of a Helical Diode Array and Planned Dose Perturbation Model for Pretreatment Verification of Volumetric Modulated Arc Therapy

by

Evan David Maynard
B.Sc., University of Victoria, 2010

Supervisory Committee

Dr. Isabelle Gagne, Co-Supervisor
(Department of Physics and Astronomy, BC Cancer Agency - Vancouver Island Centre)

Dr. Andrew Jirasek, Co-Supervisor
(Department of Physics and Astronomy)

Dr. Derek Wells, Departmental Member
(Department of Physics and Astronomy, BC Cancer Agency - Vancouver Island Centre)

Supervisory Committee

Dr. Isabelle Gagne, Co-Supervisor
(Department of Physics and Astronomy, BC Cancer Agency - Vancouver Island Centre)

Dr. Andrew Jirasek, Co-Supervisor
(Department of Physics and Astronomy)

Dr. Derek Wells, Departmental Member
(Department of Physics and Astronomy, BC Cancer Agency - Vancouver Island Centre)

ABSTRACT

The ArcCHECK® dosimeter is a novel dosimetry tool that uses a helical array of silicon diode detectors to measure dose in a cylindrical plane. 3DVH® is an associated software that can use ArcCHECK® diode measurements along with treatment planning system (TPS) data to guide a full 3D dose reconstruction. The ArcCHECK® phantom, along with 3DVH® software was evaluated as a volumetric modulated arc therapy (VMAT) pretreatment verification tool. The comprehensive evaluation of the ArcCHECK® and 3DVH® system involved a comparison of measured dose to both ECLIPSE and Monte Carlo calculated dose for open fields and intensity modulated radiation therapy (IMRT) plans. System based confidence limits for γ-pass rate and dose difference metrics were established through the measurement of prostate and head and neck VMAT plans. Using the system based confidence limits and clinically accepted tolerances, the sensitivity of the ArcCHECK® and 3DVH® system to VMAT errors was determined. Dose measured by the ArcCHECK® and reconstructed in 3DVH® agreed very well with dose calculated in ECLIPSE and Monte Carlo for both open fields and IMRT plans. The only results that fell outside of clinically accepted tolerances were a set of head and neck IMRT plans, however it was

determined that a major factor in this result was suboptimal modelling of MLC effects in the TPS, in combination with changes in linac performance since commissioning of the TPS model. VMAT measured by the ArcCHECK® and 3DVH® system were in excellent agreement with ECLIPSE results and system based confidence limits were determined to be tighter than commonly used limits. ArcCHECK® and 3DVH® were sensitive to clinically relevant VMAT errors and insensitive to errors with little dosimetric impact, although diode measurements alone required tighter tolerances than are typically used. The ArcCHECK® phantom and 3DVH® software when used together have been shown to provide useful dosimetric information when used for VMAT pretreatment verification.

Contents

List of Tables

List of Figures

ACKNOWLEDGEMENTS

This thesis would not have been possible without the guidance and support from my supervisors Isabelle Gagne and Andrew Jirasek. For their help I am sincerely grateful. I would also like to thank Derek Wells and the rest of the physics department at VIC for taking the time to provide their assistance and advice whenever it was needed. I am especially grateful to my fellow medical physics grad students for the positive and productive environment that has been established in our various work spaces. Finally, I need to thank my parents and the rest of my family for all their love and support, not just during this time, but throughout my entire academic career.

Chapter 1

Introduction

As the population of Canada continues to grow and the average life expectancy of a Canadian citizen increases, the rate at which people develop cancer in one form or another will also increase [4]. A new radiation therapy technique, volumetric modulated arc therapy (VMAT), has recently been introduced and shown to significantly decrease treatment time for certain treatment sites while delivering equal or better dose conformity when compared to the current technique of intensity modulated radiation therapy (IMRT). With better dose conformity, VMAT will produce improved outcomes for patients. VMAT will also decrease the time a patient will spend on the treatment bed receiving radiation dose. Benefits of a decrease in treatment time include decreased patient motion, resulting in improved accuracy in the delivery of dose, and improved patient comfort for patients who may not find it easy to remain still for lengthy deliveries. As treatment techniques evolve and grow more complex the quality assurance (QA) methods used to ensure safe and accurate radiation delivery, must evolve as well. The focus of this thesis is on a new dosimeter, ArcCHECK®, and reconstruction software, 3DVH®, designed for VMAT pretreatment verification.

1.1 Radiation Therapy

Radiation therapy (RT), along with surgery and chemotherapy, is one of the three major techniques for treating cancer. Chemotherapy is the least specific method of removing cancer cells. It can preferentially kill cells with characteristics that are generally associated with cancer, such as high proliferation, but often does significant damage to the rest of the body. Surgery is the most specific method of removing

cancer cells, as solid tumours are often targeted and the gross tumour volume is removed. Radiation kills cells in a more uniform manner as cancer cells are targeted by localizing high radiation doses specifically to disease sites. Radiation therapy can be used alone or in conjunction with chemotherapy and/or surgery. Radiation therapy is used as a stand alone treatment in early-stage diseases and where surgery is not a suitable treatment, but also post-operatively to remove any microscopic tumour cells or metastases left after surgery. It is also commonly used in combination with chemotherapy, targeted agents and radiosensitizers to enhance its curative power. Due to its effectiveness as a curative cancer treatment, it is estimated that more than half of all patients treatments involve a course of radiation therapy [5].

Radiation therapy uses high energy x-rays to damage and kill cells within the body. The x-ray photons used for treatment are in the MeV range which contrasts with the lower energy keV x-ray photons typically used for x-ray planar imaging and computed tomography (CT). These high energy photons interact within the patient, ejecting electrons and ionizing molecules. The ejected electrons interact with other molecules, producing more ionizations in a cascading effect until all of the energy that entered via the initial photon has either been deposited within the body or scattered away. As energy is deposited the ejected electrons travel slower and slower and interactions become more and more frequent, producing clusters of ionizations near the end of an electron track. These ionizations can cause the breaking of bonds within molecules and when ionization clusters occur within the DNA structure of a cell and produce damage that is unrepairable, it can lead to the death of that cell. The amount of damage produced by ionizing radiation can be measured, in part, by a quantity called absorbed dose which is the absorbed energy per unit mass. The absorbed dose is often quoted in gray (Gy), where one gray is equal to one joule per kilogram (J/kg). A course of radiation therapy is typically delivered over multiple days with fractions of the total dose prescription delivered per treatment day. Based on the sensitivity of normal tissue and tumour cells, fractionation of radiation therapy treatments allows for greater normal tissue sparing and escalation of the prescription dose.

Since ionizing radiation can cause significant damage to normal tissue, the localization of dose within the patient is critical to successful treatment. In order to obtain tumour control, it is necessary to kill as many tumour cells that have the ability to multiply as possible. The probability of tumour control is dependant on the remaining number of tumour cells with the ability to reproduce. The fraction

of cells killed, and therefore chance of tumour control, is dependant on the absorbed dose; the goal of radiation therapy should then be to deliver as high a dose to tumour cells within the body as possible. The limiting factor in achieving this goal is the dose delivered to normal tissue. By killing normal tissue cells the functional ability of normal tissues and organs can be diminished. Acute normal tissue toxicities are the side effects of radiation on normal tissue that occur over the time frame of the treatment and are caused by the death of a large number of normal cells. If acute toxicities become too severe, they can lead to the delay of treatment until the tissue is repaired and the symptoms pass. If allowed to repair, acute toxicities are often entirely reversible. Late normal tissue toxicities can appear months or years after a radiation therapy treatment and are never fully repaired by the body. If severe late toxicities are allowed to occur, it can lead to a severe reduction in quality life or death for the patient after the radiation treatment has been completed. For this reason the planning and delivery of a radiation treatment is an attempt to find a balance between delivering enough dose to control the tumour growth and sparing enough normal tissue to avoid unacceptable normal tissue toxicities. Therefore, to improve patient outcomes, many advancements in radiation therapy focus on delivery techniques which shield the normal tissue structures and allow for dose escalation to tumour volumes without increasing dose to normal tissues.

1.2 Radiation Therapy Delivery Techniques

One of the first high energy treatment units, the cobalt therapy unit, uses the decay of cobalt-60 to produce 1.17 MeV and 1.33 MeV photons giving the unit a fixed average beam energy of 1.25 MeV [6]. The amount of dose delivered is controlled by the length of treatment, the distance from the cobalt source to the patient and the collimation of the beam. Modern linear accelerators have the ability to not only produce a range of beam energies but also control the rate at which dose is delivered.

Beam modulation and collimation have also improved significantly in the delivery of ionizing radiation. In its simplest form, radiation therapy consists of ionizing beams of radiation delivered to a patient which is collimated into open rectangular fields to best fit the intended treatment area. By delivering multiple fields from different angles entrance and exit dose to normal tissues can be spread to a larger volume and allow for higher doses to the tumour. In modern radiation therapy open field treatment is limited to palliative care. The introduction of further collimation that is often

patient and tumour specific can offer a significant reduction in normal tissue dose. Beam collimators can be placed on the patient or in the treatment unit in the form of dense materials that are physically moulded or designed for each individual treatment and are essentially cut-outs of the desired target for irradiation. Tumour specific collimation has almost entirely been replaced by the multileaf collimator (MLC). A MLC is a collimator within the treatment machine made up of high density leaves which allow for sub-millimetre dynamic shaping of the radiation beam. Dynamic collimator allows for modulation of the radiation beam throughout delivery and is the modern basis of intensity modulated radiation therapy (IMRT) [7].

An IMRT treatment often consists of the delivery of several beams at different static gantry angles which are modulated by the MLC to deliver a high and uniform dose to the tumour volume. The precise nature of the secondary collimation allows for extreme dose escalation to the tumour while shielding normal structure and reducing the dose to the surrounding normal tissues. The modulation of the treatment beam using an MLC in radiation therapy has shown to improve patient outcomes and decrease normal tissue complications and enabled IMRT to become the standard for curative radiation therapy for many disease sites [8].

Volumetric modulated arc therapy (VMAT)is an extension of the IMRT treatment technique. Rather than using static beams and constant dose rates, VMAT delivers dose in a continuous 360° arc with the gantry in motion and a changing dose rate. VMAT treatments have several constantly varying factors that affect delivered dose which include: dose rate, MLC leaf positions, gantry position and gantry speed [9]. By delivering the treatment in a single arc, treatment time is reduced as there is often no "beam-off" time while the gantry rotates. VMAT deliveries in general require less"beam-on" time than IMRT deliveries [10–12] and the decrease in overall"beam-on" time also reduces the overall integrated dose to the patient. The increase in overall dose to the patient in IMRT treatment has been shown to be a possible cause in the increase in secondary malignancies [13]. The decrease in overall treatment time not only improves patient comfort and overall treatment efficiency, but also decreases the chance of significant patient motion during delivery. With the increased precision of treatments, the movement of only a few millimetres can have a significant impact on the way the dose is distributed to a patient. Therefore, the reduction of patient motion and image guided radiation therapy (IGRT) has become an important area of radiation therapy research. The decrease in treatment time provided by VMAT has the potential for more precise and effective IGRT techniques. One example is the

concomitant acquisition of cone beam computed tomography (CBCT) images with a VMAT delivery which would not be possible for IMRT [14]. Overall, VMAT appears to be the future of radiation therapy for many disease sites as it has been shown to provide similar or better dosimetric qualities compared to IMRT and with significant improvements in treatment time [10, 15].

With so many factors affecting the dose distribution it is a non-trivial task to find the optimal delivery plan for a patient. For IMRT and VMAT a process known as inverse-planning is used where a list of dose constraints are decided upon and the treatment planning system (TPS) calculates the optimal delivery plan to best remain within these constraints [7]. The constraints consist of doses prescribed by radiation oncologists to kill the tumour cells and dose limits for organs at risk (OAR) to minimize high grade normal tissue toxicity. The optimization algorithm of the TPS will attempt to meet all the constraints as best as possible, but there are obviously physical limits in its ability to do so [7]. The TPS then uses a dose calculation algorithm to determine the dose delivered based on the density of tissues from CT images of the patient, machine specific beam characteristics determined during linear accelerator commissioning and modelling of the MLC and other collimators.

1.3 Quality Assurance

A necessary step in the quality assurance (QA) of increasingly complex treatments, such as IMRT and VMAT is the validation of the dose distributions calculated by the TPS. There are several potential sources of discrepancy between what is physically delivered by the linear accelerator and what is virtually calculated in the TPS. These include physical characteristics of the accelerator itself such as the accuracy of gantry and MLC leaf position and speed and dose rate accuracy [16]. There also exist factors in the dose calculation that can potentially affect the dose distribution including the modelling of the MLC leaf ends and edges, calculation of leakage and transmission through the leaves, calculation of radiation scatter and modelling of the radiation source [16]. The transfer of data from the TPS to linear accelerator or corruption of treatment related files is another potential source of treatment error. Due to the tight margins and high dose gradients in IMRT and VMAT these subtle effects can have significant impacts on the overall dose distribution and require specific commissioning and periodic QA of both the treatment machine and TPS [17].

1.3.1 Pretreatment Verification for IMRT and VMAT

An important aspect of IMRT or VMAT QA is pretreatment or patient specific verification. Pretreatment verification is the verification of all the machine and planning system dosimetric factors as well as other possible unexpected errors that might arise in the chain from planning to delivery, such as corrupted or incorrect data transfer between the TPS and linear accelerator or unrecorded changes to the plan before delivery [18]. Pretreatment verification is the final check of the plan that is delivered to the patient; it is necessary to ensure that the delivery matches the planned and approved optimal treatment. Due to the complex nature of VMAT delivery and calculation, there are different challenges associated with VMAT verification when compared to IMRT verification.

Ion Chamber and Film

Individual point measurements are not an adequate test for an advanced IMRT delivery; a water equivalent two-dimensional (2D) dosimeter with sufficient detector resolution is a minimum requirement [18, 19]. One example of this type of verification dosimeter is a direct measurement of the delivery using 2D planar film combined with an ion chamber measurement. The ion chamber is the golden standard for absolute dosimetry and anchors the high resolution relative dose map measured by the film. However, film measurements tend to be fairly labour intensive and results can vary based on film orientation, film batch, scanner type or channel used, and great care needs to be taken to eliminate these factors [20].

Electronic 2D Dosimeters

Electronic 2D dosimeters can also be used for IMRT verification, each with its own strengths and weaknesses. Silicon diodes are small, highly sensitive dosimeters that can be arranged in an array to produce a 2D dose map. Diodes, however, degrade slowly over time with exposure to high doses of radiation and show directional and energy dependant responses in measurement of radiation dose which need to be accounted when they are used as part of a QA system [20–22]. One commercially available example of this type of dosimeter is the MapCHECK diode array (Sun Nuclear Corp., Melbourne, FL) [23]. Ion chambers can also be built into arrays to be used as 2D dosimeters and as mentioned earlier will provide very accurate absolute dose measurements. Ion chambers are not as sensitive as silicon diodes and need to

be much larger to acquire an adequate signal for dosimetry. Volume averaging of dose must be performed to account for the size of an ion chamber and this can often lead to discrepancies in areas of high dose gradients which are a common characteristic of IMRT [24]. Commercial examples of this type of dosimeter include MatriXX (IBA Dosimetry, Schwarzenbruck, Germany) [25] and Octavius (PTW, Freiburg, Germany) [26], the latter of which is an array embedded in an octagonal phantom with an air cavity to account for the angular dependence of the array. Another commonly used 2D dosimeter is an electronic portal imaging device (EPID), which is a flat panel detector that is used as an imaging device to verify patient positioning using the radiation therapy beam. Much work has been done to use amorphous silicon EPIDs as dosimeters as they are standard on many linear accelerators, quickly acquire data and have a high resolution [27]. Some of the challenges associated with EPID dosimetry include the lack of water-equivalence leading to some energy dependence and ghosting or image lag due to charge trapped in the photodiode layer of the detector.

It may be necessary to replace 2D and point dosimeters, that are typically used to individually verify the static fields of IMRT, with three-dimensional (3D) isotropic phantoms or dosimeters for VMAT dose verification. For IMRT it is possible to look at the fluence maps of the static fields and determine the level of agreement between delivery and plan; this is simply not possible for VMAT. Although it is possible to break a VMAT arc into its 177 sub fields that correspond to delivery control points, it is not immediately clear whether this is an adequate form of pretreatment verification. It has also been suggested that 2D planar verification of individual IMRT fields is not able to predict clinically relevant dose errors and that 3D dosimetry is necessary even for IMRT verification [28–30].

Non-Planar Arrays

Two commercially available phantoms with non-planar diode arrays have emerged as candidates for VMAT verification: ArcCHECK® (Sun Nuclear Corp., Melbourne, FL) [1, 31–33] and Delta^4 (ScandiDos AB, Uppsala, Sweden) [32, 34, 35]. Delta^4 is a cylindrical poly(methyl methacrylate) (PMMA) phantom with two perpendicular arrays of diodes producing a detector array geometry in the shape of an "X". The dose measured by the diode is corrected for a number of factors including temperature sensitivity, directional dependence, depth and field size. These corrections are performed in real time by the data acquisition software which uses trigger pulses from

the linear accelerator controller to trigger data collection and provide temporal data. The Delta^4 has been validated in several studies as a pretreatment verification device for both IMRT and VMAT [34, 36–38]. ArcCHECK® is also a cylindrical PMMA phantom, but with a helical array of diodes that form a cylinder 21 cm in diameter. The phantom has a central air cavity that can be filled with a PMMA plug which has optional slots for film or an ion chamber at its centre. The ArcCHECK® software also has real time diode corrections for field size, depth and beam direction, but rather than use a physical inclinometer attached to the gantry like Delta^4 to aid in these corrections, ArcCHECK® determines the beam angle using diode measurements at the beam entrance and exit points. [1] There have been many studies validating the ArcCHECK® as a 2D non-planar pretreatment verification device for both IMRT and VMAT [1–3, 39, 40]. Although neither the ArcCHECK®, nor the Delta^4 are true 3D dosimeters, they do provide a more viable option for VMAT verification than flat 2D planar arrays.

3D Dose Reconstruction

One form of 3D dosimetry is the combination of both measurement and calculation to produce full 3D dose without a fully 3D physical dosimeter. One example of this is full calculation of the 3D dose based on the data from the MLC log files produced by the linac controller [41–43]. This method relies on the accuracy and correct calibration of the linac controller and is arguably not an fully independent check of the system. There also exists an EPID based dose reconstruction system which uses the fluence from individual IMRT beams to reconstruct the dose into a virtual cylindrical water phantom [44]. This is the system currently used for IMRT pretreatment verification at the British Columbia Cancer Agency - Vancouver Island Centre (BCCA-VIC). Other systems using EPID measurements combined with independent dose calculation engines to reconstruct the dose into patient CT images have also been developed [27]. Similar EPID-based techniques are currently being developed for VMAT verification as well. A commercially available software called 3DVH® (Sun Nuclear Corp., Melbourne, FL) has recently been released for use in conjunction with either MapCHECK or ArcCHECK® diode detectors [45, 46]. The 3DVH® software uses a technique called planned dose perturbation (PDP) to create a full 3D dose reconstruction for IMRT or VMAT verification. Due to the planar nature of the MapCHECK's diode array, VMAT verification is only possible using

the ArcCHECK® phantom. The PDP method uses data from the TPS and the dose measured by the ArcCHECK®'s diode array to guide a 3D dose reconstruction in the phantom itself or in the patient's CT images. It has been suggested that the traditional reconstruction of dose into a phantom for comparison with that calculated by the TPS may be insufficient to catch clinically relevant dose errors in pretreatment verification [47]. The ArcCHECK® phantom combined with 3DVH® has the ability to measure dose directly at the individual diode level, but is also able to reconstruct a full 3D dose distribution within a phantom or into a patient CT image set. The flexibility to combine the clinically relevant 3D patient dose with the more intuitive direct diode measurement and more familiar reconstructed phantom dose make the ArcCHECK® and 3DVH® an intriguing and novel QA system. Although a large set of studies have investigated the ArcCHECK® detector alone, there is little published work on ArcCHECK® detector combined with 3DVH® reconstruction software.

1.4 Thesis Scope

With VMAT as an emerging delivery technique it is necessary to evaluate the potential options for 3D pretreatment verification. VIC recently acquired an ArcCHECK® device with accompanying 3DVH® software. The aim of this thesis is to perform a comprehensive evaluation of this system's ability in 2D and 3D pretreatment dose verification and determine its sensitivity to errors. The focus will be largely on the 3DVH® reconstruction software, for which there is little published work. Although this system has the ability to reconstruct dose into a patient's CT image set, this work focuses solely on direct diode measurements and dose reconstruction into the ArcCHECK® phantom. This is because current IMRT patient-specific verification procedures at VIC uses phantom dose reconstruction and the results of a similar verification method would be more beneficial to the advancement of VMAT verification procedures. The phantom dose reconstruction is an important initial step in the patient dose reconstruction performed by 3DVH® and will provide valuable insight into the potential quality of the patient dose reconstruction. The evaluation was broken down into 4 sequential parts. The first was to establish that the basic requirements of a dosimetric tool were met with this system by analysing fundamental results such as dose linearity, dose rate dependence and field size dependence. The manufacturer has published work on these types of results for this system and a verification of these initial tests was necessary. The second step was to establish confidence in the ability

of the ArcCHECK® system to accurately measure and reconstruct dose distributions by comparing its results, at both the diode level and in 3DVH®, to open fields and IMRT plans calculated by the TPS. As the plans used for this section have passed the well-established IMRT verification procedures at VIC there was confidence in the TPS to accurately calculate these IMRT dose distributions. The third step was to establish baseline results for VMAT plans for two different treatment sites: prostate and head and neck. With no reference for what results to expect for VMAT plans measured using the ArcCHECK® system, it was necessary to establish baselines for VMAT plans before determining the sensitivity of the system to errors. The two treatment sites were chosen because they are two of the most commonly treated site by IMRT at VIC. Prostate will be the first site treated by VMAT at VIC and VMAT treatment of head and neck gives the greatest reduction in overall delivery time of any treatment site when compared to IMRT. These two treatment sites also contrast each other well as head and neck treatments are often very complicated with very large treatment areas and high fluence modulation, whereas prostate treatments have a simpler deliveries with smaller treatment areas and lower fluence modulation. The final step was to determine the sensitivity of the ArcCHECK® system to treatment errors. This was accomplished by delivering plans which had several types of potential treatment errors, and comparing the ArcCHECK® measured and reconstructed results to the TPS calculations of error free plans. The results of this work provides valuable information in determining the role of the ArcCHECK® system in the QA and pretreatment verification of VMAT at VIC.

Chapter 2 discusses the delivery and calculation of complex radiation therapy treatments and the characteristics and response of detectors and software used in this work.

Chapter 3 outlines the methods used to establish the accuracy of the ArcCHECK® and 3DVH® system, as well as the steps taken to determine the system's sensitivity to VMAT errors.

Chapter 4 presents the results and analysis of the ArcCHECK® and 3DVH® system's measurements of open fields and IMRT dose distributions.

Chapter 5 presents the results and analysis of the ArcCHECK® and 3DVH® system's measurements of VMAT plans and the system's sensitivity to VMAT errors.

Chapter 6 will conclude with an overall assessment of the ArcCHECK® detector and 3DVH® software and discuss its future use for VMAT pretreatment verification.

Chapter 2

Background

This chapter discusses the delivery of complex radiation therapy treatment and the factors which affect the final outcome of the delivery. Also discussed are the methods by which the dose to be delivered can be calculated. The characteristics and response of detectors used in this work are also presented. Finally, the methods by which dose distributions are typically compared to one another are examined in an attempt to provide context for the methods that are described in Chapter 3.

2.1 Delivery of VMAT

2.1.1 Linear Accelerator

The delivery of IMRT and VMAT treatment plans is facilitated by a linear accelerator. A linear accelerator produces a beam of high energy electrons, which is used to produce a photon beam for delivery of radiation therapy [48]. Figure 2.1 is a schematic diagram of the major components within the accelerator treatment head when it is used for photon therapy. The mono-energetic electron beam is directed towards a high atomic number target, often tungsten, where bremsstrahlung interactions occur to produce x-ray photons. Bremsstrahlung, or braking radiation, is the name given to radiation produced by the slowing of high speed electrons, which is typically caused by the Coulomb interactions near atomic nuclei. An electron will convert some fraction of its energy to one or multiple photons, so the mono-energetic beam of electrons will produce a radiation beam with a spectrum of photon energies. The maximum energy of the photon beam will be the same as the electron energy and the mean energy photon beam will be approximately one-third of the electron energy

[48]. A photon beam is typically designated by the voltage required to accelerate an electron to the energy that produced the beam. For example, a beam of 6 MeV electrons will produce a 6 MV photon beam.

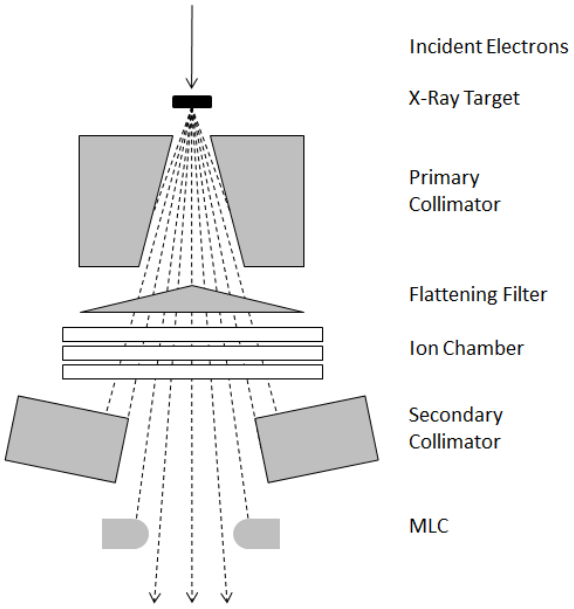

Figure 2.1: Diagram of the major components in a linear accelerator treatment head as used for photon therapy.

The fixed primary collimator is located just beyond the target and removes a large number of scattered photons which are not directed towards the treatment area. The flattening filter is a high density attenuating device used to create a photon beam of uniform intensity at a specific depth. The photon beam produced by megavoltage electrons is largely forward peaked, therefore it is necessary to preferentially attenuate photons near the centre of the beam. A set of ion chambers above the secondary collimation provides a dosimetry check as well as ensures that the electron beam hits the x-ray target in the correct location to produce a flat photon beam. The secondary collimator is made up of two sets of movable jaws (X and Y jaws) which can shape the beam into rectangular open fields. The tertiary collimation on modern linear accelerators is performed by the multileaf collimator (MLC) which is discussed in more detail in the next section. The entire treatment head sits on a gantry which allows the x-ray source to rotate about the patient and deliver radiation from any angle in the plane of rotation. The gantry rotates around a single point, called the isocentre, which is located 100 cm from the x-ray source.

The total integrated dose which is measured by the monitor ion chamber (before

secondary collimation) is described by a unit known as the monitor unit (MU). The MU of a linear accelerator is often calibrated so that for a 6 MV photon beam, 1 MU is equal to 1 cGy at isocentre and a depth of maximum dose in water for a 10×10 cm^2 field. The dose rate of radiation delivery is measured in units of MU per minute.

The two types of accelerators used to deliver radiation in this evaluation of the ArcCHECK® and 3DVH® software were a Varian 21-EX Clinac and a Varian Truebeam (Varian Medical Systems, Palo Alto, CA, USA). These accelerators are shown in figure 2.2.

(a) (b)

Figure 2.2: Varian 21-EX Clinac (a) and Truebeam (b) linear accelerators used at BCCA.

2.1.2 Multileaf Collimator

The Varian MLC is usually comprised of either 40 or 60 pairs of high density leaves that can provide precise shaping of the delivery beam. Both treatment units used Varian 120 Millennium MLCs which are comprised of 60 pairs of leaves, with the 20 outer pairs projecting a 10 mm width at isocentre and the 40 inner pairs projecting a 5 mm width at isocentre. The sides of the MLC leaves are not flat, with an indentation

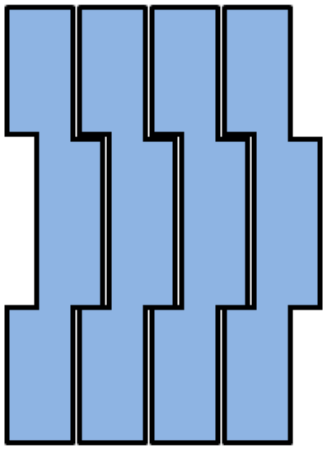

Figure 2.3: Diagram of Varian MLC leaves arranged in a tongue and groove pattern.

on one side and a corresponding outward projection on the other which slides into the neighbouring leaf. This is commonly referred to as a "tongue and groove" design, which is used to reduce leakage between the leaves. A diagram of the tongue and groove design is shown in figure 2.3. Transmission through the MLC leaves, both midleaf and interleaf, is not entirely eliminated but has been shown to be less than 3% [49]. Unlike the X and Y jaws of the secondary collimator, the MLC leaves do not move in an arc which matches the divergence of the radiation beam, but rather in a simple planar motion. In off-axis positions the beam will pass through the leaf at different angles, and if flat leaf ends were used there would be significant differences in transmission through the leaf ends at different positions within the field. To maintain an equal transmission at different beam angles, rounded leaf ends are used. One issue with rounded leaf ends is that the transmission through the leaves is greater near the tip of the leaf and this must be accounted for in any dose calculation. Usually, the leaf end is not explicitly modelled in dose calculations and the excess transmission is treated dosimetrically as a shift in the position of the leaf, slightly increasing the gap between a leaf pair. This factor is often referred to as the dosimetric leaf separation (DLS) or dosimetric leaf gap (DLG) and is on the order of millimetres [49]. Note that the DLG will contribute a more significant portion of the total calculated leaf opening for deliveries with smaller physical leaf openings and the correct modelling of this factor can be important for plans with small average leaf openings.

2.2 Treatment Planning System

Due to the complexity of IMRT and VMAT treatments, the planning of these treatments requires inverse planning. Inverse planning is the process of working backwards from a set of dose prescriptions and constraints in an attempt to find the optimal set of beam fluences that will achieve these goals [7]. For IMRT, these fluences are determined for a set of beams delivered at static gantry angles. For VMAT a single continuous arc is broken up into a number of control points and the fluences are optimized at intervals throughout the arc. Once the optimal set of fluences has been found the TPS will calculate the motion of MLC leaves that will best achieve these fluences. The actual fluences that can be delivered are derived from the motion of the leaves and these fluences will include factors such as the DLG and leaf transmission. From the fluences calculated based of the MLC leaf motions a dose calculation within a patient CT set is possible.

All treatment planning and calculations in this work were performed using the Varian ECLIPSE treatment planning system (Version 10.0.45) with the dose calculations using the anisotropic analytical algorithm (AAA). AAA is a fast pencil beam dose calculation model that is configured using Monte Carlo physical parameters and measured beam data. In AAA the photon beam is separated into smaller beamlets and the patient's CT data is divided in smaller 3D voxels along the beamlets each with a uniform electron density. Calculations from Monte Carlo simulations supply kernels for narrow beams of mono-energetic photons. For each beamlet a weighted superposition of these mono-energetic kernels is used to build a poly-energetic kernel for each voxel along the beamlet which models the depth component of energy deposition. The lateral component is modelled by a poly-energetic scatter kernel which is also a superposition of mono-energetic scatter kernel calculated in Monte Carlo. The lateral scatter kernel is scaled by the electron density in neighbouring voxels to correct for heterogeneity in the medium. Secondary photons generated in the flattening filter and collimator are modelled in the same way as the primary source with the secondary source located at the bottom plane of the flattening filter. The contamination of the primary photon beam by electrons originating in the treatment head is also modelled. The total energy deposited is then a superposition of the contributions from the primary photons, secondary photons and electron contamination for all beamlets. The energy distribution is then converted to dose using the electron density from the CT data set [50].

2.3 Monte Carlo

Monte Carlo simulations calculate dose distributions by simulating the transportation and interactions of millions of particles within the patient. The interactions of particles are sampled from probability distributions based on fundamental laws of physics [51]. In theory the only limiting factor in the accuracy of Monte Carlo simulations is the uncertainty in simulating a finite number of particles using random numbers to sample the probability distributions of the particle interactions. In practice the cost of computing time to simulate a large numbers of particles in dose calculations often requires Monte Carlo codes to trade off absolute accuracy for efficiency. However, despite the necessary trade off for computing times Monte Carlo is still the most accurate method of calculating dose distributions [48]. One method to improve the efficiency of electron interactions is the condensed history technique, where a number of similar interactions which produce small changes in a particle's energy and direction are combined into a single larger step. Other techniques to improve the efficiency of Monte Carlo simulations include bremsstrahlung splitting, photon forcing and range rejection [52]. The Vancouver Island Monte Carlo (VIMC) system used in this work models the linear accelerator treatment head using Beamnrc[53] and DOSXYZnrc[54] to calculate dose distributions within the patient. VIMC has been thoroughly validated for IMRT and VMAT calculations [55–57]. In this work Monte Carlo simulations are used to provide a standard with which the ArcCHECK® measurements and 3DVH® dose distributions can be compared to for open fields and IMRT plans. The dose calculate in Monte Carlo is more accurate and reliable than the dose calculated using AAA.

2.4 ArcCHECK® QA System

The ArcCHECK® detector, seen in figure 2.4, consists of 1386 n-type silicon diode detectors arranged in a 2D helical pattern embedded 2.9 cm from the outer surface of the phantom and which forms a cylinder 10.4 cm from the centre of the doughnut shaped phantom. The outer and inner diameters of the poly(methyl methacrylate) (PMMA) phantom are 26.6 cm and 15.5 cm, respectively. The cavity at the centre of the phantom can be filled with a PMMA plug which can be machined to contain a slot for an ion chamber. The detector separation is 1 cm along both the circumference and length of the helical array. The total length of the detector array is 21 cm with

and length of the phantom is 32.4 cm. Figure 2.5 shows an example of a dose map produced by the ArcCHECK® diode measurements with the dose measured by the diode detectors unwrapped onto a flat plane. The location of each diode is represented by a square marker.

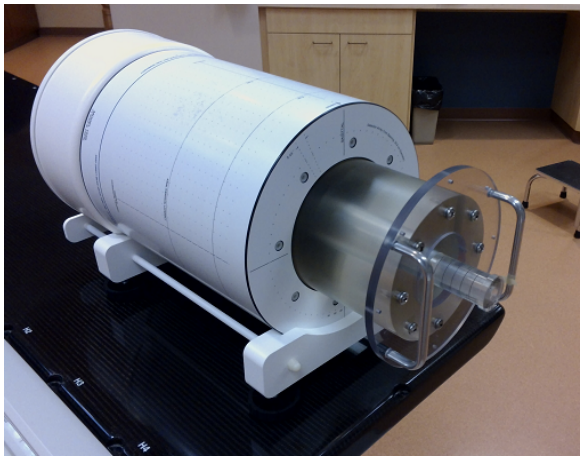

Figure 2.4: Image of the ArcCHECK® detector with central cavity plug and ion chamber insert.

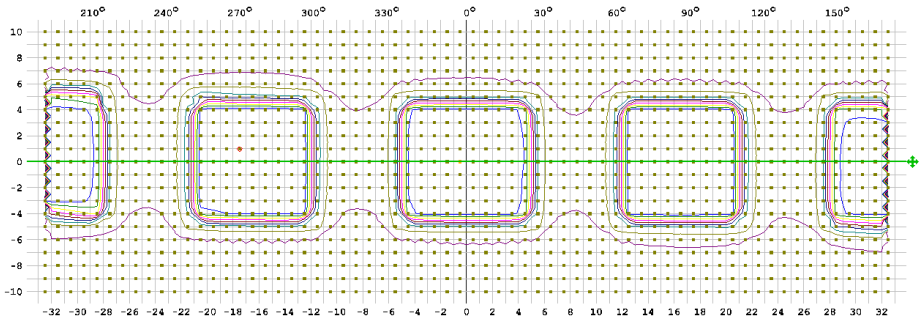

Figure 2.5: Dose map displayed in the ArcCHECK® software with the diodes unwrapped onto a flat plane. The centre of the map corresponds to the top of the phantom and edges correspond to the bottom of the phantom. Each square marker corresponds to a diode detector.

2.4.1 Diode Detectors

An n-type silicon diode detector consist of a silicon substrate lightly doped with phosphorus to produce an n-type region and a surface heavily doped with boron to produce a p-type region. The n-type region receives carriers of negative charge and

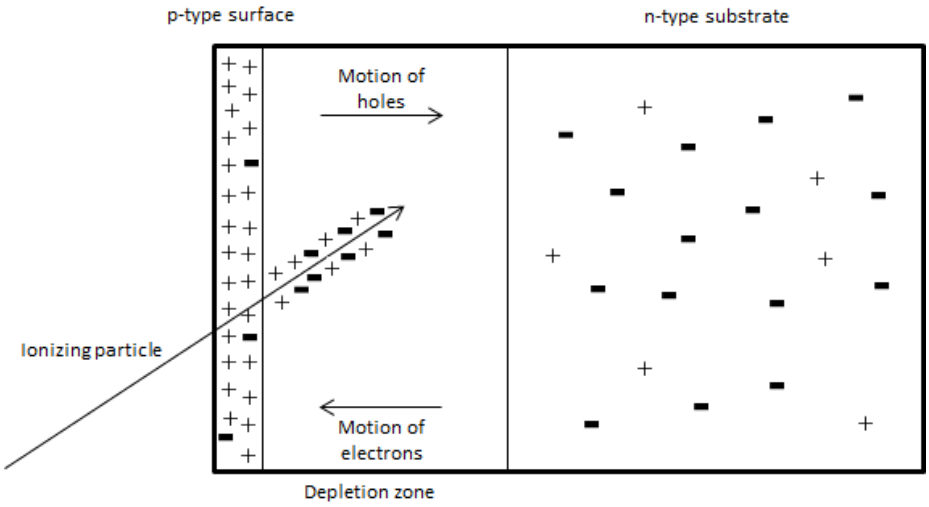

Figure 2.6: Diagram of an n-type diode exposed to ionizing radiation.

contains excess electrons and the p-type region is deficient in electrons and is an electron receptor, or said to contain holes. When a positive voltage is applied to the n-type region, as seen in figure 2.6, electrons and holes are pulled from the region near the substrate-surface border and a depletion region is formed over which little or no current can flow. When an ionizing particle passes through this depletion zone and interacts to produce electron-hole pairs, they are immediately separated to by the electric field created in the depletion zone. This will produce a current in the diode which is relative to the number of ion pairs produced by ionizing radiation.

Diode detectors are highly sensitive to ionizing radiation (18 000 times more sensitive than an air filled ionization chamber) [48], therefore the sensitive volume of diode detectors can be small while still achieving adequate sensitivity. However, the high atomic number of silicon relative to water and therefore, increased cross-section of the photoelectric effect for silicon, causes diode detectors to be overly sensitive to low energy photons. This leads to a field size effect in diode measurements, as diodes will over respond to scattered low energy photons in larger field sizes [20]. The sensitivity of silicon diodes have also been shown to be dependant on temperature, dose rate and beam direction [22, 23, 58]. For many diode detector devices, such as the ArcCHECK® and MapCHECK®, the field size and angular dependence of the diode detectors is significant, and correction factors are necessary to account for these effects.

In the ArcCHECK® detector several correction factors are used to account for

the various dose dependencies of the diode detectors. The intrinsic sensitivity of each individual diode within the array is calibrated by a set of wide field measurements. A factory calibration file is provided with the ArcCHECK® detector, and the procedure for performing the array calibration is provided to enable for future calibrations. This individual diode calibration applies corrections to the raw readings for each diode to ensure equal sensitivity of all diodes [1]. To account for field size dependence, there is a set of field size corrections for diode measurements. The field size corrections vary based on angular position of the diode relative to beam entry, beam energy and whether or not the central plug is used [1]. A heterogeneity correction is included to account for the air cavities, diodes, and electronics within the detector array. This correction converts the dose measured in the heterogeneous phantom to dose in a homogeneous phantom for comparison with a virtual homogeneous phantom provided for TPS calculations. Finally, a set of angular corrections is included to account for the sensitivity changes for the diodes based on the angle of beam entry. These correction factors all require information about the angle of beam entry in the correction of the diode's doses. To determine the beam entry angle the ArcCHECK® detector uses a virtual inclinometer, which projects the dose measured by diodes in the top and bottom half of the detector to create two dose images projected onto the same plane at the centre of the phantom. The beam angle used to determine this projection plane is varied until the difference between the images is minimized. This method of determining beam angle has been shown to produce accurate results [1].

2.4.2 Ionization Chamber

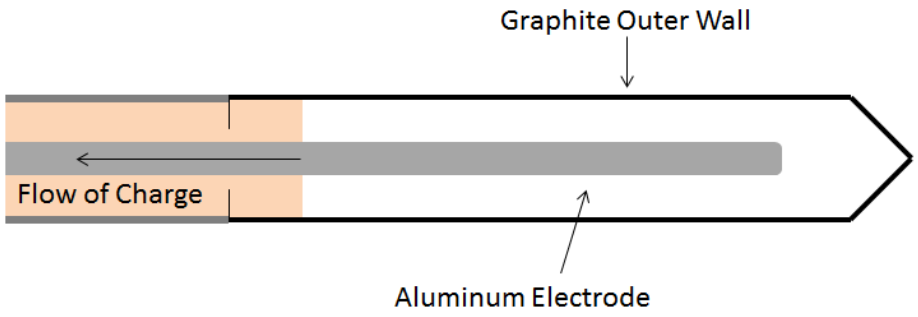

Figure 2.7: Diagram of a Farmer type ion chamber.

The ionization chamber, or ion chamber, is the most commonly used dosimeter in radiation therapy and when calibrated correctly provide accurate absolute point

dose measurements. The use of ion chambers in IMRT and VMAT pretreatment verification is discussed in chapter 1. The ion chamber used in this work was a Farmer type chamber which has an active volume 0.6 cc. A diagram of a Farmer type ion chamber is shown in figure 2.7. The chamber consists of a pure aluminium electrode at the centre of air-filled cavity with a pure graphite surrounding wall. When ionizing radiation interacts with the air within the chamber cavity, ion pairs are produced. If a potential difference (usually -300 V) is held between the electrode and chamber wall, the charge produced by the electrons will be collected at the electrode. This collected charge will be proportional to the absorbed dose to the gas at that point. The advantages of using ion chambers include accurate dosimetry, near tissue equivalence and little to no directional dependence.

2.4.3 3DVH®

3DVH® is a dose reconstruction software which has the ability to take measurements from the ArcCHECK® diodes and perform a measurement guided dose reconstruction to estimate the 3D dose that was delivered. The reconstruction relies on the ArcCHECK® data file that is generated when an ArcCHECK® measurement is made, and the DICOM RT Plan file generated in ECLIPSE for the plan that was delivered. The ArcCHECK® measurement file is logged with updates at 50 ms intervals which stores the updated dose and gantry angle determined by the virtual inclinometer at each interval [46]. The time resolved gantry measurements are used to synchronize the RT Plan's control points to corresponding points in the ArcCHECK® measurement file. If the virtual inclinometer determination of gantry angles does not match up with the gantry angles in the ECLIPSE plan, the synchronization will fail and the reconstruction will be aborted. Next the RT Plan file is used to create a set of sub-beams at 2° intervals and interpolate control point data to create a modulated fluence for each sub-beam. A 3D grid of the total energy released per unit mass (TERMA) is then calculated for each sub-beam and convolved with a 3D dose scatter depth kernels to generate a relative 3D dose grid for each sub-beam. The TERMA and scatter kernels are modelled for specific linear accelerator models and beam energies which must be specified before the 3D reconstruction is performed. The relative dose grids for each sub-beam are then normalized to absolute dose using entrance and exit diode measurements from each sub-beam. The 3D normalization is not uniform, as scaling factors are interpolated between entrance and exit dose. Diodes with less

than 80% of the sub-beam's maximum dose at each surface (entrance and exit) and diodes in areas of high gradient are not used in this normalization procedure [46]; an addition to latest version of the software called "high sensitivity mode" disregards these conditions and uses all diodes in the normalization. Note that the volume of reconstruction is limited to the volume within the diode array as this is the limit of the absolute dose scaling.

Once an absolute dose grid for each sub-beam has been calculated; these dose grids are then summed to create a full 3D absolute dose grid. The final step in the reconstruction process is a global correction factor which is a uniform normalization of the 3D dose grid to minimize cumulative dose differences between the 3D reconstructed dose and diode measurements; only diode with greater than 30% of the maximum diode dose are used in the global normalization [46]. The final result is a 3D distribution of absolute dose within a homogeneous phantom which can be compared to the dose calculated in the homogeneous phantom in ECLIPSE. Dose reconstruction within the PMMA phantom is the focus of this work, but the 3DVH® does have the capability to reconstruct dose into a patient CT image set which provides more clinically relevant dose comparisons. 3DVH® uses the differences between reconstruction and ECLIPSE phantom doses to predict differences between reconstruction and ECLIPSE patient doses, so the reconstruction of dose into the phantom is an important step towards the calculation of dose into a patient CT set.

The 3DVH® software also has the ability to perform comparisons of the reconstructed dose to the dose calculated in ECLIPSE. The software allows for 3D gamma analysis with variable gamma criteria and dose thresholds, 3D mean dose difference calculations and DVH comparisons.

2.5 Dose Distribution Evaluation Techniques

2.5.1 Gamma Analysis

Gamma analysis, or γ-analysis, is a convenient method of condensing the comparison of dose distributions into a single metric. A simple comparison of dose difference is not a sufficient method to compare measured and calculated dose distributions, especially in areas of high dose gradient, where a small spatial misalignment of either the measured or calculated dose can produce a significant difference in dose. A more useful way to evaluate high dose gradient areas is the distance-to-agreement metric,

which is the smallest distance between a measured data point and a data point in the calculated dose distribution that have the same dose. Low et al. [59] suggested combining dose difference and DTA comparisons in a quantity now commonly referred to as the γ-index.

Given dose difference and DTA criteria, ΔD_C and Δd_C respectively, the gamma index for the point in the measurement $\mathbf{r}_m$ is as follows:

$$\gamma(\mathbf{r}_m) = min\{\Gamma(\mathbf{r}_m, \mathbf{r}_c)\}\forall\{\mathbf{r}_c\}, \tag{2.1}$$

where,

$$\Gamma(\mathbf{r}_m, \mathbf{r}_c) = \sqrt{\frac{(\mathbf{r}_c - \mathbf{r}_m)^2}{\Delta d_C^2} + \frac{(D_c(\mathbf{r}_c) - D_m(\mathbf{r}_m))^2}{\Delta D_C^2}}, \tag{2.2}$$

$\mathbf{r}_c$ is a point in the calculation, $D_m(\mathbf{r}_m)$ is the dose at $\mathbf{r}_m$ and $D_c(\mathbf{r}_c)$ is the dose at $\mathbf{r}_c$. A point with a γ-index less than or equal to 1 passes the given γ criterion and a point with a γ-index greater than 1 fails. It is common for the dose difference, $D_c(\mathbf{r}_c) - D_m(\mathbf{r}_m)$, to be normalized to the maximum dose within the dose distribution (global normalization), however the dose difference can also be normalized to the dose at the point of interest (local normalization). When global normalization is used, errors in the low dose region can be masked by the global normalization, however it is not clear whether these errors are clinically relevant [20]. When using γ analysis, points below a certain dose threshold, usually a percentage of the maximum dose, are often eliminated from the analysis.

At the diode level the ArcCHECK® software calculates the γ-index using a simplified method, where the individual dose difference and DTA criteria are tested first; only if they both fail will a full γ-index calculation be made. This focuses the results on the γ-pass rate, the percentage of points that pass the γ criterion, rather than the actual γ-index values for each point. The ArcCHECK® software also provides the option of 2D and 3D DTA analysis. When analysing a measurement point, the 2D DTA analysis searches only for points in the calculation along the detector plane, whereas the 3D DTA analysis searches above and below the detector plane in the calculation dose distribution. In this work all diode level analysis used the 3D DTA option.

The most common γ criteria used for pretreatment verification is 3%/3 mm with global dose difference normalization [20]. This is also the γ criteria suggested in the TG-119 report on IMRT commissioning [17], which also used a dose threshold of 10%

for γ analysis. TG-119 suggested acceptable γ-pass rates of 90% for per field IMRT analysis and 88%-90% for composite irradiations analysed with film, with the caveat that gamma pass rates will strongly depend on the specific details of the procedure used. Basran et. al [60] suggested that acceptable IMRT QA pass rates may be site dependant, with 95% suggested for non-head and neck IMRT plans and 88% for head and neck IMRT plans using a 3%/3mm gamma criterion and a 10% dose threshold. Finally, Sanghangthum et al. [40] found that when using the ArcCHECK® detector (but not 3DVH®) for VMAT QA, a lower limit on γ-pass rates should be 90%. At BCCA-VIC the IMRT pretreatment verification procedure uses a χ-evaluation developed by Bakai et. al [61] which is similar to the γ-index. The criterion used for the χ-evaluation at BCCA-VIC is 3%/3 mm with a 90% lower limit on pass rates. The χ-evaluation is performed in two regions: for points above 80% of the reference dose and for points within 40% and 80% of the reference dose, where the reference dose is a point within the high dose region and is similar to the prescription dose.

2.5.2 Dose Differences

Another way to compare dose distributions is to calculate point dose differences for points within the dose distributions and to calculate the mean dose differences for volumes of interest. TG-119 recommends that point measurements within an ion chamber remain within 5% of the calculated dose [17].

At BCCA-VIC a 3% action level is used for reference point dose measurements where the dose at the reference point must be greater than 90% of the prescription dose and in a region with a low dose gradient. Mean dose differences, as with γ-pass rates, are evaluated in a high dose region for points with dose greater than 80% of the maximum dose and in a lower dose region for points with dose falling between 40% and 80% of the maximum dose. The action level for the mean dose difference in these regions is 2%.

Chapter 3

Methods and Materials

To evaluate the ArcCHECK® device a number of radiation therapy plans, from open fields to more complicated IMRT and VMAT plans, were delivered using a Varian 21-EX Clinac and Varian Truebeam (Varian Medical Systems, Palo Alto, CA, USA) at the BCCA-VIC. This chapter outlines the measurements that were performed and the forms of analysis used to evaluate the ArcCHECK® and 3DVH® dosimetry system. A summary of these measurements and analysis are shown in figure 3.1, along with overall goal of each set of measurements. Section 3.1 outlines the methods used to analyse the ArcCHECK® diode response and the models used in ECLIPSE for the ArcCHECK® phantom and treatment couches. Section 3.2 describes the dose comparison metrics used to compare calculated and measured doses. Section 3.3 and 3.4 describe the procedure for the measurement of open fields and IMRT plans. Section 3.5 outlines the methods used to establish baseline results for VMAT plans and section 3.6 describes the introduction of errors into VMAT plans and the methods that were used to determine the sensitivity of the ArcCHECK® phantom and 3DVH® software to errors.

3.1 Initial Characterization

3.1.1 Diode Response

The response of the diode detectors embedded within the ArcCHECK® phantom was evaluated to ensure an accurate response of the diodes. The ArcCHECK® phantom makes real time corrections to diode measurements to account for factors affecting diode response such as field size, beam direction and beam energy. In depth studies

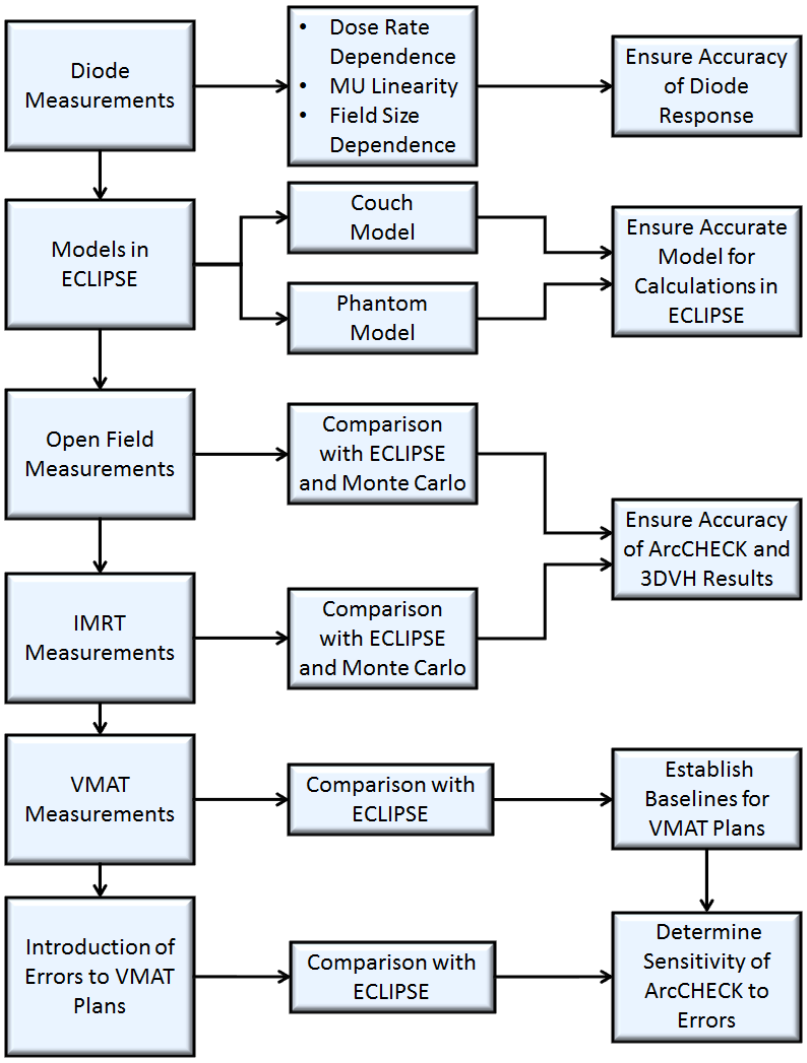

Figure 3.1: Flow chart describing the measurements performed and the overall goal of each type of measurement.

of these effects and corrections factors have been performed for the ArcCHECK® system [1, 2, 32, 33] and the following diode response tests were performed to confirm the application of these factors. Diode response to dose rate, MU linearity, and field size were investigated. An outline of the different parameters that were tested are shown in table 3.1. In all measurements testing diode response, the dose was averaged between 6 diodes surrounding the central axis at the top of the ArcCHECK® device as shown in figure 3.2; a set of similarly arranged diodes at the bottom of the device was also used. Diodes at the top and bottom of the device were investigated separately to determine the magnitude of these effects at both the entrance and exit plane of

the beam.

Table 3.1: Summary of the parameters varied to test the response of the diode detectors.

	Values Tested
Dose Rate (MU/min)	100, 200, 300, 400, 500, 600
MU Linearity (MU)	5, 10, 20, 100, 200, 300
Field Size (cm^2)	3×3, 5×5, 8×8, 10×10, 15×15, 25×25

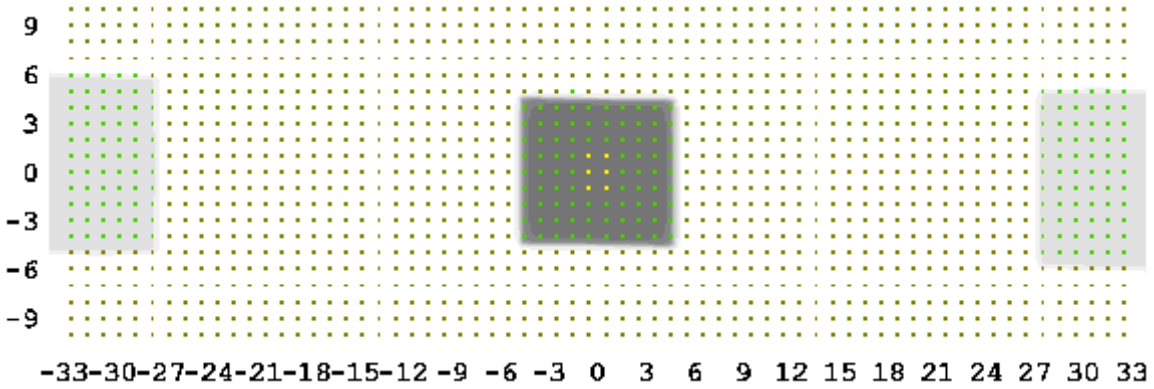

Figure 3.2: Image highlighting the positions of the 6 diodes (yellow markers) at the top of the ArcCHECK® used in testing the factors which affect diode response.

The effect of dose rate was studied by delivering 200 MU in an open 10×10 cm^2 field at different dose rates and determining the sensitivity of each measurement relative to 400 MU/min. Dose linearity was investigated by delivering an increasing number of MU in 10×10 cm^2 fields. The effect of field size was examined by delivering 200 MU at different field sizes and comparing the sensitivity of diodes relative to a 10×10 cm^2 field. In the case of field size, the dose at the centre of the field is not the same at different fields size due to scatter considerations, so dose calculated in ECLIPSE provided a standard for comparison with measurements and the difference between measurement and ECLIPSE provided a measure of diode sensitivity.

3.1.2 Modelling ArcCHECK® Phantom in ECLIPSE

Virtual CT images of the ArcCHECK® phantom were provided by Sun Nuclear for use in ECLIPSE with an electron density of 1.15 assigned to the virtual homogeneous ArcCHECK® phantom. For optimal results, Sun Nuclear recommends adjusting the

density to match ECLIPSE results to measurements. When using the original electron density in ECLIPSE it was discovered that the attenuation in the ArcCHECK® phantom calculated in ECLIPSE did not match measurements. When this electron density was used in ECLIPSE and a 10×10 cm^2 open field was delivered, dose measured by the diodes where the beam entered the phantom matched dose calculated in ECLIPSE, but dose measured by the diodes where the beam exited the phantom was lower than in ECLIPSE. The electron density was increased to account for this discrepancy, increasing the calculated attenuation of the beam, until the calculated entrance and exit dose matched what was physically measured by the diodes.

Three-dimensional dose distributions were calculated in 3DVH® for open fields using different electron densities in ECLIPSE and the agreement between ECLIPSE and 3DVH® was compared. The electron densities that produced the best agreement was different for the two types of linear accelerators used: The optimal electron densities were 1.18 and 1.20 for the 21-EX and Truebeam, respectively. The optimization of the phantom electron density improved agreement between ECLIPSE and measurement for both open fields and for a preliminary subset of IMRT plans.

3.1.3 Modelling Treatment Couch in ECLIPSE

Attenuation by the treatment couch on both the 21-EX and Truebeam linear accelerators can have a significant impact on dosimetry and plan verification for both IMRT and VMAT [62–66]. Since the ArcCHECK® phantom must be placed on the treatment couch during pretreatment verification measurements, the couch will affect the measurements and it therefore must be modelled in ECLIPSE if the calculations are to be an accurate comparison.

The 21-EX is equipped with a Varian Exact couch which holds a grid couch insert supported by two movable rails, all made of carbon fibre to reduce attenuation. For all 21-EX measurements the ArcCHECK® phantom was placed on the couch grid and the support rails were moved to their furthest position from the centre of the couch so as to provide a consistent setup. Positioning the rails at the edge of the couch was also ideal, as the majority of the prostate and head and neck IMRT cases studied were designed to avoid the rails using this setup. The setup on the 21-EX linear accelerator is shown in figure 3.3a. The insert and rails were modelled in ECLIPSE as shown in figure 3.4a. The couch insert centre was assigned an electron density of 0, and the frame was assigned an electron density of 1.00. The couch

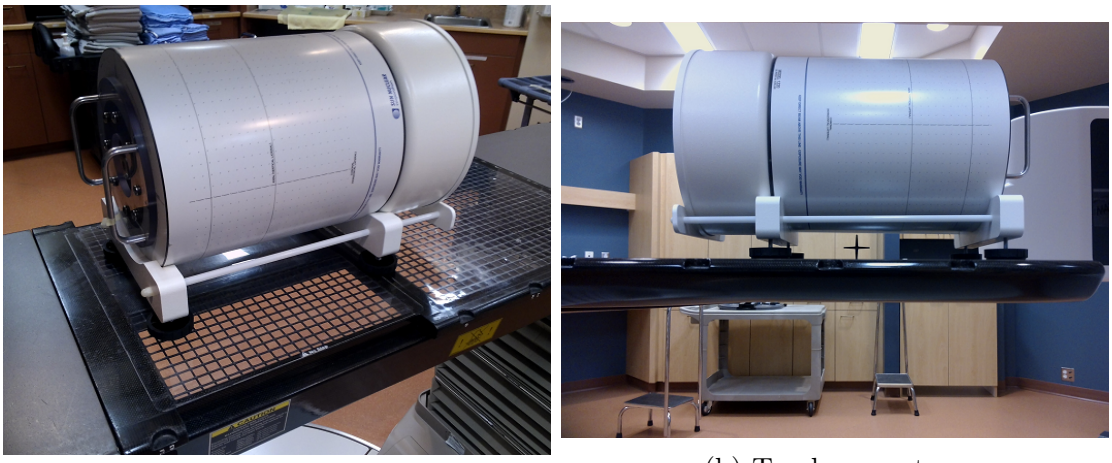

(a) 21-EX Clinac setup.

(b) Truebeam setup.

Figure 3.3: Images showing the setups of the ArcCHECK® used on the two different linear accelerators.

density values were verified by delivering a posterior 10×10 cm^2 open field to the ArcCHECK® phantom directly through the bottom of the couch and comparing the dose distribution in ECLIPSE to diode measurements and 3DVH® reconstructions. The interior and outer frames of the two rails were assigned electron densities of 0 and 1.10, respectively. The rail density values were verified by delivering a 10×10 cm^2 open field to the ArcCHECK® phantom directly through the rail at a gantry angle of 150° and comparing the dose distribution in ECLIPSE to diode measurements and a 3DVH® reconstruction. Ion chamber measurements at isocentre were also used to help asses the amount of attenuation by the couch.

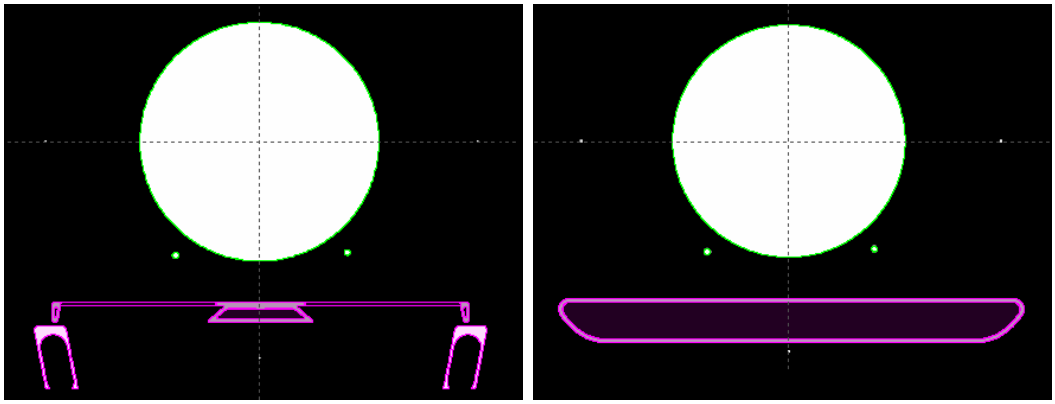

(a) Clinac Couch

(b) Truebeam Couch

Figure 3.4: Models of couches used in ECLIPSE for dose calculations.

The Truebeam is equipped with a Varian Exact IGRT couch which is a carbon fibre shell filled with foam and, unlike the couch on the 21EX machine, has no support rails. The thickness of the couch varies along the longitudinal axis from 5 cm at one end of the couch to 7.5 cm at the thicker end with a transition section between the two. The couch model used in ECLIPSE was for the thin section of the IGRT couch shown in figure 3.4b, and for all measurements performed on the Truebeam the ArcCHECK® was aligned so that the entire phantom was sitting above only the thin section of the couch. The setup for the ArcCHECK® on the Truebeam couch is shown in figure 3.3b. The central foam portion and carbon fibre shell were assigned electron densities of 0.10 and 0.69, respectively. The Truebeam couch densities were determined by delivering several 10×10 cm^2 open fields at gantry angles between 180° and 130° in 10° intervals and matching the dose calculated in ECLIPSE to the dose measured at the diodes in ArcCHECK®. The couch densities were further verified by delivering a 10×10 cm^2 open field partial arc through the couch to the ArcCHECK® phantom and comparing the dose distribution in ECLIPSE to diode measurements and a 3DVH® reconstruction. Ion chamber measurements at isocentre were also used to help asses the amount of attenuation by the couch.

Once the phantom and couch structures had been set and assigned electron densities in ECLIPSE it was possible to create verification plans using the virtual phantom CT image set and calculate dose in the phantom. The ECLIPSE dose distributions were then available for comparison with diode measurements and use in the 3DVH® software.

3.2 Dose Comparison Metrics

For open field, IMRT and VMAT plans, several metrics were used to compare the dose calculated ECLIPSE or Monte Carlo to dose measured by the ArcCHECK® diodes or reconstructed in 3DVH®.

The SNC Patient software (Sun Nuclear Corp., Melbourne, FL) allowed for comparison of the diode point dose measurements to the ECLIPSE dose distributions. The main method of comparison was the 3D γ passing rate, which was calculated with γ criteria of 2%/2mm and 3%/3mm using a 10% dose threshold. Both the more commonly used global dose difference, and more stringent local dose difference, were used in the γ analysis.

In 3DVH®, 3D γ analysis was used as to compare 3D reconstructed dose to

ECLIPSE calculated dose; the same range of γ criteria used SNC Patient was used in 3DVH®. The same analysis was repeated using 40% and 80% dose thresholds to determine passing rates specific to the high and intermediate dose regions of the dose distributions. Along with γ passing rates the mean dose differences in the 40% and 80% isodose regions was also calculated for each dose distribution. The 80% isodose region is specific to the high dose region covering the dose prescription to the tumour and the 40% isodose region includes some of the surrounding tissues which will also receive a significant amount of dose. Examples of the isodose structures can be seen in figure 3.5.

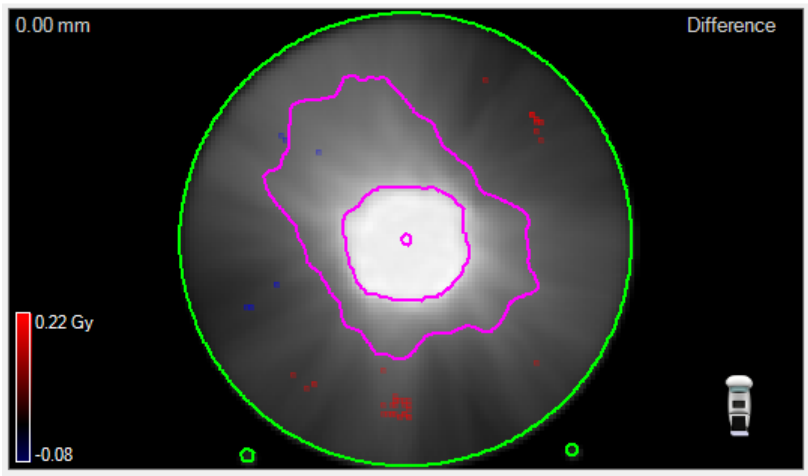

Figure 3.5: Example of 40% and 80% isodose structures as seen on a prostate plan in 3DVH®. Also shown at the centre of the distribution is the ion chamber structure.

To compare ion chamber measurements to dose in ECLIPSE, an ion chamber structure, shown in figure 3.5, was created and the mean dose inside the chamber's collection volume was calculated to account for the finite size of the chamber. The same ion chamber structure was used to calculate the mean dose at isocentre in the 3DVH® dose reconstruction which could then be compared to mean dose at isocentre in ECLIPSE and the physical ion chamber measurement. To further avoid volume averaging effects, any verification plans where the isocentre fell in a region of high dose gradient were shifted to place the isocentre in a more uniform dose region.

3.3 Measurement of Open Fields

Open fields were delivered to ArcCHECK® on both the 21-EX and Truebeam linear accelerators to asses the accuracy of the diode detectors and 3DVH® reconstructions for the simplest configurations. The open fields were 10×10 cm^2, with 200 MU delivered at a dose rate of 400 MU/min on the 21-EX and 600 MU/min on the Truebeam. These fields were delivered individually at gantry angles of 0°, 90°, 180°, and 270° and together in one measurement in a delivery known as a "4-field box" with 50 MU delivered per gantry angle to give the same total dose at isocentre as the individual open fields. These open field measurements were then compared to results calculated by ECLIPSE. The open field measurements were compared dose calculated in Monte Carlo simulations as an additional test of the accuracy of the ArcCHECK® and 3DVH® system.

3.4 Measurement of IMRT plans

IMRT plans were chosen from a pool of patient plans that had passed the IMRT pretreatment verification process at VIC and therefore were established as accurate dose distributions. Eight prostate and eight head and neck plans were selected for comparison. On the 21-EX machine the original patient plans were converted into verification plans on the ArcCHECK® phantom and the dose distributions were calculated in ECLIPSE. The patient plans were then exported to a treatment machine and delivered to the ArcCHECK® phantom for comparison with ECLIPSE results. As with open fields, dose distributions for the IMRT plans were calculated independently using Monte Carlo simulation for comparison with measurement. The same 16 patient plans, with the exception of two prostate plans which were replaced for Truebeam measurements, were converted from 21-EX to Truebeam IMRT plans. As with the 21-EX, verification plans were created and calculated in ECLIPSE followed by delivery to the ArcCHECK® phantom for comparison with ECLIPSE results. Monte Carlo dose distribution calculations were not performed for plans delivered on the Truebeam because a model for the Truebeam had not yet been validated on the VIMC system.

All IMRT measurements were accompanied by an ion chamber measurement at the centre of the ArcCHECK® phantom, which coincides with the isocentre of the delivery, for comparison with the isocentre dose in ECLIPSE. This ion chamber mea-

surement was also compared to the dose at isocentre calculated in the 3DVH® dose reconstruction. All IMRT plans were also delivered to a 20.4 cm diameter water phantom with an ion chamber measurement at isocentre. This ion chamber measurement was compared to the isocentre dose in ECLIPSE for a water phantom verification plan. The dose difference at isocentre between ion chamber measurements and ECLIPSE were calculated for both the water phantom and the ArcCHECK® phantom. This was done to verify the validity of the ion chamber dose measurement in the PMMA material as ion chamber measurements and IMRT pretreatment verification is typically performed on a water phantom at VIC. The water phantom measurement also had the added benefit of acting as a further verification of the couch model as the water phantom measurement is performed without the couch in the way to attenuate any of the beams. The setup of the water phantom is shown in figure 3.6.

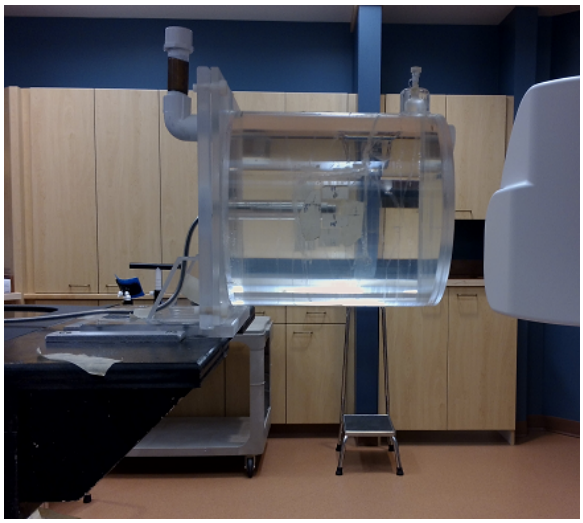

Figure 3.6: An image showing the setup of the water phantom used to perform ion chamber measurements at isocentre for IMRT and VMAT plans.

3.5 Establishing VMAT Baselines

As there is little in the way of published results for the use of 3DVH® with the ArcCHECK® phantom and no established pretreatment verification technique for VMAT delivery at VIC it was necessary to establish a baseline set of results for VMAT plans. This baseline was essentially an expected γ-pass rate for a VMAT plan and a range over which one would expect typical VMAT passing rates to fall. Then, when errors were intentionally induced, if the passing rate fell outside the expected

range the plan failed and the ArcCHECK® system was deemed to have caught the potential error.

3.5.1 VMAT Interplan Variation

The optimization objectives used for the 16 IMRT plans delivered on the Truebeam were used to optimize two-arc VMAT plans. For each site, prostate and head and neck, the results from these measurements provided a range of passing rates one might expect from error free plans for each site. These plans used the same targets and dose constrains as the IMRT optimizations. As with the IMRT plans, verification plans were created and calculated in ECLIPSE followed by delivery to the ArcCHECK® phantom for comparison with ECLIPSE results. Each VMAT measurement included an ion chamber measurement at the center of the ArcCHECK® phantom for comparison with ECLIPSE and 3DVH® isocentre dose. As with IMRT plans, the VMAT plans were delivered to a water phantom with an ion chamber measurement at isocentre and compared to results in ECLIPSE.

3.5.2 VMAT Intraday and Interday Variation

It is important for any pretreatment verification device to not only be sensitive to significant dosimetric errors, but also have high specificity. This ensures that plans which are free from significant dosimetric errors do not fail the verification and resources are not wasted in reinvestigating and potentially replanning a dosimetrically sound plan. For an individual VMAT delivery there are many factors that can fluctuate on a day-to-day and even delivery by delivery basis, but will in most cases not introduce significant dosimetric errors. It is necessary for a pretreatment verification device to be able to distinguish the significant errors from an insignificant one. To test the consistency of the ArcCHECK® system over multiple measurements, a single prostate and single head and neck plan were chosen for measurement. Each plan was tested in two ways: by taking 8 measurements in a single day and by taking 8 measurements over 8 different days. The intraday measurements were necessary to determine the consistency of the ArcCHECK® results when small changes in the delivery of the plan occur, where the variation in the results is affected by factors such as machine output, MLC leaf accuracy, gantry angle accuracy, MU accuracy, and dose rate accuracy. These factors are routinely subject to QA procedures to ensure that they do not produce significant dosimetric errors. The intraday measurements would

also show any affect or trend in the ArcCHECK® results caused by taking many consecutive measurements over a short period of time. The interday variation was affected by the same factors as the intraday variation plus changes in temperature and pressure and differences in the setup over the 8 days of measurements.

3.6 Sensitivity of VMAT Plans to Errors

In order to determine the sensitivity of the ArcCHECK® system to treatment errors the same two plans used for the intraday and interday variation test were investigated. The effect of MU normalization errors, MLC position errors, gantry position errors, delivery of a partial plan and changes in dosimetric leaf gap were investigated. A summary of the parameters varied for the VMAT error investigation is shown in table 3.2. In all cases, except for the changes dosimetric leaf gap, the delivery of the plan was altered in order to acquire a measurement with errors. At the diode level, the measurement with errors was compared to an error free ECLIPSE calculation to determine the change in pass rate when errors were induced. In 3DVH®, the 3D dose reconstruction was guided by the measurement with errors and the error-free ECLIPSE plan. The final reconstructed dose was then compared to the error-free ECLIPSE plan.

For the MLC and normalization errors, a second set of ECLIPSE plans was calculated with the same errors that were induced for delivery. These plans with calculated errors were compared to the 3DVH® results to determine the accuracy with which 3DVH® can predict the final outcome of the error-filled delivery in a 3D dose reconstruction. Note that in this case the 3DVH® reconstruction was still guided using the error-free ECLIPSE plan, but then compared to the ECLIPSE plan with errors. This was done to simulate the type of situation that would arise in normal pretreatment verification procedures.

3.6.1 Monitor Unit Normalization Errors

An MU normalization error is a difference in the machine output from what is expected, effectively changing the dose normalization of the plan. This was tested by adjusting the total number of MU of each plan. The plans with altered MU were delivered to the ArcCHECK® phantom and the results were compared to the unaltered plans calculated in ECLIPSE.

Table 3.2: Summary of the parameters varied to test sensitivity of the ArcCHECK® and 3DVH® to VMAT errors.

Type of Error	Values Tested
MU Normalization Error	±1%, ±2%, ±3%, ±5%
Systematic MLC Error (mm)	±1, ±2, ±3, ±5
Random MLC Error (mm)	1, 2, 3, 5
Systematic Gantry Error (°)	1, 2
Random Gantry Error (°)	0.5, 1
Percentage of Second Arc Delivered	95%, 90%, 85%
Dosimetric Leaf Gap Used (mm)	1.2, 1.4, 1.6, 1.8

3.6.2 MLC Leaf Position Errors

The MLC leaves are used to modulate the beam and control the distribution of dose. Therefore, the accuracy of the leaf positions is critical in ensuring a predictable delivery. Although the MLC is subject to its own set of QA procedures it is still important that any significant error with the leaf positions is detectable in pretreatment verification. The original error free plans calculated in ECLIPSE were exported, and each MLC leaf position for every control points of the delivery was altered. This was done in both a random and systematic manner. For the random errors, each leaf position was changed by a random number sampled from a uniform probability distribution and each gap was either increased or decreased. The values in table 3.2 are the maximum random errors induced. All gaps less than zero were reset to 0 to avoid any crashing of the MLC leafs. For the systematic errors, the gap between each leaf pair was changed by the same amount so that there was a systematic change in the overall MLC gap. The gaps were either increased or decreased creating a set of plans where all the gaps were more open and a set where all the gaps were more closed. The plans with MLC errors were delivered to the ArcCHECK® phantom and the results were compared to the unaltered plans calculated in ECLIPSE.

3.6.3 Gantry Position Errors

The position of the gantry is a factor which affects the distribution of dose delivered in each control point. The accuracy of the gantry position can potentially have an effect on the dose distribution as a whole. As with MLC leaf position errors, the gantry positions in the error free plans were altered either randomly or systematically. For random gantry angle errors the gantry angle of each control point was changed by a

random number sampled from a uniform probability distribution. The gantry position was either increased or decreased and the maximum random gantry position changes are listed in table 3.2. Setting the maximum random gantry angle change greater than 1.0° created plans where the gantry changed direction during a single arc, so 1.0° was the maximum random change used. The plans with random gantry angle errors were delivered to the ArcCHECK® phantom and the results were compared to the unaltered plans calculated in ECLIPSE. For the systematic errors, ECLIPSE would not allow the calculation or export of a plan with systematic gantry angle changes because it would create control points with gantry angles beyond the maximum point of rotation, 180°. So, for systematic gantry angles shifts of 1.0° and 2.0°, an error free plan was delivered with the phantom itself rotated. The accuracy of the phantom rotation was ensured by using the physical inclinometer within the ArcCHECK® phantom.

3.6.4 Partial Deliveries

The partial delivery of a VMAT plan has the obvious effect of decreasing the overall dose delivered. Partial deliveries were tested by turning off the beam after a fraction of the MU in the second arc of each plan had been delivered. The measurements and 3DVH® reconstructions were compared to the full delivery of each plan.

3.6.5 Dosimetric Leaf Gap Errors

The dosimetric leaf gap, as defined in ECLIPSE, is used to take into account for leaf end transmission due to the rounded leaf end shape. The value of this parameter is determined during commissioning of the linear accelerator and TPS. By changing this leaf gap value the dose distribution calculated in ECLIPSE for a given plan will change. As this parameter is used in the dose calculated in ECLIPSE it will have no effect on the dose that is actually delivered by the linear accelerator. So a single measurement made by the ArcCHECK® was compared to ECLIPSE plans with the different dosimetric leaf gaps.

Chapter 4

Results and Discussion I: Open Field and IMRT Measurements

This chapter presents the results of the initial characterization of the ArcCHECK® phantom's diode response to radiation and a comparison of the ArcCHECK® and 3DVH® dose to known methods for open fields and IMRT deliveries. The ArcCHECK® phantom's diode response is evaluated for several factors which are outlined in section 3.1.1, with the results displayed in section 4.1. The results of optimizing the treatment couch and ArcCHECK® densities in ECLIPSE are presented in sections 4.2 and 4.3. A comparison of the ArcCHECK® and 3DVH® system to results from ECLIPSE, Monte Carlo and ion chamber measurements are shown and discussed in section 4.4 for open field and sections 4.5 for IMRT plans.

4.1 Diode Response

Figure 4.1 shows the diode response to changes in dose rate as described in section 3.1.1. Each data point represents an average of six diode measurements and includes the standard error of the averaged diode measurements. The sensitivity of the diode response is relative to the response at a dose rate of 400 MU/min. In figure 4.1a the measurements were made by diodes at the beam entrance and in figure 4.1b the measurements were made by diodes at the beam exit.

The change in dose rate had little effect on the sensitivity of the diodes in beam entrance or beam exit. A single measurement in the exit beam at a dose rate of 100 MU/min fell outside the statistical uncertainty of the measurement, however

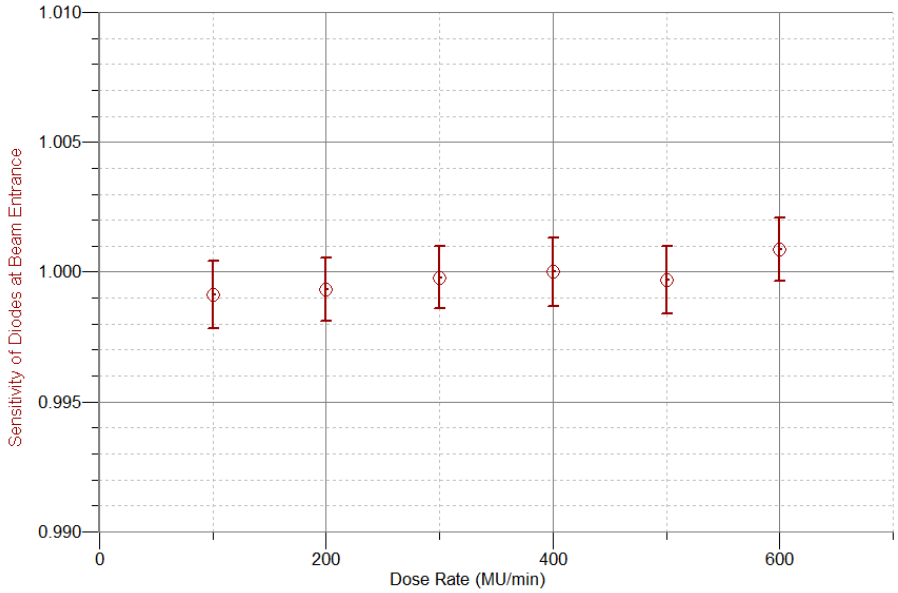

(a)

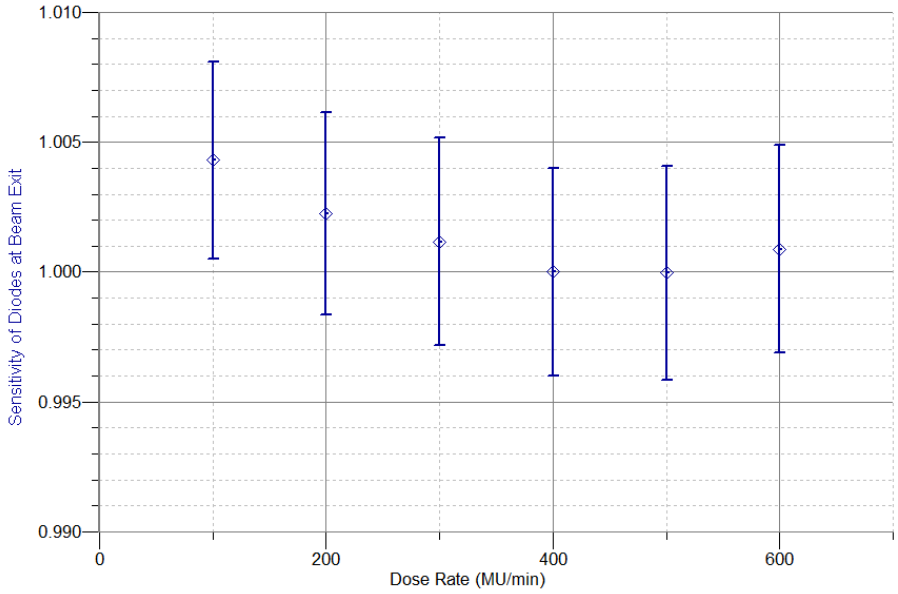

(b)

Figure 4.1: Plot of diode response to changes in dose rate relative to 400 MU/min. Figure (a) shows response of diodes at the top the phantom at the beam entrance and figure (b) shows the response of diodes at the bottom of the phantom at the beam exit.

the measurement falls just outside the uncertainty and the sensitivity is still within 0.5% of unity. The over sensitivity of this measurement may be a result of the a uniform correction factor used in the ArcCHECK® software to account for changes in sensitivity at different dose rates [1]. The correction factor is based on the sensitivity of the entrance diodes but is used for both entrance and exit diodes despite a small difference in sensitivity between entrance and exit diodes at lower dose rates.

Figure 4.2 shows the linearity of both the entrance and exit diode response to the number of MU delivered. Each data point represents an average of six diode measurements, as described in section 3.1.1, with the error derived from the standard deviation of the averaged diode measurements.

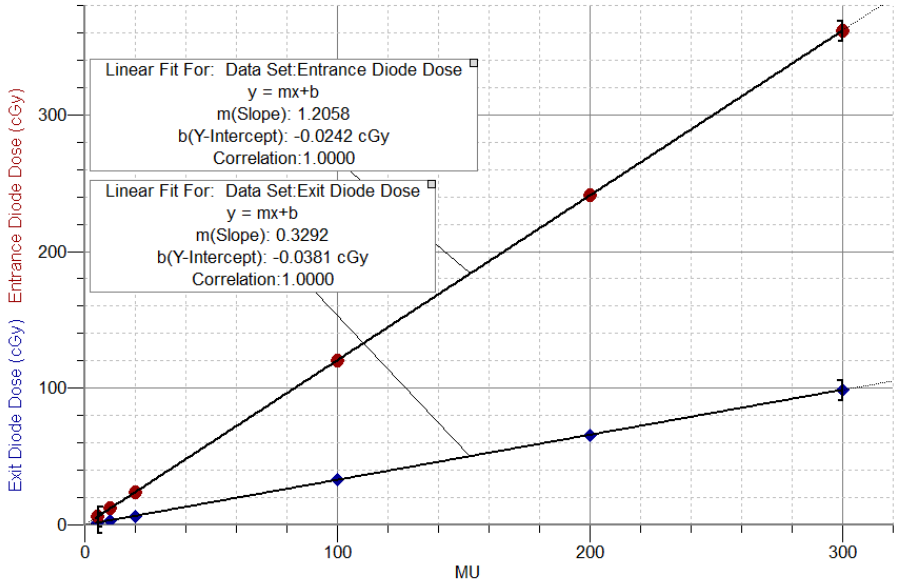

Figure 4.2: Plot of the linearity of diode response with increasing number of MU.

The response of the diodes at both the entrance and exit of the beam showed little deviation from a linear fit. This result is in agreement with measurements performed on the linearity of diode response in the MapCHECK device which uses the same diode detectors as the ArcCHECK® phantom [23, 58]. A similar result was found by Li et. al [2] when dose linearity was measured using the ArcCHECK® phantom.

Figure 4.3 shows the diode response to changes in field size as described in section 3.1.1. As with the previous experiments in this section each data point represents an average of six diode measurements with the error derived from the standard deviation of the averaged diode measurements. The sensitivity of diode response to field

size changes is calculated from the difference between diode measurement and value calculated in ECLIPSE, relative to this difference for a field size of 10×10 cm^2.

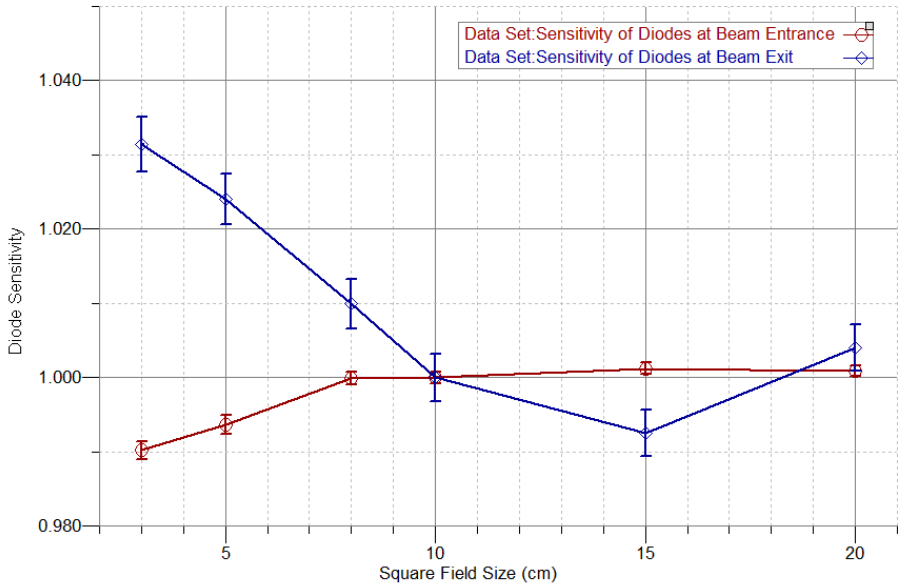

Figure 4.3: Plot of field size corrected diode response to changes in field size relative to a 10×10 cm ^{2} field.

The entrance diodes showed almost no change in sensitivity as field size increased and sensitivity trended slightly downward as field size decreased, with no deviation from 1 greater than 1%. The exit diodes also showed no apparent trend in sensitivity for larger field sizes with no deviation from 1 greater than 1%. However, for field sizes less than 10×10 cm^2 the sensitivity increased significantly with decreasing field size, with a deviation from unity of more than 3% at a field size of 3×3 cm^2.

There is a significant field size effect that is corrected for by the ArcCHECK® software [1]; the factors used for this correction are displayed in figure 4.4a. Dose measured by the diodes is divided by the correction factor to obtain the corrected dose. In figure 4.3 the exit diode dose appears to be over corrected, and is higher than the dose calculated in ECLIPSE. An adjustment was made to the field size corrections for the exit diodes in the ArcCHECK® software in an attempt to account for the over correction at lower field sizes; this adjustment can be seen in figure 4.4a. Note that no adjustments were made to the correction factors of the top diodes or at larger field sizes because in these cases there was little deviation in sensitivity. Figure 4.4b shows the diode response for field sizes less than 10×10 cm^2 after the adjusted

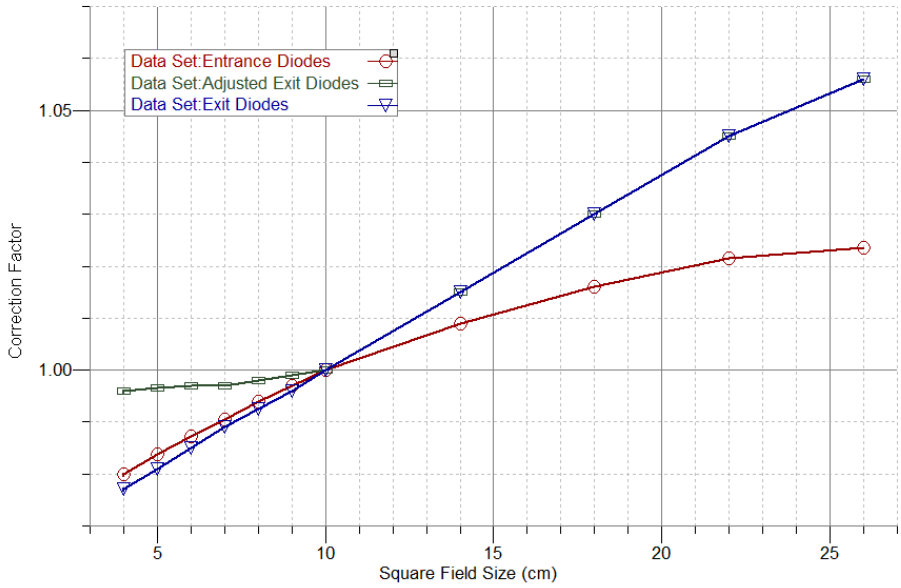

(a)

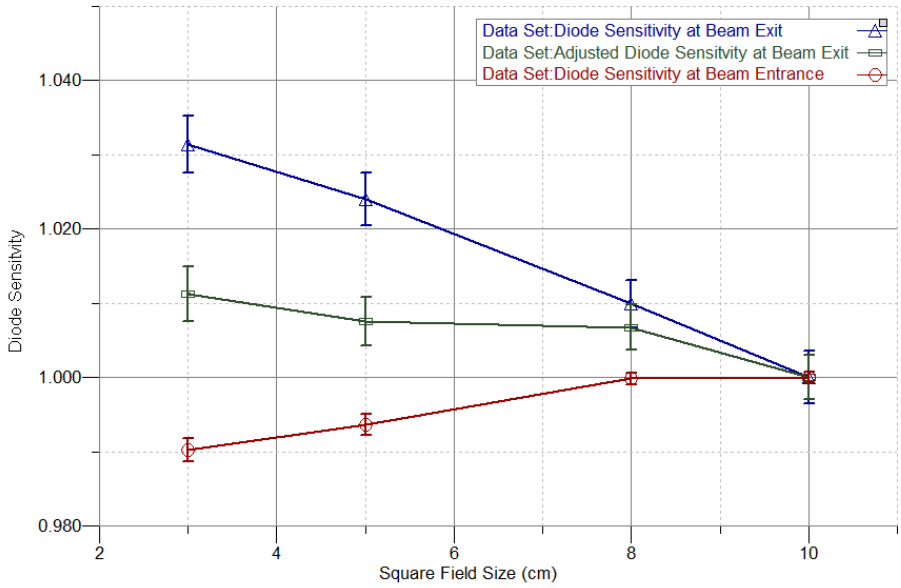

(b)

Figure 4.4: The effect of adjusting field size corrections in the ArcCHECK® software. Figure (a) shows the changes made to the field size corrections and figure (b) shows the effect that this adjustment had on the sensitivity of the diode response to changes in field size.

corrections factors had been applied. Adjusting the correction factors produced a significant drop in the dose measured by the exit diodes at smaller field sizes, with the maximum deviation from 1 close to 1%.

4.2 ArcCHECK® Phantom Modelling

In ECLIPSE the ArcCHECK® phantom was modelled using a virtual homogeneous phantom. The electron density of this phantom was adjusted in ECLIPSE from the electron density that was recommended by the manufacturer. The procedure for this adjustment is described in section 3.1.2. Figure 4.5 shows dose differences between diode measurements and dose calculated in ECLIPSE for a 10×10 cm^2 open field using electron densities of 1.15 and 1.20. With an electron density of 1.15 used in ECLIPSE, figure 4.5a shows that many diode measurements in the bottom diodes, where the beam exited the phantom, failed the 2%/2mm γ criterion with dose lower than what was calculated in ECLIPSE. This is a possible indication that the calculation in ECLIPSE was not attenuating the beam enough, causing the exit dose to be too high in ECLIPSE and causing the failure seen in the dose map. This over estimation at the beam exit by ECLIPSE is also seen in a profile horizontally through the dose map seen in figure 4.6a.

In figure 4.5b, when the electron density in ECLIPSE was increased to 1.20, the number of failing points in the exit diodes decreased dramatically. The agreement between ECLIPSE and exit diode measurement can also be seen in figure 4.6b. This improved agreement indicated that the attenuation of the beam calculated by ECLIPSE now matched what was physically measured in ArcCHECK® phantom diodes. It should be noted that increasing the electron density caused a small increase in the off-axis dose at the position of the entrance diodes in the ECLIPSE calculation; this lead to an increase in the number of failing points near the edge of the field, as seen in figure 4.5a, and a larger difference between ECLIPSE and diode doses at the edge of the field in the dose profile in figure 4.6b. Despite slightly worse agreement at beam entrance, the overall agreement between diode measurements and ECLIPSE improved with an increase in the virtual phantom's electron density. This conclusion was further validated by measurements in 3DVH®.

Figure 4.7 shows the 3D dose difference map between 3DVH® dose reconstructions and dose calculated in ECLIPSE for a 10×10 cm^2 open field using electron densities of 1.15 and 1.20. Figure 4.7a shows many points in the 3DVH® reconstruc-

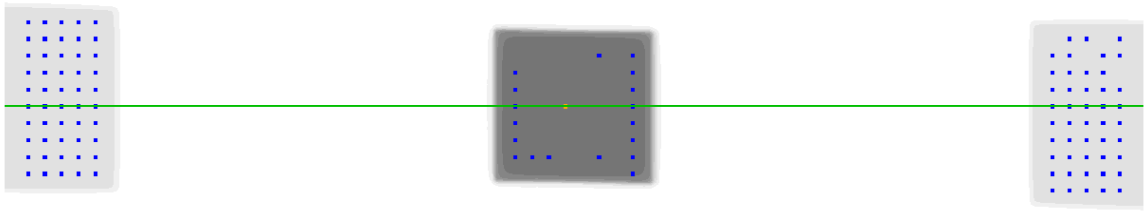

(a)

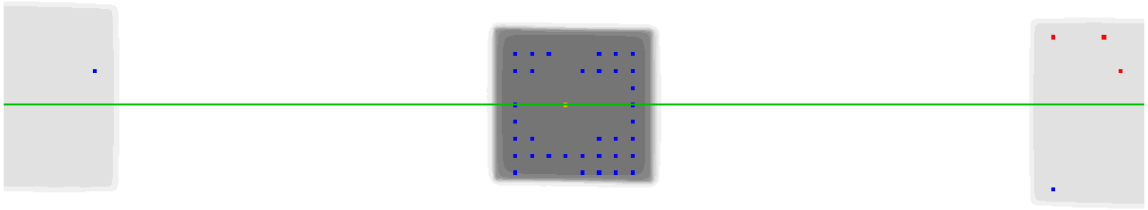

(b)

Figure 4.5: Dose difference maps showing the effect of changing the electron density of the ArcCHECK® phantom in ECLIPSE from 1.15 in figure (a) to 1.20 in figure (b). Square markers indicate a diode measurements failing a 2%/2mm, local dose difference, γ criterion with red and blue indicating high and low measurement dose, respectively.

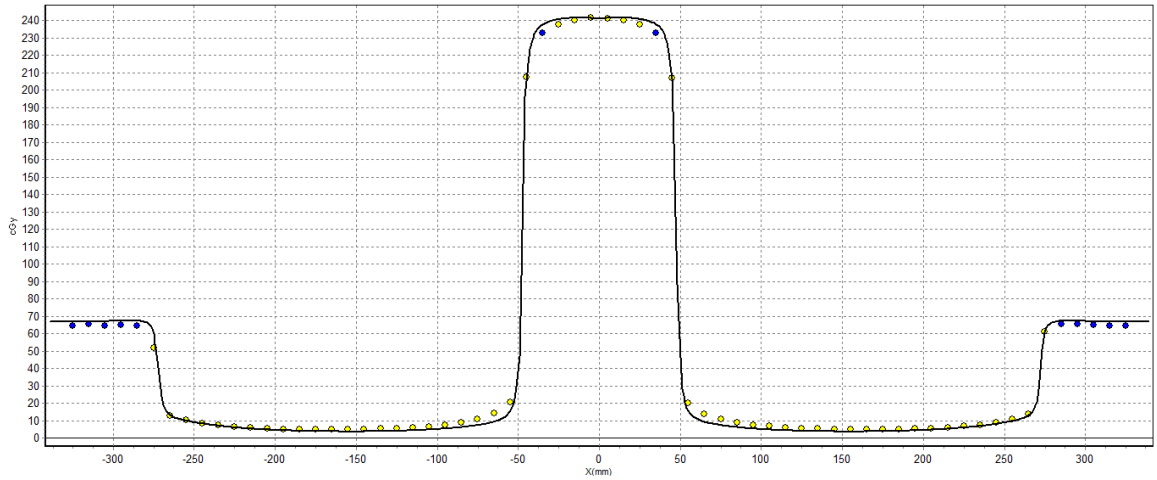

(a)

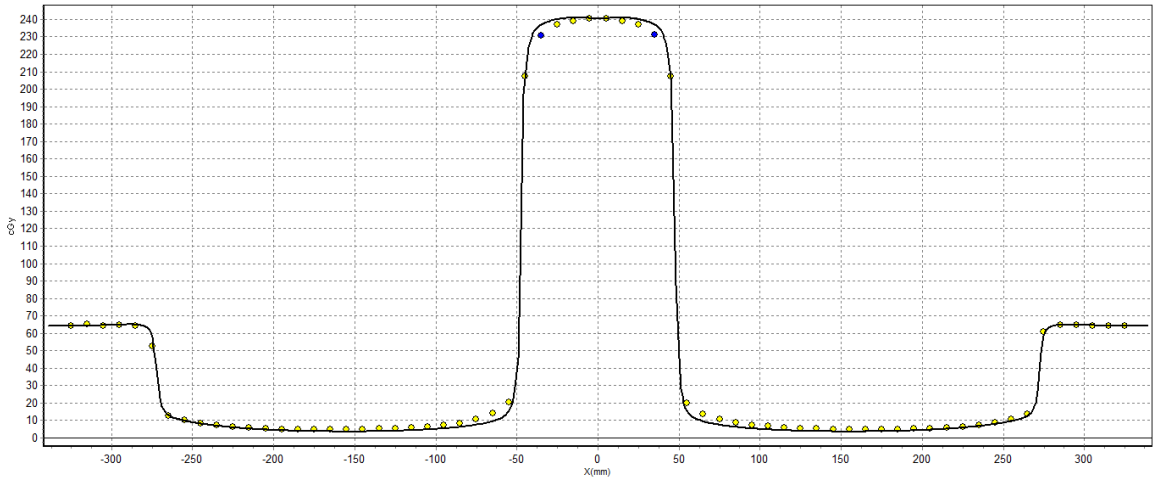

(b)

Figure 4.6: Dose profiles indicated by the green line in figure 4.5 showing the effect of changing the electron density of the ArcCHECK® phantom in ECLIPSE from 1.15 in figure (a) to 1.20 in figure (b). Circle markers indicate diode measurements with red and blue indicating high and low measurements failing a 2%/2mm, local dose difference, γ criterion.

tion failing the γ criterion with lower dose than what was calculated in ECLIPSE. Additionally, in the PDD curve along the central axis, it can be observed that at further depths within the phantom the reconstructed dose is less than the dose calculated in ECLIPSE. The volumes of discrepancy between 3DVH® and ECLIPSE are due to the overestimation of dose in ECLIPSE at the location of the exit diodes as discussed above. The differences between ECLIPSE and diode measurements at the exit diodes propagated into the 3DVH® dose reconstruction; the 3DVH® system reconstructed the dose with areas of lower dose, relative to ECLIPSE, near the exit diodes to match to the diode measurements. Figure 4.7b shows the 3D dose difference map after the electron density in ECLIPSE had been increased to 1.20 and the dose at the location of the exit diodes in ECLIPSE matched dose measured by the diodes. In this instance the 3DVH® reconstruction produced much better agreement with ECLIPSE, particularly near the exit surface of the phantom. There are volumes of disagreement off the central axis near the entrance surface of the phantom which are related to the increased disagreement seen in the off-axis diode measurements in figures 4.5b and 4.6b. Using a γ criteria of 2%/2mm, local dose difference, pass rates increased by over 30% for diode measurements and over 15% in 3DVH® when the electron density in ECLIPSE was increased from 1.15 to 1.20. The decision was made to use 1.20 for the electron density of the ArcCHECK® phantom in ECLIPSE calculations as the attenuation of the beam in ECLIPSE matched what was determined by diode measurement and subsequent 3DVH® reconstruction. The results and discussion on the modelling of the ArcCHECK® phantom in this section are based on measurements using the Truebeam linear accelerator. Similar work was performed using the 21-EX linear accelerator with similar results observed in both diode measurements and 3DVH® reconstruction. In the case of the 21-EX, the electron density which produced matching attenuation between ECLIPSE and diode measurements was 1.18.

Another observation from this section's results is the advantage provided by using both 3DVH® dose reconstructions and the individual diode measurements in assessing results. When the lower electron density was used in ECLIPSE calculations, simply looking at a 3DVH® reconstruction somewhat obscured the root of the underlying problem and the path to a solution was not entirely clear. Looking at the diode measurements was somewhat more illuminating and provided valuable information in determining the appropriate course of action.

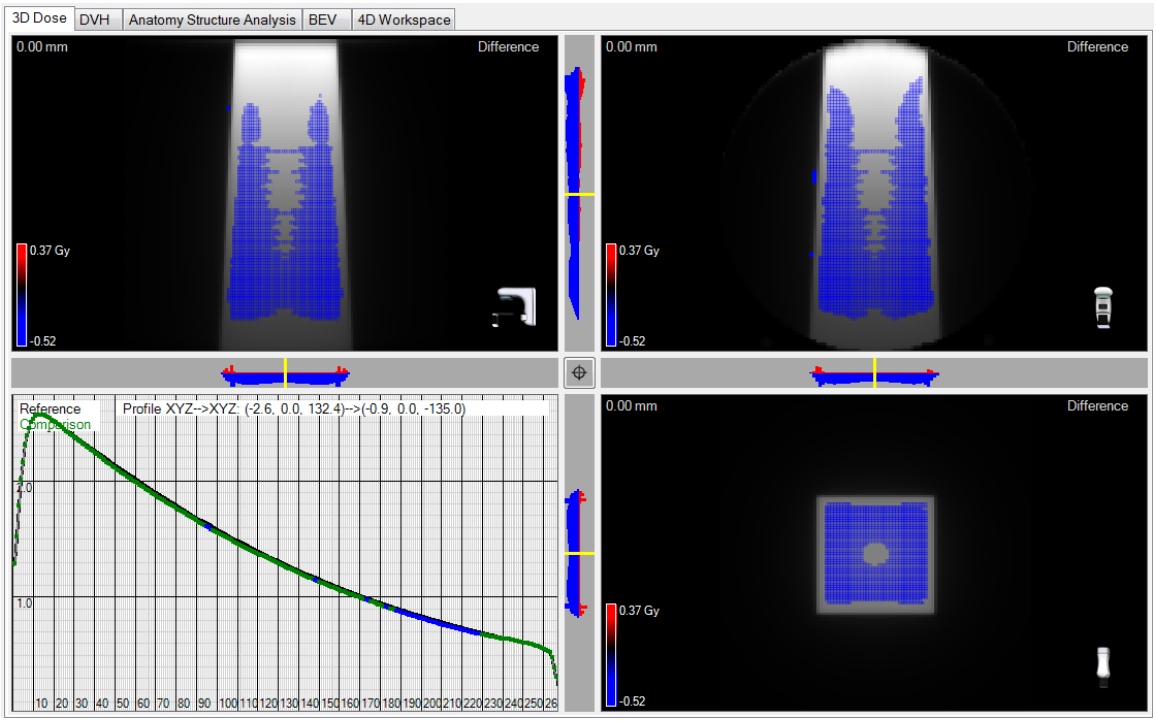

(a)

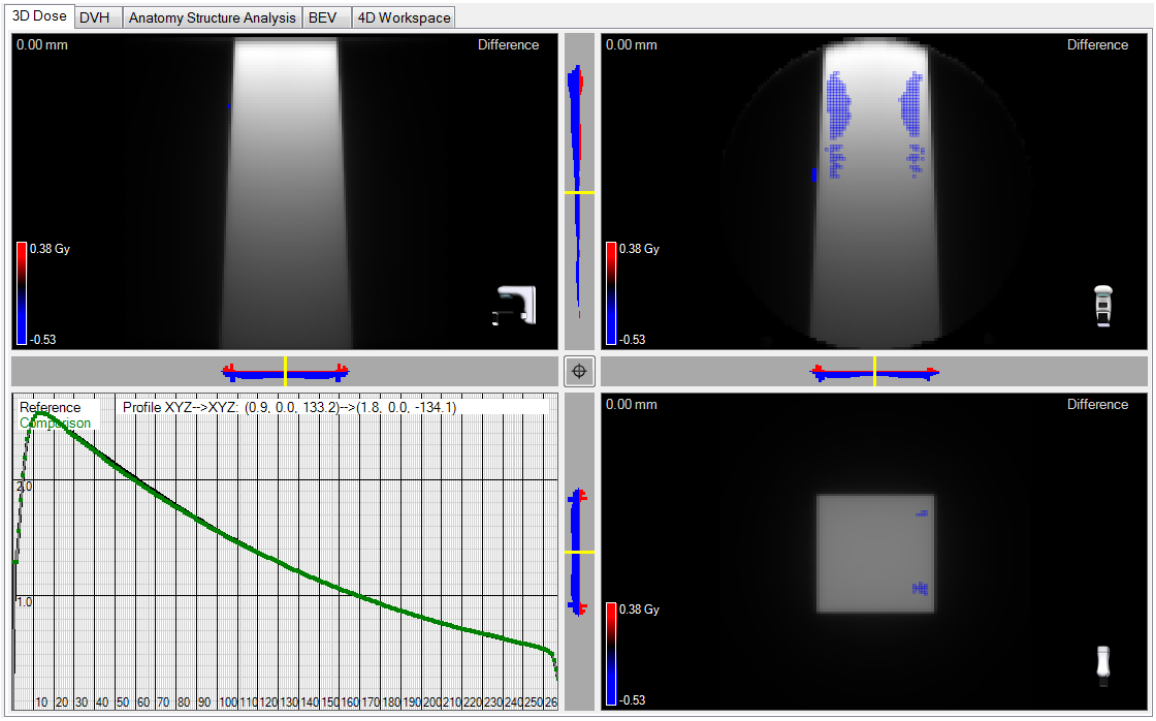

(b)

Figure 4.7: 3DVH® dose maps and PDD curves showing the effect of changing the electron density of the ArcCHECK® phantom from 1.15 (a) to 1.20 (b) in ECLIPSE calculations. Coloured areas indicates voxels failing a 2%/2mm, local dose difference, γ criterion with red and blue indicating high and low reconstructed dose, respectively.

4.3 Linear Accelerator Couch Modelling

Measurements of open fields delivered through the couches on both the 21-EX and Truebeam were used to determine appropriate models for these couches in ECLIPSE. The procedure for these couch measurements is described in section 3.1.2.

Figure 4.8 shows the results of a 10×10 cm^2 open field to the ArcCHECK® directly through the couch. In figure 4.8a excellent agreement was seen between ECLIPSE and diode measurements at both the entrance and exit of the beam when using a 2%/2mm, local dose difference, γ criterion. The results from this posterior beam showed similar, if not better, agreement to that seen with an anterior beam and no couch attenuation, which is an indication of an adequate model used in ECLIPSE. Figure 4.8b shows excellent agreement between ECLIPSE and a 3DVH® dose reconstruction as seen in the 3D dose difference map and PDD curve along the central axis. As with the results in section 4.2, there was excellent agreement at the diode level which led to excellent agreement in the 3DVH® reconstruction. The 3DVH® results for the posterior beam were also similar to or better than those seen with an anterior beam and no couch attenuation. Overall, the results showed good agreement between measurement and ECLIPSE when beams were delivered through the couch, therefore the couch modelled in ECLIPSE for the 21-EX was determined to be adequate for subsequent measurements.

The results for a posterior beam through the Truebeam couch were similar to those seen in figure 4.8 for the 21-EX couch. Due to the nature of VMAT delivery it was also necessary to determine the result of deliveries though the couch at various angles; this is most easily observed with a partial arc through the couch. Figure 4.9 shows the results of a 10×10 cm^2 open field partial arc delivered from 180° to 130°. In figure 4.9a there is excellent agreement between ECLIPSE and diode measurements along the whole arc at the entrance and exit diodes when using a 2%2/mm, local dose difference, γ criterion. Figure 4.9b shows excellent agreement between ECLIPSE and a 3DVH® dose reconstruction as seen in the 3D dose difference map and PDD curve along the central axis. The attenuation by the couch on the Truebeam seems to match what was predicted by ECLIPSE with the assigned couch model at all angles through the couch. Overall, these results showed good agreement between measurement and ECLIPSE when beams were delivered through the couch. It was important that an accurate model for the Truebeam couch was used as the VMAT plans delivered on the Truebeam required a significant portion of the delivery to go through the couch.

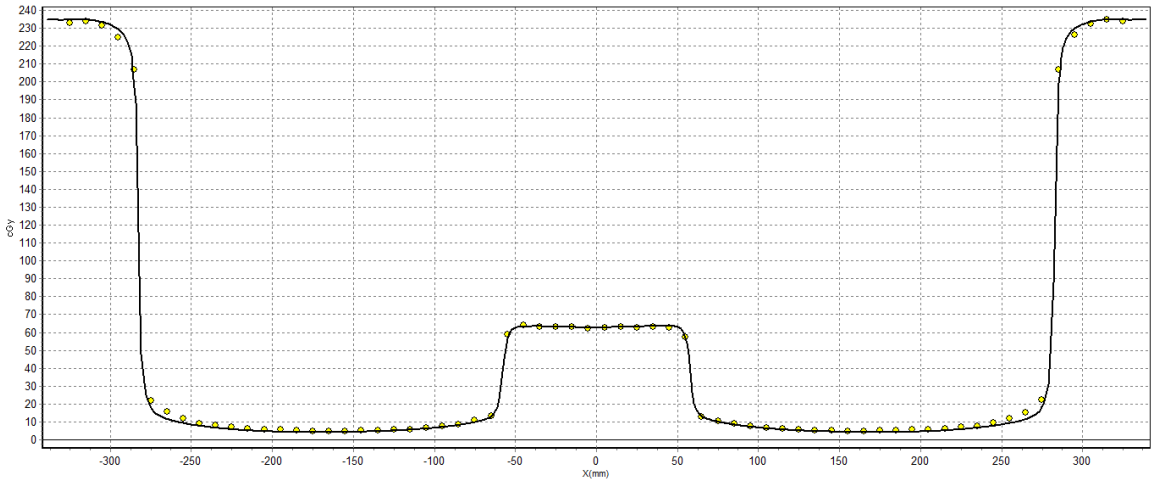

(a)

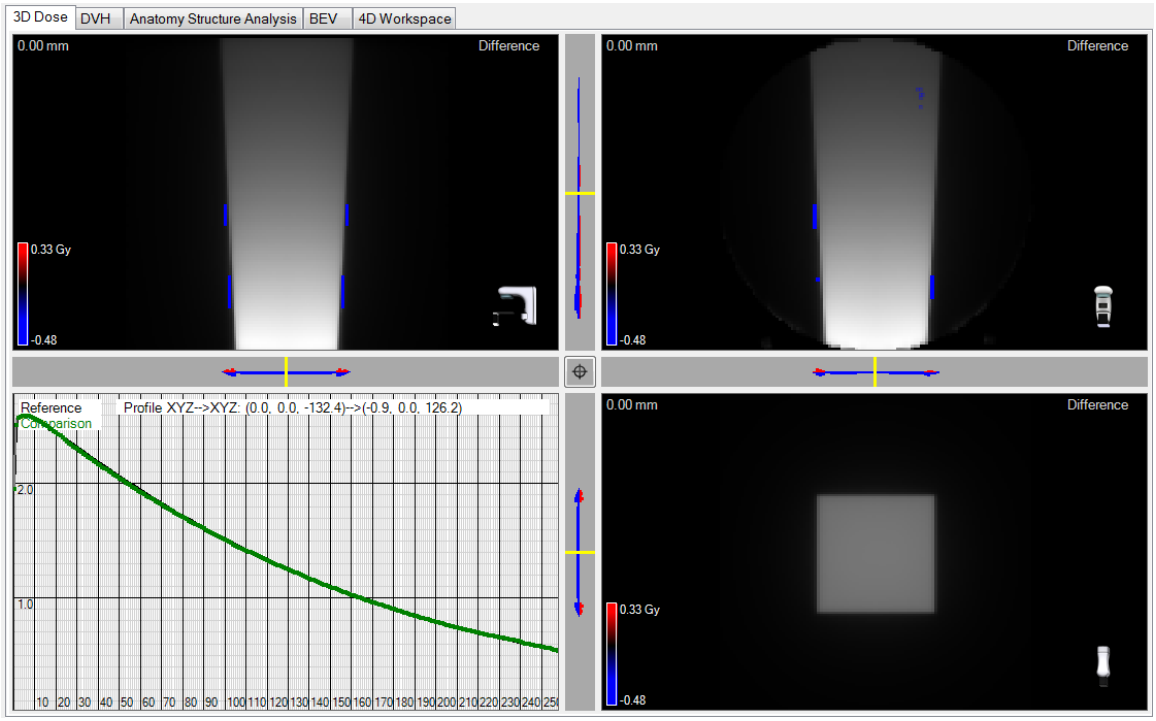

(b)

Figure 4.8: Data showing agreement between measurements and ECLIPSE calculations for a posterior beam through the couch on the 21-EX. Figure (a) shows a dose profile comparing diode measurements to ECLIPSE. Figure (b) shows a dose map and PDD curve comparing 3DVH® reconstruction to ECLIPSE.

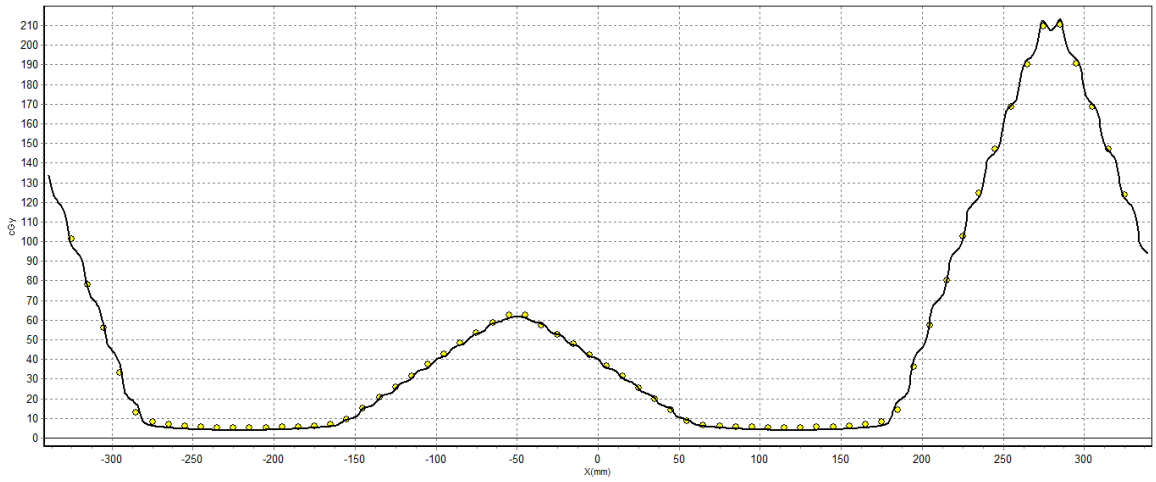

(a)

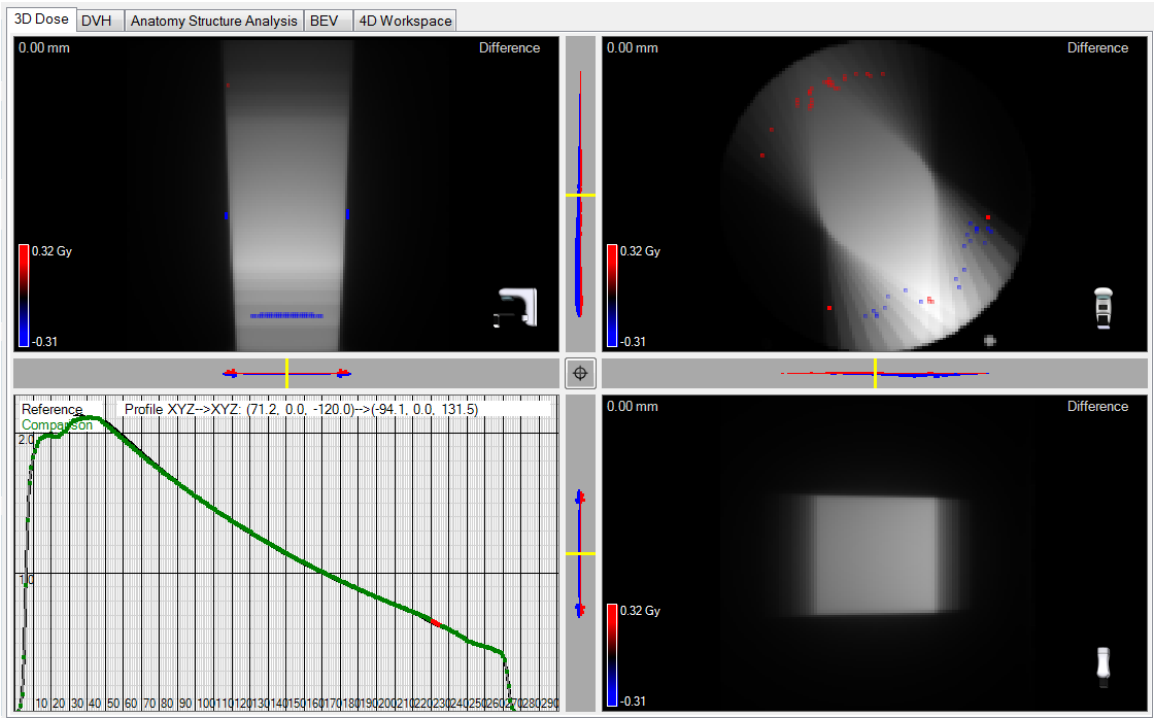

(b)

Figure 4.9: Data showing agreement between measurements and ECLIPSE calculations for a partial arc through the couch on the Truebeam. Figure (a) shows a dose profile comparing diode measurements to ECLIPSE. Figure (b) shows a dose map and PDD curve comparing 3DVH® reconstruction to ECLIPSE.

4.4 Measurement of Open Fields

4.4.1 ArcCHECK® Comparison with ECLIPSE

The summary of γ-pass rates comparing diode measurements to ECLIPSE for single 10×10 cm^2 open fields at gantry angles of 0°, 90°, 180° and 270° is shown in table 4.1. The procedures used to obtain these results are described in section 3.3. Also included in table 4.1 are the results from Kozelka et al. [1] comparing diode measurements for a 10×10 cm^2 open field delivered at 0° to a Pinnacle (Philips Radiation Oncology Systems, Fitchburg, WI) TPS. The pass rates for both the 21-EX and Truebeam were excellent even when the most stringent γ criteria of 2%2/mm, local dose difference, was used. Figures 4.5b and 4.6b show the results of the anterior open field delivered on the Truebeam. Table 4.2 shows the γ-pass rates comparing 3DVH® dose reconstructions to ECLIPSE for the same fields as in table 4.1. Again the agreement between measurement and ECLIPSE was excellent and the Truebeam results showed slightly better agreement than the 21-EX results. Figure 4.7b shows the 3DVH® result of the anterior open field delivered on the Truebeam. Table 4.3 is a summary of the dose differences at isocentre comparing 3DVH® to both ECLIPSE and ion chamber measurements. On average the dose at isocentre in 3DVH® agreed within 0.5% of what was calculated in ECLIPSE and measured by an ion chamber. It should be noted that the mean dose difference within the entire ArcCHECK® phantom between 3DVH® and ECLIPSE was, on average, -0.79% (SD: 0.34) and -0.54% (SD: 0.30) for the 21-EX and Truebeam, respectively. Although the isocentre doses matched within 0.5% on average, there were volumes within the phantom where the dose reconstructed in 3DVH® was lower than what was calculated in ECLIPSE. Examples of this disagreement can be seen in figure 4.7b near the diode array within the phantom where there are several points in 3DVH® that failed with dose lower than what was calculated in ECLIPSE. The effect looked similar in the results from the fields delivered on the 21-EX. For both types of accelerators this effect was relatively small and did not effect the overall dose distribution significantly as the passing rates were still high and doses at isocentre were still in good agreement.

Another area of discrepancy between ECLIPSE calculations and measurements can be seen in figure 4.6b in tail of the dose distribution just outside the field. The dose measured by the diodes in the tail region is significantly higher than what was calculated in ECLIPSE. These points do not fail the γ criteria because they are not

Table 4.1: Average γ-pass rates of diode measurements compared to ECLIPSE for 10×10 cm^2 open field beams delivered on the Truebeam and 21-EX using both local and global dose difference. Also included are results from Kozelka et al. [1]. All γ comparisons used a dose threshold of 10%.

γ criteria	2%/2mm Local (σ)	3%/3mm Local (σ)	2%/2mm Global (σ)	3%/3mm Global (σ)
21-EX	98.3%(1.2)	100%(0.0)	98.9%(1.3)	100%(0.0)
Truebeam	99.2%(0.6)	100%(0.0)	99.5%(0.6)	100%(0.0)
Kozelka et al.	95.4%	100%	99.6%	100%

Table 4.2: Average γ-pass rates of 3DVH® dose reconstructions compared to ECLIPSE for 10×10 cm^2 open field beams delivered on the Truebeam and 21-EX using both local and global dose difference. All γ comparisons used a dose threshold of 10%.

γ criteria	2%/2mm Local (σ)	3%/3mm Local (σ)	2%/2mm Global (σ)	3%/3mm Global (σ)
21-EX	93.0%(5.8)	100%(0.0)	99.3%(0.6)	100%(0.0)
Truebeam	97.2%(3.7)	100%(0.0)	99.5%(0.6)	100%(0.0)

within the 10% threshold of the maximum dose, but the local dose difference is greater than 5% for these points, and in some cases, as high as 20%. One potential reason is that the diodes are over responding to low energy scattered photons in this region. This tail region discrepancy also appears to have no effect on the 3DVH® dose reconstruction as these diode measurements are likely excluded from the reconstruction for not reaching the dose threshold required as discussed in section 2.5.

Table 4.4 shows the γ-pass rates when comparing diode measurements and 3DVH® dose reconstructions to ECLIPSE for an open 4-field box delivery as described in section 3.3. On both the 21-EX and the Truebeam the γ-pass rates decrease significantly when compared to the results for simple open fields, when using for the more stringent

Table 4.3: Average dose differences at isocentre between 3DVH® and ECLIPSE and between ion chamber measurements and ECLIPSE for single 10×10 cm^2 open fields.

	Isocentre Dose Difference (σ)	
	3DVH® verus ECLIPSE	Ion Chamber versus ECLIPSE
21-EX	+0.37%(0.41)	+0.08%(0.29)
Truebeam	+0.18%(0.24)	-0.09%(0.33)

γ criteria. Li et al. [2] have published results for 4-field box deliveries with field sizes ranging from 10×30 cm^2 to 20×30 cm^2 to the ArcCHECK® phantom, and found that at the diode level γ-pass rates were around 95% using a γ criterion of 3%/3mm, global dose difference. The results in table 4.4 compare favourably to the results from Li et al. Figure 4.10 shows that on the Truebeam the majority of the failing points at the diode level occurred at diodes in between the 4 fields and failed with dose measured higher than in ECLIPSE. The results on the 21-EX were similar to those seen on the Truebeam. The trend of over estimation of dose in the tail region for the single open fields is compounded for measurements of the 4-field box. In the case of the 4-field box, the dose is high enough to reach the 10% dose threshold causing the points to fail the γ criterion. When global dose difference was used, the number of failing points in this tail region decreased dramatically as the dose difference at these points was small relative to the maximum dose in the centre of the open fields. Figure 4.11 shows the results in 3DVH® of the 4-field box delivered on the Truebeam. The failure of points at the edge of the field seen in figure 4.7b seemed to accumulate over multiple fields and caused a drop in γ-pass rates when compared to individual open fields. The results in 3DVH® for 4-field box measurements on the 21-EX were similar to those seen on the Truebeam.

Table 4.4: γ-pass rates of diode measurements and 3DVH® dose reconstructions compared to ECLIPSE for open field 4-field box delivered on the Truebeam and 21-EX using both local and global dose difference. All γ comparisons used a dose threshold of 10%.

γ criteria	2%/2mm Local	3%/3mm Local	2%/2mm Global	3%/3mm Global
21-EX Diode Measurements	73.1%	82.9%	93.3%	98.9%
21-EX 3DVH® 3DVH® Reconstructions	74.2%	96.2%	88.5%	99.9%
Truebeam Diode Measurements	80.4%	92.4%	85.3%	100%
Truebeam 3DVH® Reconstructions	80.8%	99.4%	91.7%	100%

Table 4.5 displays the dose differences at isocentre for the 4-field box measurements on both the 21-EX and the Truebeam. The doses at isocentre are considerably lower compared to ECLIPSE than was seen for individual open fields indicating that what were originally off-axis dose discrepancies for single fields began to effect dose on the

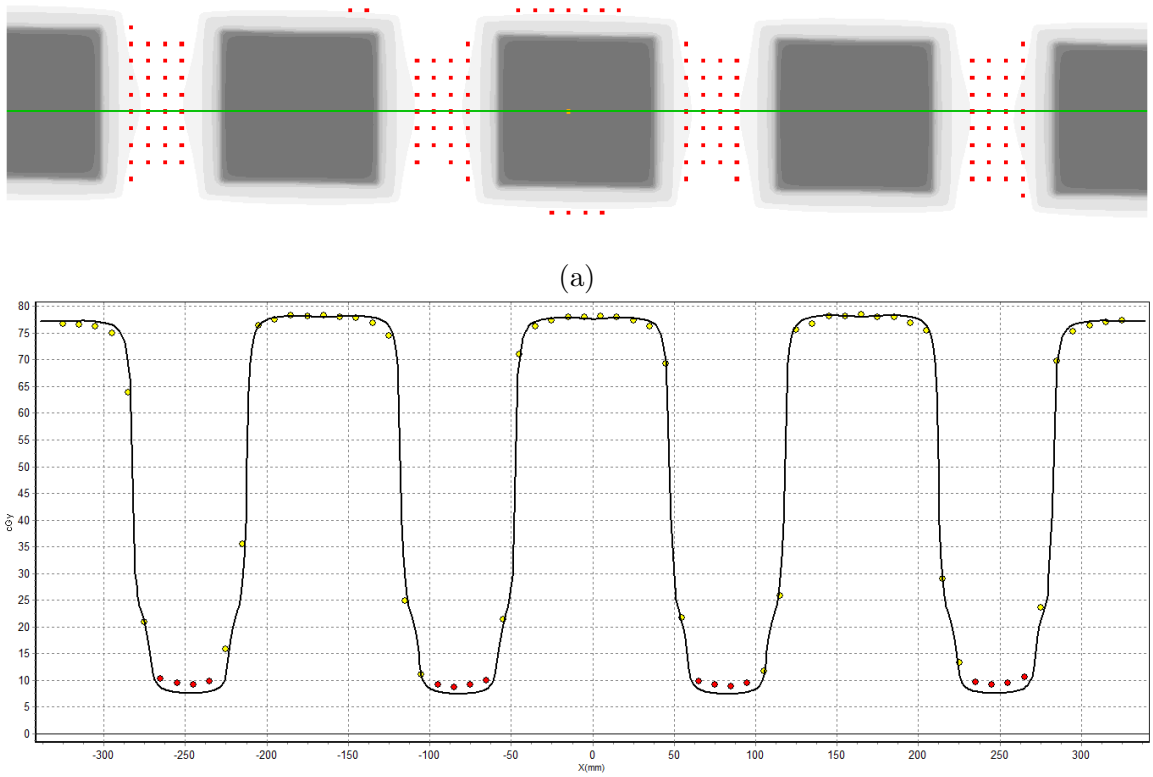

(a)

(b)

Figure 4.10: A dose difference map (a) and dose profile (b) of a 4-field box delivered on the Truebeam comparing diode measurements to ECLIPSE. Markers indicate diode measurements with red and blue indicating high and low measurements, respectively, failing a 2%/2mm, local dose difference, γ criterion.

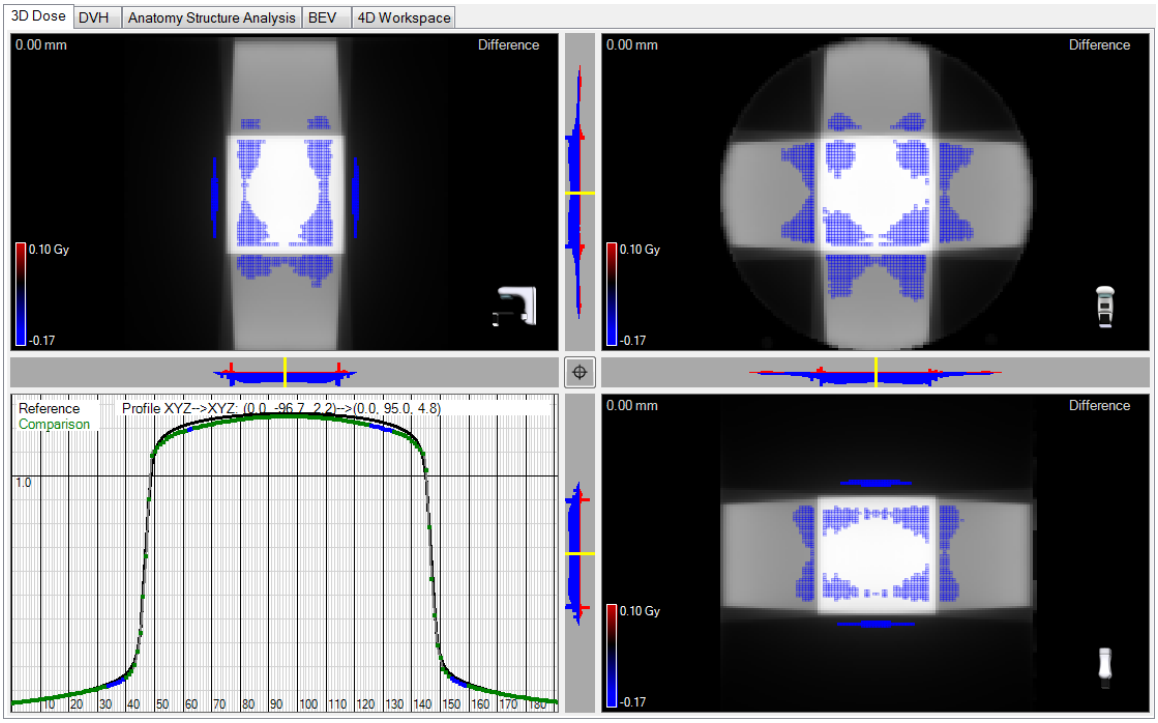

Figure 4.11: 3DVH® dose maps and a dose profile for a 4-field box delivered on the Truebeam comparing 3DVH® dose to ECLIPSE. Coloured areas indicate voxels failing a 2%/2mm, local dose difference, γ criterion with red and blue indicating high and low reconstructed dose, respectively.

central axis when 4 fields were used. The ion chamber measurements showed a similar effect, indicating that the differences at isocentre were more likely based on errors in ArcCHECK® measurements and or errors in 3DVH® reconstructions than errors in ECLIPSE or due to machine output. The mean dose differences within the entire phantom for the 4-field box were -1.54% and -0.84% on the 21-EX and Truebeam, respectively. These mean dose differences values also dropped when moving from single fields to a 4-field box.

Table 4.5: Dose differences at isocentre between 3DVH® and ECLIPSE and between ion chamber measurements and ECLIPSE for a 4-field box.

	Isocentre Dose Difference	
	3DVH® verus ECLIPSE	Ion Chamber versus ECLIPSE
21-EX	-0.83%	-0.28%
Truebeam	-0.95%	-0.79%

Overall, the errors for single open fields were magnified, especially in 3DVH® reconstructions, for the 4-field box. However, the results from the 4-field box still showed excellent agreement with ECLIPSE. The γ-pass rates were high when less stringent γ criteria were used and isocentre dose differences were less than 1%.

4.4.2 ArcCHECK® Comparison with Monte Carlo

As a further comparison for measurements, dose distributions for an anterior 10×10 cm^2 and a 4-field box were calculated in Monte Carlo on the 21-EX. Table 4.6 summarizes the γ-pass rates when diode measurements and 3DVH® reconstructions were compared to Monte Carlo calculations. For the single 10×10 cm^2 field the γ-pass rates were similar to those when measurements were compared to ECLIPSE in tables 4.1 and 4.2. In figure 4.12 the points near the edge of the field are no longer failing, as was seen in figures 4.5b and 4.6b. Although the dose at these off-axis diodes is still lower than what was calculated in Monte Carlo, the difference is not as large as when compared to ECLIPSE. The calculation of off-axis dose may have be over estimated by ECLIPSE, but the diode measurements in this region also appear to have been slightly low. The problem of high diode dose seen in the tail region persists when Monte Carlo calculations are compared to diode measurements, but again the effect is not as significant as when ECLIPSE calculations were used. In the tail region, when

compared to Monte Carlo, the diodes still appeared to over estimate dose but not to the extent that was suggested by comparison with ECLIPSE. Figure 4.13 shows the comparison of 3DVH® reconstructed dose to a Monte Carlo calculation for a single open field. The result is similar to that seen in figure 4.7b when the 3DVH® result was compared to ECLIPSE. The number of failing points off the central axis near the top surface of the phantom was reduced due to better agreement between Monte Carlo and the off-axis entrance diode measurements. There were more failing points deeper within the phantom which could be attributed to slightly different attenuation between ECLIPSE and Monte Carlo calculations and the uncertainty, around 1%, associated with the Monte Carlo calculations.

Table 4.6: γ-pass rates of diode measurements compared to Monte Carlo for a 10×10 cm^2 open field and a 4-field box delivered on the 21-EX using both local and global dose difference. All γ comparisons used a dose threshold of 10%.

	2%/2mm Local	3%/3mm Local	2%/2mm Global	3%/3mm Global
Single Field Diode Measurements	96.1%	100%	96.1%	100%
Single Field 3DVH® Reconstructions	91.4%	99.9%	99.7%	100%
4-field box Diode Measurements	73.5%	79.8%	79.2%	99.2%
4-field box 3DVH® Reconstructions	89.4%	98.3%	95.3%	99.2%

For a 4-field box delivery the γ-pass rates comparing measurements and Monte Carlo were similar to those when the measurements where compared to ECLIPSE. Looking at diode measurements in tables 4.4 and 4.6 it can be observed that γ-pass rates decrease when Monte Carlo was used as a comparison instead of ECLIPSE, particularly at the 2%/2mm, local dose difference, γ criterion where the pass rate drop by more than 10%. The dose map in figure 4.14 shows an increase in failing points outside the high dose region when Monte Carlo was used as a comparison. For 3DVH® reconstructions the trend is reversed, with Monte Carlo comparisons producing roughly 10% higher γ-pass rates when the 2%/2mm γ criterion is used. In figure 4.15 the 3DVH® comparison with Monte Carlo suffers from the same types of points failing as with ECLIPSE comparisons.

Overall, the comparison of diode measurements and 3DVH® reconstructions with Monte Carlo produce similar results to those seen when compared to ECLIPSE.

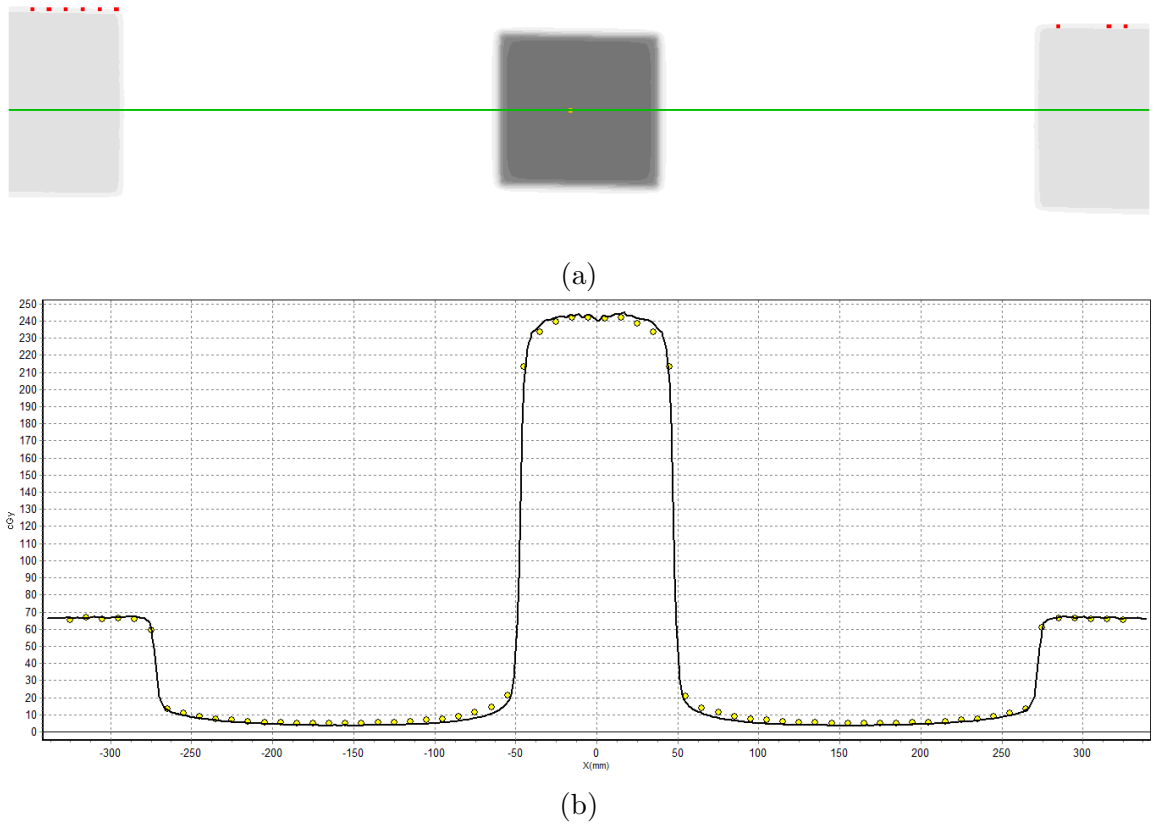

Figure 4.12: A dose difference map (a) and dose profile (b) of a 10×10 cm^2 open field delivered on the 21-EX comparing diode measurements to Monte Carlo. Markers indicate diode measurements with red and blue indicating high and low measurements, respectively, failing a 2%/2mm, local dose difference, γ criterion.

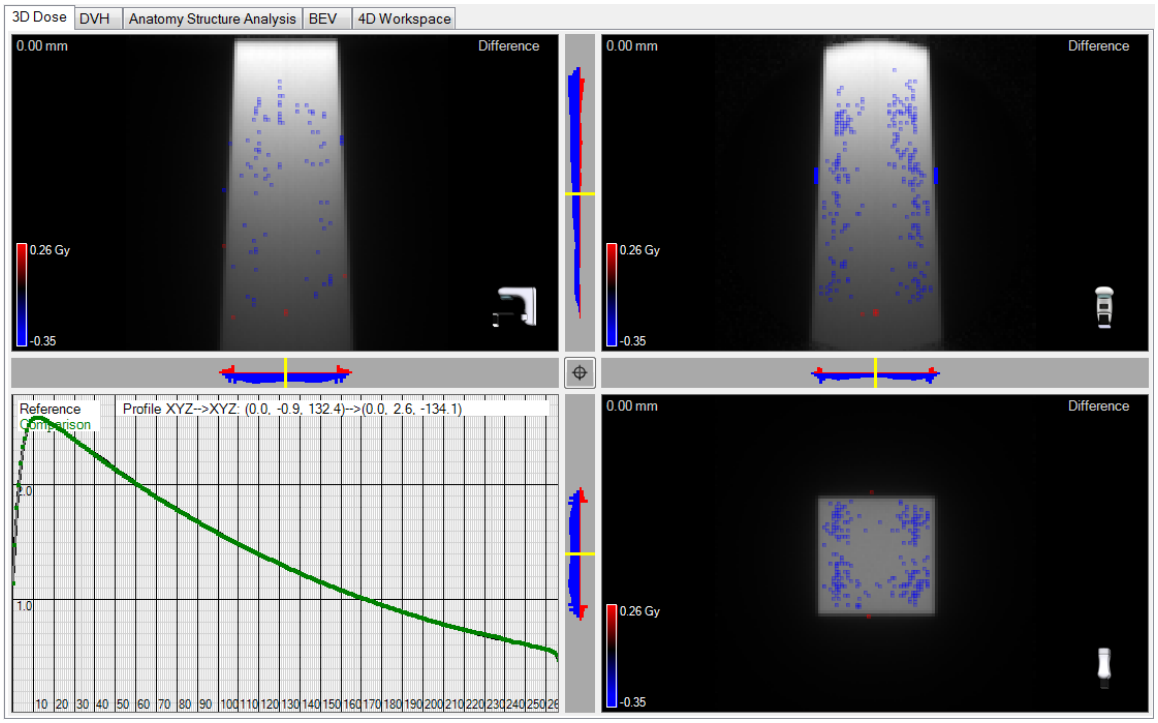

Figure 4.13: 3DVH® dose maps and PDD curves for a 10×10 cm^2 open field delivered on the 21-EX comparing 3DVH® dose to Monte Carlo. Coloured areas indicate dose voxels failing a 2%/2mm, local dose difference, γ criterion with red and blue indicating high and low reconstructed dose, respectively.

This provides some validation of the ECLIPSE comparisons and confirms that the differences with ECLIPSE are not caused solely by problems with the ECLIPSE calculation. The persistence of the over estimation of dose in the tail region and under estimation of dose by the entrance diodes at the edge of the field indicates that these differences are caused by small failures in the ArcCHECK® system. These problems may be somewhat overstated in the comparisons with ECLIPSE as the Monte Carlo calculations fall somewhere in between the ArcCHECK® results and ECLIPSE calculations. In either case these errors remain small and there is good agreement for ArcCHECK® results with open field deliveries.

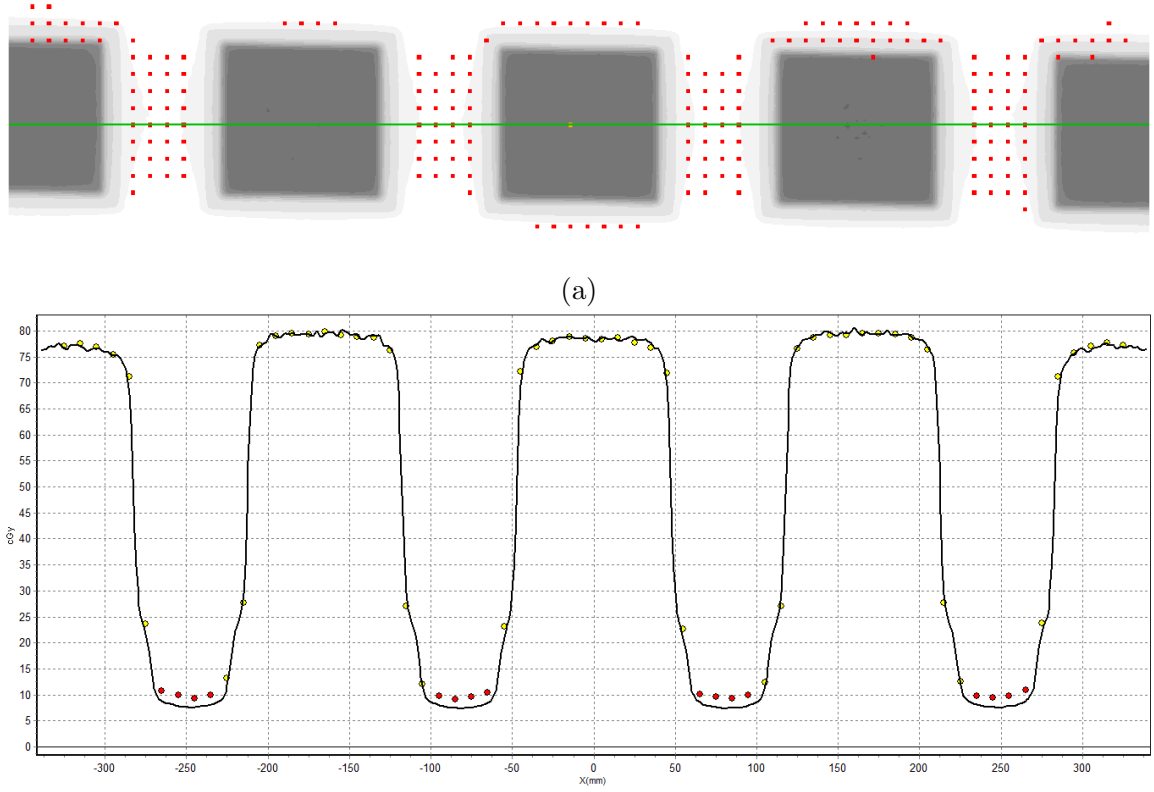

(a)

(b)

Figure 4.14: A dose difference map (a) and dose profile (b) of a 4-field box delivered on the 21-EX comparing diode measurements to Monte Carlo. Markers indicate diode measurements with red and blue indicating high and low measurements, respectively, failing a 2%/2mm, local dose difference, γ criterion.

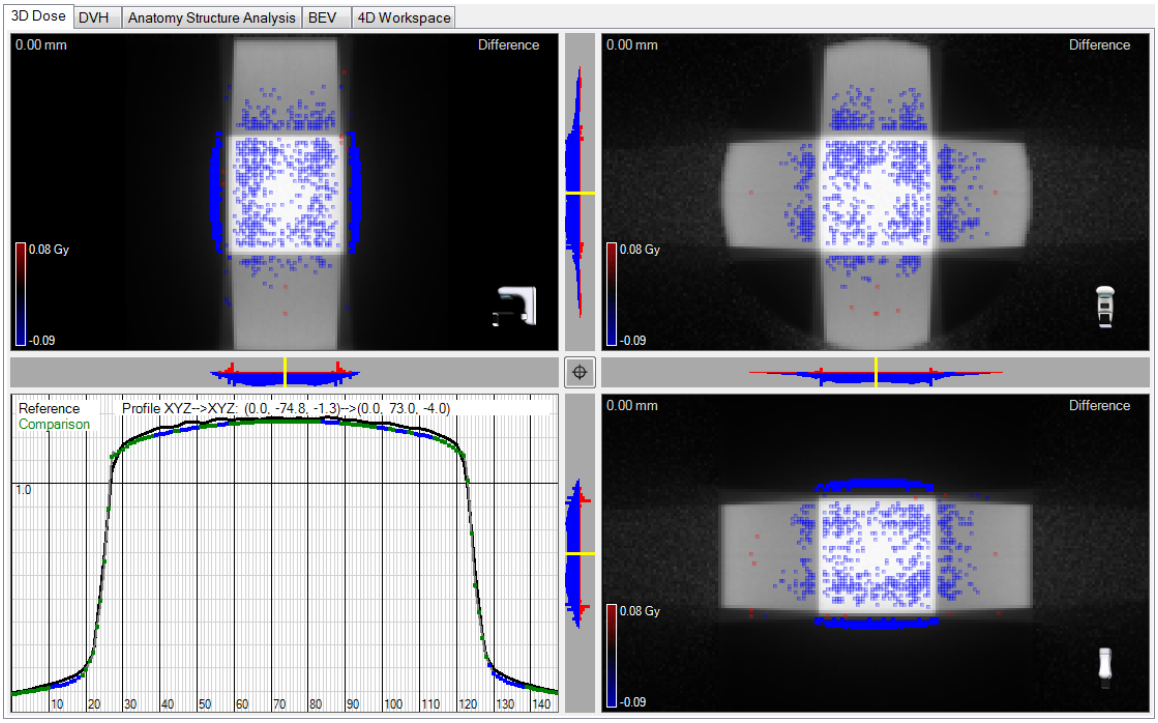

Figure 4.15: 3DVH® dose maps and a dose profile for a 4-field box delivered on the 21-EX comparing 3DVH® dose to Monte Carlo. Coloured areas indicate dose voxels failing a 2%/2mm, local dose difference, γ criterion with red and blue indicating high and low reconstructed dose, respectively.

4.5 Measurement of IMRT Plans

4.5.1 Prostate Plans

ArcCHECK® Comparison with ECLIPSE

The summary of γ-pass rates comparing diode measurements to ECLIPSE for 8 prostate IMRT plans is shown in table 4.7. The procedures used to obtain these results are described in section 3.4. Also included in table 4.7 are results from Li et al.[2] and Garcia-Vicente et al. [3] comparing diode measurements to a TPS for IMRT plans. Li et al. have results from only one prostate step-and-shoot IMRT plan, whereas the prostate plans used in this work were sliding window IMRT plans. Garcia-Vicente et al. have combined results for 3 prostate and 3 head and neck sliding window IMRT plans, and in their γ analysis use relative dose differences and a two-dimensional distance-to-agreement search, whereas this work uses absolute dose differences and a three-dimensional distance-to-agreement search. The results for

prostate IMRT show excellent agreement with ECLIPSE and there is little difference between the 21-EX and the Truebeam. The results also compare favourably to published work, with the results in this work showing slightly better agreement with the TPS. The γ-pass rates for prostate IMRT plans are also well within the action level of 90% at 3%/3mm, global dose difference, set out by TG-119 for IMRT commissioning [17].

Table 4.7: Average γ-pass rates of diode measurements compared to ECLIPSE for 8 prostate IMRT plans delivered on the Truebeam and 21-EX using both local and global dose difference. Also included are results from Li et al. [2] and Garcia-Vicente et al. [3]. All γ comparisons used a dose threshold of 10%.

γ criteria	2%/2mm Local (σ)	3%/3mm Local (σ)	2%/2mm Global (σ)	3%/3mm Global (σ)
21-EX	82.8%(4.1)	95.1%(1.5)	99.6%(0.2)	100%(0.0)
Truebeam	81.7%(8.1)	94.1%(3.9)	99.0%(0.6)	100%(0.0)
Li et al.	-	-	88.6%	96.9%
Garcia-Vicente et al.	-	-	-	99.1%

Figure 4.16 displays γ-pass rates comparing 3DVH® and ECLIPSE for IMRT prostate plans delivered on both the 21-EX and Truebeam. The γ-pass rates were analyzed using 10%, 40% and 80% dose thresholds. For the prostate IMRT plans, excellent agreement was seen between 3DVH® and ECLIPSE with γ-pass rates at all dose thresholds exceeding 95% using even the most stringent γ criterion of 2%/2mm, local dose difference. There is little difference in results between the 21-EX and Truebeam. At 3%/3mm, global dose difference, the pass rates in the high and intermediate dose region are well within the 90% action level used for the χ-evaluation used at BCCA-VIC for IMRT pretreatment verification.

Table 4.8 displays the dose differences at isocentre on both the 21-EX and Truebeam for prostate IMRT plans. On the 21-EX the isocentre dose in 3DVH® was on average significantly higher than in ECLIPSE. Ion chamber measurements were closer to the 3DVH® results and indicate that there may have been some underestimation by ECLIPSE, but there was still a significant difference between ion chamber measurements and 3DVH®. The isocentre doses in 3DVH® for Truebeam measurements show good agreement with both ECLIPSE and ion chamber measurements. Also shown in table 4.8, are the isocentre dose differences between ion chamber measurements and ECLIPSE are compared for measurements taken in the ArcCHECK® phantom and in a water phantom. For both the 21-EX and Truebeam the measure-

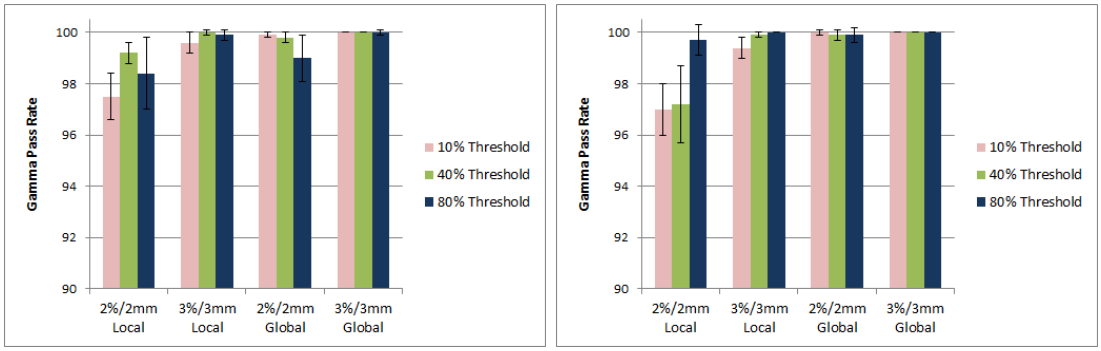

(a) (b)

Figure 4.16: γ-pass rates of 3DVH® dose reconstructions compared to ECLIPSE using various γ criterion and dose thresholds for prostate IMRT plans. Results displayed for both 21-EX (a) and Truebeam (b) deliveries.

ments in the ArcCHECK® phantom produced results that were within one standard deviation of the measurements taken in the water phantom. The agreement between water and ArcCHECK® measurements validates the ion chamber measurements in the ArcCHECK®, as ion chamber measurements in water phantoms are frequently used in IMRT QA. The comparison to the water measurements also provides additional validation of the couch model used in ECLIPSE, as deliveries to the water phantom were not obstructed by the couch. Overall the dose differences at isocentre showed good agreement with ECLIPSE as all results, on average, fell within the 5% dose difference action level recommended by TG-119 for ion chamber point dose measurements [17], and the 3% action level used at BCCA-VIC for reference point dose measurements. In fact, no single prostate IMRT plan had a 3DVH® dose difference that fell outside of a 3% difference when compared to ECLIPSE or ion chamber measurement.

Table 4.9 displays the mean dose difference averages within various volumes for the prostate IMRT plans. For plans delivered on the 21-EX the dose in 3DVH® was, on average, higher than in ECLIPSE within the 80% isodose region, indicating that the dose reconstructed by 3DVH® was slightly higher in the high dose regions. In the 40% isodose region there was little difference between 3DVH® and ECLIPSE, but the fact that the 40% region contains the 80% region must be considered. For points that are within the 40% region and not the 80% region, the mean dose must be lower than ECLIPSE to balance out the high mean dose in the 80% region. For Truebeam deliveries, 3DVH® reconstructed dose was, on average, lower than ECLIPSE in high dose regions and higher than ECLIPSE in lower dose regions. In this case, the mean dose difference for the 40% and 80% isodose region are similar and the dose difference within the entire phantom is higher. Again when considering the fact that the body structure contains both the 40% and 80% regions, it can be concluded that the region outside the 40% isodose has a much higher mean dose difference. However, these mean dose differences are relatively small with no difference for either accelerator greater than 1%. These results are within the 2% action level used at BCCA-VIC used for mean dose differences in the high and intermediate dose regions for IMRT pretreatment verification.

Overall, for prostate IMRT plans both diode measurements and 3DVH® reconstructions showed good agreement with ECLIPSE. On the 21-EX, doses in the high dose region and near the isocentre were higher in 3DVH® than in ECLIPSE. Ion chamber measurements suggest that this may be an underestimation of dose in

ECLIPSE, which could potentially be caused by issues with ECLIPSE calculation factors such as the dosimetric leaf gap or the MLC transmission factor. Both γ-pass rates and dose difference metric fell within action level suggested by TG-119 [17] and used at BCCA-VIC for IMRT pretreatment verification.

Table 4.8: Average dose differences at isocentre between 3DVH® and ECLIPSE and between ion chamber measurement and ECLIPSE for prostate IMRT plans. Also included is the dose difference for an ion chamber in water.

	Isocentre Dose Difference (σ)		
	3DVH® verus ECLIPSE	Ion Chamber versus ECLIPSE	Ion Chamber versus ECLIPSE (in water)
21-EX	+1.86%(0.51)	+0.96%(0.43)	+1.06%(0.25)
Truebeam	-0.12%(0.48)	+0.23%(0.30)	+0.66%(0.22)

Table 4.9: Average mean dose differences between 3DVH® and ECLIPSE within the entire ArcCHECK® phantom, the 40% isodose and the 80% isodose for prostate IMRT plans.

	Mean Dose Difference (σ)		
	ArcCHECK® Body	40% Isodose	80% Isodose
21-EX	+0.01%(0.22)	-0.11%(0.24)	+0.63%(0.26)
Truebeam	+0.23%(0.24)	-0.66%(0.25)	-0.44%(0.25)

ArcCHECK® Comparison with Monte Carlo

The summary of γ-pass rates comparing diode measurements to Monte Carlo for 8 prostate IMRT plans delivered on the 21-EX is shown in table 4.10. The results using Monte Carlo as a comparison are not significantly different from those seen in table 4.7 where ECLIPSE is used. Figure 4.17 shows a side by side comparison of γ-pass rates for 3DVH® reconstructions compared to both ECLIPSE and Monte Carlo. Note that the data in figure 4.17a is the same as seen in figure 4.16a. As with the results for the diode measurements there is little difference in 3DVH® γ-pass rates whether ECLIPSE or Monte Carlo is used as a comparison. The results from Monte Carlo provide validation for the ArcCHECK® comparisons with ECLIPSE.

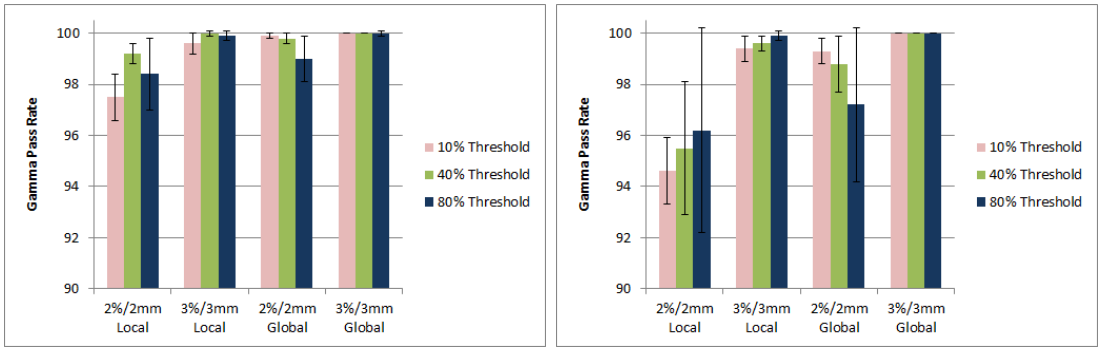

(a) (b)

Figure 4.17: γ-pass rates of 3DVH® dose reconstructions compared to ECLIPSE (a) and Monte Carlo (b) using various γ criterion and dose thresholds for prostate IMRT plans.

Table 4.10: Average γ-pass rates of diode measurements compared to Monte Carlo for 8 prostate IMRT plans delivered on the 21-EX using both local and global dose difference. All γ comparisons used a dose threshold of 10%.

γ criteria	2%/2mm Local (σ)	3%/3mm Local (σ)	2%/2mm Global (σ)	3%/3mm Global (σ)
21-EX	84.7%(2.8)	95.9%(2.5)	99.5%(0.2)	100%(0.0)

4.5.2 Head and Neck Plans

ArcCHECK® Comparison with ECLIPSE

The summary of γ-pass rates comparing diode measurements to ECLIPSE for 8 head and neck IMRT plans is shown in table 4.11. The procedures used to obtain these results are described in section 3.4. Also included in table 4.11 are results from Li et al. [2] and Garcia-Vicente et al. [3] comparing diode measurements to a TPS for IMRT plans. Li et al. have results from six nasopharyngeal step-and-shoot IMRT plans, whereas the head and neck plans used in this work were for a variety of sites and were also sliding window IMRT plans. Garcia-Vicente et al. have combined results for 3 prostate and 3 head and neck sliding window IMRT plans, and in their γ analysis use relative dose differences and a two-dimensional distance-to-agreement search, whereas this work uses absolute dose differences and a three-dimensional distance-to-agreement search. The γ-pass rates for head and neck plans when comparing diode measurements and ECLIPSE were significantly worse than those seen for prostate plans. The pass rates were high when a global dose difference was used in the γ criteria, but the pass rates with local dose difference are much lower. As seen in figure 4.18, there are many points which fail the γ criteria in the lower dose regions; many of these points pass the γ criteria when global dose difference is used. The pass rates for deliveries on the Truebeam are higher than those on the 21-EX, but still lower than the pass rates for prostate IMRT plans. Overall, despite lower pass rates at the more stringent γ criteria, when the clinically standard 3%/3mm, global dose difference, criteria is used the pass rates are well within the 90% action level suggested by TG-119 [17] for IMRT commissioning and the 85% lower confidence limit found by Sanghangthum et. al [40] for head and neck IMRT diode measurements using the ArcCHECK®.

Figure 4.19 displays γ-pass rates comparing 3DVH® and ECLIPSE for head and neck IMRT plans delivered on both the 21-EX and Truebeam. The γ-pass rates

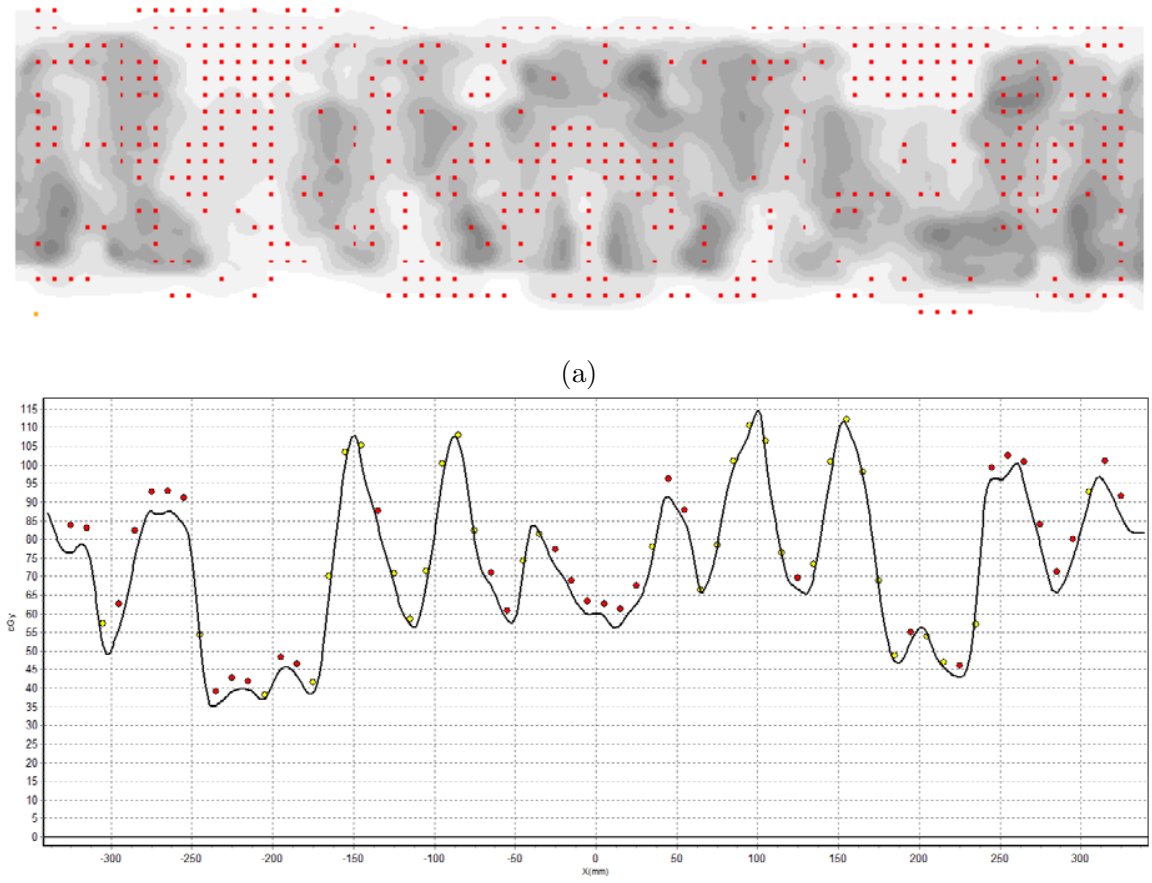

(a)

(b)

Figure 4.18: A dose difference map (a) and dose profile (b) of a HN IMRT plan delivered on the 21-EX comparing diode measurements to ECLIPSE. Markers indicate diode measurements with red and blue indicating high and low measurements, respectively, failing a 2%/2mm, local dose difference, γ criterion.

Table 4.11: Average γ-pass rates of diode measurements compared to ECLIPSE for 8 head and neck IMRT plans delivered on the Truebeam and 21-EX using both local and global dose difference. Also included are results from Li et al. [2] and Garcia-Vicente et al. [3]. All γ comparisons used a dose threshold of 10%.

γ criteria	2%/2mm Local (σ)	3%/3mm Local (σ)	2%/2mm Global (σ)	3%/3mm Global (σ)
21-EX	67.5%(7.7)	83.3%(6.0)	85.7%(9.3)	98.4%(1.6)
Truebeam	75.8%(3.5)	87.8%(4.4)	91.4%(5.0)	99.6%(0.4)
Li et al.	-	-	89.5%	97.4%
Garcia-Vicente et al.	-	-	-	99.1%

were analysed using 10%, 40% and 80% dose thresholds. As with the diode level measurements γ-pass rates are significantly lower for the head and neck IMRT plans when compared to the prostate plans. As with the diode level measurements the pass rates for the Truebeam measurements are higher than for the 21-EX, although in 3DVH® this difference is much larger. In figure 4.19a the γ-pass rates when 10% and 40% dose thresholds are used are much higher than when an 80% dose threshold is used. This suggests that the majority of points failing the γ criterion in 3DVH® are in the high dose region. A similar effect can be seen in figure 4.19b, although the difference in results between threshold levels is much smaller. At the 3%/3mm global dose difference γ criteria, the pass rates for the 21-EX measurements in the 80% dose threshold fall outside the 90% action level used for the χ-evaluation used at BCCA-VIC for IMRT pretreatment verification. For the Truebeam measurements, all results are well within this lower limit.

Overall the results γ-pass rates for head and neck IMRT are much lower than those seen for prostate IMRT plans, especially for the 21-EX. The agreement between 21-EX measurements and ECLIPSE is poor, particularly in 3DVH® where, on average, less than half of points in the high dose region pass the more stringent 2%/2mm γ criteria. Measurements on the Truebeam show significantly better agreement with ECLIPSE, and in 3DVH® the γ-pass rates for any dose threshold never dropped below 80%, even for the most stringent γ criteria used. The better agreement in the Truebeam results could be a result of more consistent and accurate delivery by the newer linear accelerator, more accurate leaf motion calculation in ECLIPSE, or better dosimetric calculation factors on the more recently commissioned accelerator. If an incorrect dosimetric leaf gap were a cause of the poor results on the 21-EX, the effect would produce a more exaggerated effect for head and neck IMRT plans as they

generally are more modulated and use smaller leaf gaps.

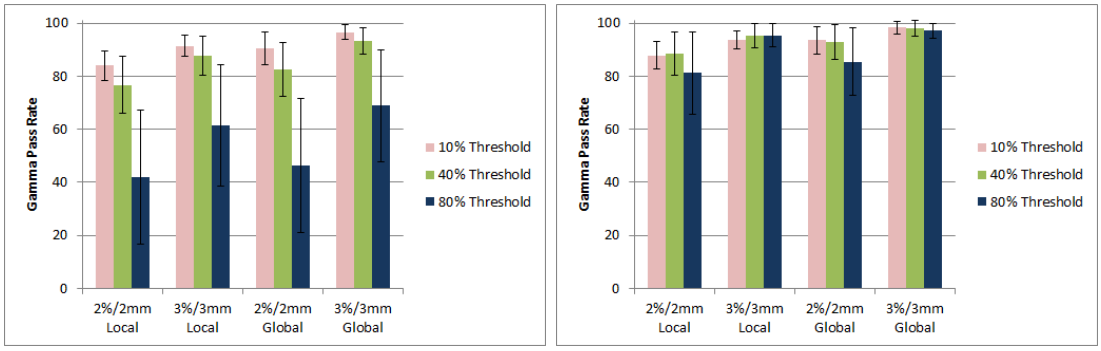

(a) (b)

Figure 4.19: γ-pass rates of 3DVH® dose reconstructions compared to ECLIPSE using various γ criterion and dose thresholds for head and neck IMRT plans. Results displayed for both 21-EX (a) and Truebeam (b) deliveries.

Table 4.12 displays the dose differences at isocentre on both the 21-EX and Truebeam for head and neck IMRT plans. On the 21-EX the isocentre dose in 3DVH® was on average more than 4% higher than in ECLIPSE. This average dose difference falls outside the 3% action level used at BCCA-VIC for reference points measurements. Six of the eight head and neck plans fell outside this 3% action level and four fell outside the 5% action level suggested by TG-119 [17]. When compared to ion chamber measurements the 3DVH® results were, on average, within a 3% dose difference and only 2 plans fell outside this action level. The better agreement with ion chamber measurements indicates that there may have been some underestimation in the ECLIPSE calculations. The isocentre doses in 3DVH® for Truebeam measurements are still greater, on average, than both ECLIPSE and ion chamber measurements, but the average differences are less than 2% and lower than the 21-EX results. As with the prostate IMRT water measurements, the measurements in the water phantom for head and neck IMRT plans produced results that were similar to measurements taken in the ArcCHECK® phantom.

Table 4.13 displays the mean dose difference averages within various volumes for the head and neck IMRT plans. For plans delivered on the 21-EX the dose in 3DVH® was, on average, more than 2% higher than that in ECLIPSE within all regions examined and almost 3% higher in the 80% isodose region. This falls outside the 2% action level used at BCCA-VIC for mean dose differences. These large mean dose differences indicate that the dose reconstructed by 3DVH® was higher

in practically all volumes within the ArcCHECK® phantom. The large number of failing points seen in figure 4.19a when an 80% dose threshold is used is not surprising when the almost 3% mean dose difference within the 80% isodose region is considered. The Truebeam mean dose differences, as with the γ-pass rates and isocentre dose differences, show better agreement with ECLIPSE than the 21-EX results and are within the 2% action level.

Table 4.12: Average dose differences at isocentre between 3DVH® and ECLIPSE and between ion chamber measurement and ECLIPSE for head and neck IMRT plans. Also included is the dose difference for an ion chamber in water.

	Isocentre Dose Difference (σ)		
	3DVH® verus ECLIPSE	Ion Chamber versus ECLIPSE	Ion Chamber versus ECLIPSE (in water)
21-EX	+4.14%(1.28)	+1.83%(1.06)	+1.91%(0.53)
Truebeam	+1.81%(0.69)	+1.01%(0.51)	+0.47%(0.41)

Table 4.13: Average mean dose differences between 3DVH® and ECLIPSE within the entire ArcCHECK® phantom, the 40% isodose and the 80% isodose for head and neck IMRT plans.

	Mean Dose Difference (σ)		
	ArcCHECK® Body	40% Isodose	80% Isodose
21-EX	+2.08%(0.71)	+2.11%(0.86)	+2.95%(1.04)
Truebeam	+1.83%(0.75)	+1.14%(0.86)	+1.23%(0.83)

Table 4.14 summarizes the average global correction factors used in 3DVH® reconstructions for IMRT plans on both the 21-EX and Truebeam. The global correction factor is used to scale the dose in the last step of the 3DVH® reconstruction and should in most cases be very close to 1.0 [46]. As discussed in section 2.4.3, the global correction factor minimizes the cumulative dose differences between the initial 3DVH® reconstruction and the diode measurements. In the case of 21-EX head and neck plans the global correction factor was, on average, almost 3% greater than unity. In all other cases the average global correction factors were within 1% of unity. The abnormal global correction factor seen for 21-EX head and neck plans suggests there is some issue with the 3DVH® reconstructions which was causing such poor agreement with ECLIPSE.

	Prostate	Head and Neck
21-EX	1.005	1.029
Truebeam	0.999	0.999

Table 4.14: A summary of the average global correction factors used in 3DVH® reconstructions for head and neck and prostate IMRT plans.

Overall, for head and neck IMRT plans, diode measurements showed good agreement with ECLIPSE at less stringent γ criteria, but pass rates dropped significantly when more stringent criteria were used. For the 21-EX diode measurements, the γ-pass rates at the clinically used 3%/3mm, global dose difference, criterion remained within accepted coincidence limits. In 3DVH®, the γ-pass rates were poor, especially in the high dose regions and the pass rates fell outside clinically used action levels. Isocentre doses and mean doses within the ArcCHECK® phantom were much higher in 3DVH® reconstructions when compared to ECLIPSE and also fell outside the action levels used at BCCA-VIC for reference point dose measurements and mean dose differences. Ion chamber measurements, however, were within these tolerances suggesting that part of this disagreement may be an underestimation of dose in ECLIPSE. For Truebeam deliveries, γ-pass rates and dose difference metrics had significantly better agreement with ECLIPSE, and all metrics remained within the clinically used action levels. The better agreement for Truebeam measurements provides further evidence that the ECLIPSE calculation for the 21-EX plans may be underestimating the dose. The most likely cause of this underestimation is an incorrect calibration of the dosimetric leaf gap. If the leaf gap were too small, the dose calculated in ECLIPSE would be lower than what is actually delivered on the linear accelerator. This effect was also seen for prostate plans delivered on the 21-EX, as there was a 1% underestimation of dose at isocentre by ECLIPSE when compared to ion chamber measurements. Since the average leaf gap for the head and neck plans (16.1 mm) is much lower than for prostate plans (31.0 mm), this dosimetric leaf gap error had a more significant impact on the head and neck plans.

ArcCHECK® Comparison with Monte Carlo

The summary of γ-pass rates comparing diode measurements to Monte Carlo for 8 head and neck IMRT plans delivered on the 21-EX is shown in table 4.15. The results using Monte Carlo as a comparison are not significantly different from those seen in table 4.11 where ECLIPSE is used. Figure 4.20 shows a side by side comparison of γ-

pass rates for 3DVH® reconstructions compared to both ECLIPSE and Monte Carlo. Note that the data in figure 4.20a is the same as seen in figure 4.19a. The 3DVH® γ-pass rates increase dramatically when Monte Carlo is used as a comparison. The pass rates for the 21-EX head and neck plans when compared to Monte Carlo are similar to the results for Truebeam head and neck plans compared to ECLIPSE seen in figure 4.19b. These Monte Carlo results provide further evidence that part of the reason for the poor agreement between 21-EX head and neck results and ECLIPSE is due to suboptimal modelling of MLC effects in the ECLIPSE calculation.

γ criteria	2%/2mm Local (σ)	3%/3mm Local (σ)	2%/2mm Global (σ)	3%/3mm Global (σ)
21-EX	67.8%(8.1)	83.6%(6.3)	84.4%(8.4)	98.0%(1.9)

Table 4.15: Average γ-pass rates of diode measurements compared to Monte Carlo for 8 head and neck IMRT plans delivered on the 21-EX using both local and global dose difference. All γ comparisons used a dose threshold of 10%.

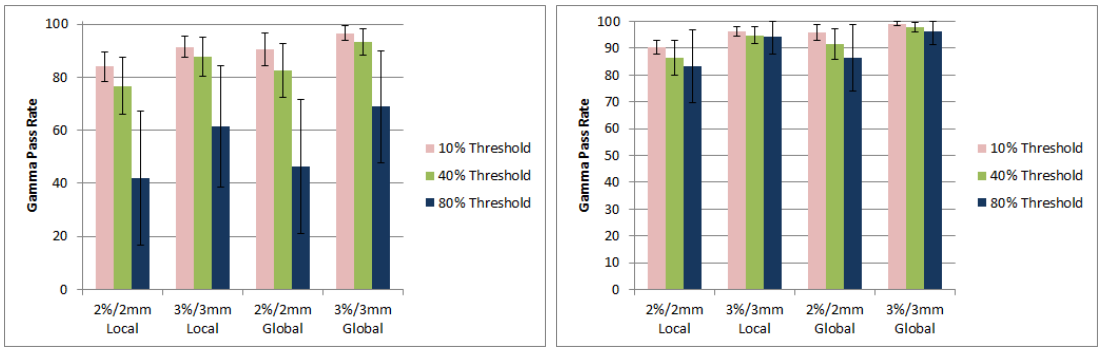

(a) (b)

Figure 4.20: γ-pass rates of 3DVH® dose reconstructions compared to ECLIPSE (a) and Monte Carlo (b) using various γ criterion and dose thresholds for head and neck IMRT plans.

Chapter 5

Discussion and Results II: VMAT Measurements

This chapter summarizes the results of the ArcCHECK® phantom and 3DVH® system's measurements of VMAT deliveries and the sensitivity of the system to errors. Section 5.1 presents the results for a population of both prostate and head and neck VMAT plans delivered to the ArcCHECK®. The intraday and interday variation in measurements are summarized in section 5.2, along with a set of confidence limits for γ-pass rates and dose difference metrics. Finally, the sensitivity of ArcCHECK® diode measurements and 3DVH® dose reconstructions to delivery and ECLIPSE calculation errors is determined in section 5.3.

5.1 Measurement of VMAT Plans

The summary of γ-pass rates comparing diode measurements to ECLIPSE for 8 prostate and 8 head and neck VMAT plans is shown in table 5.1. The procedures used to obtain these results are described in section 3.5. Also included in table 5.1 are results from several studies comparing diode measurements to a TPS for VMAT plans. It should be noted that some of the studies listed in table 5.1 did not use the optional PMMA plug and the use of the plug is noted in the table. The results for both prostate and head and neck VMAT plans showed excellent agreement with the TPS. In both cases 100% of points passed the 3%/3mm, global dose difference, γ criterion and greater than 95% passed the 2%/2mm, global dose difference, γ criterion. When local dose difference was used the performance of the head and neck plans de-

creased compared to prostate plans. Note that a decrease in γ-pass rates when moving from prostate to head and neck plans is seen for all studies quoted in table 5.1 which includes both types of plans. This decrease is likely due to the increased complexity of head and neck treatments, which for IMRT, often results in reduced tolerances for γ-pass rates compared to less complex sites [60]. For both sites, the γ-pass rates are well within the action level of 90% at 3%/3mm, global dose difference, set out by TG-119 for IMRT commissioning [16]. A lower control limit of 90% is also the limit suggested by Sanghangthum et. al [40] for VMAT pretreatment verification of head and neck plans using diode measurements with the ArcCHECK®. The prostate and head and neck VMAT γ-pass rates are higher than the pass rates for IMRT plans included in chapter 4.

Comparing the results to other work, one must consider the effect of the PMMA plug on pass rates. The highest γ-pass rates are seen in measurements for which the PMMA plug was used. The difference in results between measurements with and without the plug can be attributed to the difficulties in calculating dose within a phantom containing a 15 cm air cavity, as was done in the other three sets of results. There is also a difficulty in comparing the results in this work to those from Feygelman et al. [32], Nelms et al. and Kozelka et al. [1], as each study only evaluated a single prostate and single head and neck plan. Overall for both prostate and head and neck plans, the results were comparable to those seen in other studies and when the most clinically relevant γ criterion, 3%/3mm global dose difference, was used the pass rates were well within suggested control limits.

Figure 5.1 displays γ-pass rates comparing 3DVH® and ECLIPSE for prostate and head and neck VMAT plans. The γ-pass rates were analysed using 10%, 40% and 80% dose thresholds. The prostate VMAT plans showed excellent agreement between 3DVH® and ECLIPSE with γ-pass rates at all dose thresholds exceeding 95%, even when using the most stringent 2%/2mm, local dose difference, γ criterion. The head and neck VMAT plans showed little difference from prostate results when global dose difference was used. As with diode measurement comparisons, the results for head and neck 3DVH® reconstructions were not in as good agreement with ECLIPSE when local dose difference was used but pass rates still exceeded 90% for all dose threshold and γ criteria used. Overall, for both prostate and head and neck plans the 3DVH® dose reconstructions showed excellent agreement with ECLIPSE, and pass rates using the 3%/3mm, global dose difference, criterion were well within the 90% lower limit used at BCCA-VIC for χ-pass rates within the high and intermediate dose

Table 5.1: Average γ-pass rates of diode measurements compared to ECLIPSE for 8 prostate and 8 head and neck VMAT plans using both local and global dose difference. Also included are results from other ArcCHECK® studies. All gamma comparisons used a dose threshold of 10%.

γ criteria	2%/2mm Local (σ)	3%/3mm Local (σ)	2%/2mm Global (σ)	3%/3mm Global (σ)	Plug Used?
Prostate					
This work	92.1%(3.8)	97.0%(2.8)	99.5%(0.3)	100%(0.1)	YES
Feygelman et al. [32]	-	-	95.8%	99.4%	NO
Kozelka et al. [1]	88.5%	95.8%	96.8%	99.5%	NO
Nelms et al. [46]	97%	100%	99.7%	100%	YES
Koren et al. [39]	-	-	-	98.8%	NO
Head and Neck					
This work	88.2%(4.9)	94.9%(2.3)	99.1%(1.1)	100%(0.0)	YES
Feygelman et al.	-	-	85.8%	94.2%	NO
Kozelka et al.	85.9%	94.9%	93.1%	98.3%	NO
Nelms et al.	97.8%	99.7%	99.7%	100%	YES
Li et al. [2]	-	-	85.5%	95.3%	YES
Koren et al.	-	-	-	96.1%	NO

regions.

Table 5.2 displays the dose differences at isocentre for prostate and head and neck VMAT plans. As with IMRT results seen in chapter 4, there was a systematic difference between ion chamber measurements and ECLIPSE calculations in ArcCHECK® greater than 1% for both prostate and head and neck VMAT plans. For prostate VMAT plans, the average 3DVH® isocentre dose fell between the ECLIPSE and ion chamber results and was within 1% of both. For head and neck plans, the average 3DVH® isocentre dose agreed more closely with ECLIPSE than ion chamber measurements, but showed only about 1% difference, on average, from ion chamber measurements. It is important to note the larger standard deviation for head and neck dose differences compared to prostate, indicating that the head and neck VMAT plans covered a wider range of results. The isocentre dose differences between ion chamber measurements and ECLIPSE in ArcCHECK® are also compared for measurements in a water phantom. For both prostate and head and neck VMAT plans the measurements in the ArcCHECK® phantom produced results that were not significantly different from measurements taken in the water phantom. Overall, the isocentre dose calculated in 3DVH® for both prostate and head and neck VMAT plans showed good agreement with both ECLIPSE and ion chamber measurements.

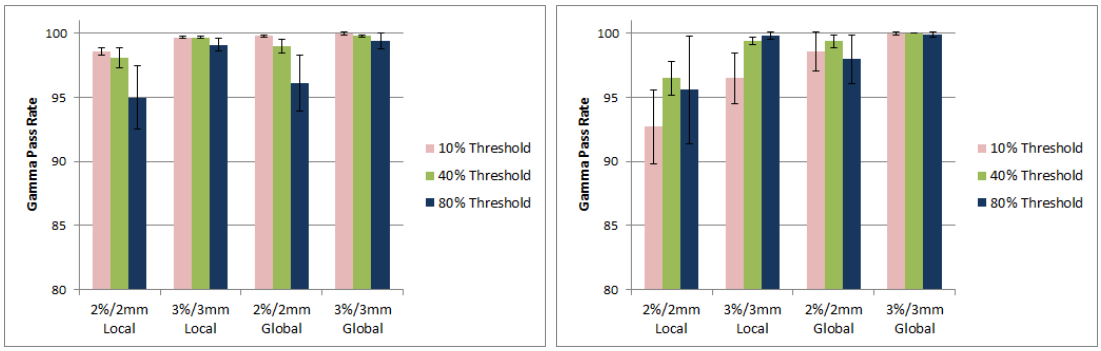

(a) (b)

Figure 5.1: γ-pass rates of 3DVH® dose reconstructions compared to ECLIPSE for prostate (a) and head and neck (b) VMAT plans.

All results, on average, fell within the 5% dose difference action level recommended by TG-119 for ion chamber point dose measurements [17], and the 3% action level used at BCCA-VIC for reference point dose measurements. In fact, no single prostate or head and neck plan had a 3DVH® isocentre dose that fell outside of a 3% difference when compared to ECLIPSE or ion chamber measurement.

Table 5.3 displays the mean dose difference averages within the volumes described in section 3.2 for the prostate and head and neck plan 3DVH® reconstructions compared to ECLIPSE. For prostate plans the dose in 3DVH® was, on average, slightly higher than in ECLIPSE within all regions analysed; the differences between the body, 40% isodose and 80% isodose results were not significant. The positive dose difference for prostate plans was in line with the isocentre dose difference between 3DVH® and ECLIPSE in table 5.2. For head and neck plans the dose in 3DVH® was, on average, lower than in ECLIPSE within the 40% and 80% isodose regions, but higher than ECLIPSE when the whole phantom was analysed. The difference between the low and high dose regions for head and neck plans is caused by points in the peripheral regions near the diode detectors, where 3DVH® seems to overestimate the dose compared to ECLIPSE. Overall for both prostate and head and neck VMAT plans, the average mean dose differences between 3DVH® and ECLIPSE in all regions analysed were less than 1%. These results are within the 2% action level used at BCCA-VIC used for mean dose differences in the high and intermediate dose regions analysed for pretreatment verification.

Overall for prostate and head and neck VMAT plans, both diode measurements and 3DVH® reconstructions showed excellent agreement with ECLIPSE. The mean

Table 5.2: Average dose differences at isocentre between 3DVH® and ECLIPSE and between ion chamber measurement and ECLIPSE for VMAT plans. Also included is the dose difference for an ion chamber measurement in water.

	Isocentre Dose Difference (σ)		
	3DVH versus ECLIPSE	Ion Chamber versus ECLIPSE	Ion Chamber versus ECLIPSE (in water)
Prostate	+0.72%(0.41)	+1.30%(0.33)	+1.29%(0.79)
Head and Neck	+0.05%(0.94)	+1.08%(0.55)	+0.64%(0.55)

Table 5.3: Average mean dose differences between 3DVH® and ECLIPSE within the entire ArcCHECK® phantom, the 40% isodose and the 80% isodose for VMAT plans.

	Mean Dose Difference (σ)		
	ArcCHECK Body	40% Isodose	80% Isodose
Prostate	+0.76%(0.35)	+0.35%(0.55)	+0.70%(0.61)
Head and Neck	+0.92%(0.28)	-0.16%(0.28)	-0.58%(0.49)

3DVH® reconstructed dose for prostate plans was high compared to ECLIPSE but this difference was less than 1% for all regions analysed. Head and neck plans showed dose lower than ECLIPSE in the high dose regions and higher than ECLIPSE in the intermediate dose regions, but within 1% for all regions analysed. Results for all metrics fell within the limits set by TG-119 [17] and the action levels used at BCCA-VIC for IMRT pretreatment verification.

5.2 VMAT Intraday and Interday Variation

The summary of intraday and interday diode measurements for one prostate and one head and neck plan is shown in figure 5.2; also included are the interplan results from section 5.1. Using a global dose difference, there was almost no interday or intraday variance in the results for either the prostate or head and neck plan. When looking at all 8 prostate plans from section 5.1, the standard deviation in the γ-pass rates were only 0.1% and 0.3% for the 2%/2mm and 3%/3mm γ criteria, respectively. For the 8 head and neck plans there was no variation at the 3%/3mm γ criterion but the standard deviation when 2%/2mm was used was over three times larger than the standard deviation seen for prostate plans.

For both prostate and head and neck plans, the interday variance was larger than the intraday variance which is likely due to the uncertainty introduced in setting up the phantom between each measurement in the interday measurements. The variance in both the interday and intraday γ-pass rates was lower than the interplan variance as one would expect from a stable dosimeter when comparing the results from one plan compared to a population of plans from the same treatment site.

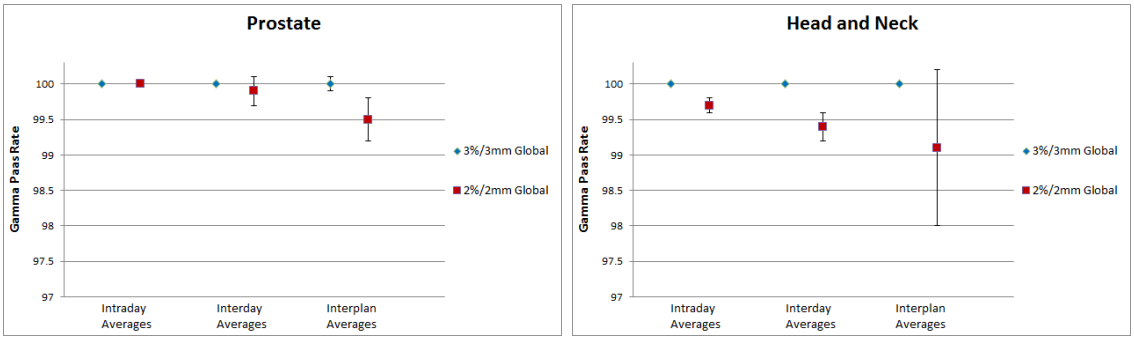

(a) (b)

Figure 5.2: Interday and intraday γ-pass rates for diode measurements compared to ECLIPSE for a single prostate (a) and single head and neck (b) VMAT plan. Also shown are the interplan average γ-pass rates for 8 prostate (a) and 8 head and neck (b) VMAT plans from section 5.1. All gamma comparisons used a dose threshold of 10%. Error bars represent standard deviation of the average γ-pass rates.

Figure 5.3 displays the results from intraday and interday 3DVH® dose reconstructions when compared to ECLIPSE; also included are the interplan results from section 5.1.

For prostate plans, the standard deviations of the γ-pass rates at the 40% threshold are less than 1% for the intraday, interday and interplan averages. When an 80% dose threshold was used the standard deviations in the γ-pass rates increased and were over 4 times larger than with a 40% dose thresholds at the 2%/2mm γ criterion. This indicates that when the 80% dose threshold was used the γ-pass rates were more sensitive to small changes in delivery than when the 40% dose threshold was used. This is partially due to the fact that at the 80% dose threshold a smaller number of points were used in the gamma analysis, so small changes in the number of passing points had a greater effect on the γ-pass rate. The standard deviations of the intraday, interday and interplan average γ-pass rates were similar for prostate plans with approximately 20% higher standard deviations seen in the interplan results. The similarity between the intraday and interday results indicated that the

set up of the the phantom for the interday results was reasonably consistent as there was no significant addition of uncertainty in the results when multiple set ups were used. There was a small increase in uncertainty for the interplan results, which arose from differences between prostate VMAT plans, but overall the γ-pass rates were remarkably consistent from plan to plan.

For head and neck plans, the γ-pass rates at the 40% dose threshold had similar interplan standard deviations to the those seen for prostate plans. The standard deviations of the intraday and interday averages however, were less than half of those measured for prostate plans at the 2%/2mm γ criterion. At an 80% dose threshold, the interplan standard deviations of the head and neck plans were again similar to the the standard deviations of the prostate plans. In this case the standard deviations of the intraday and interday averages were less than one fifth of those seen for prostate plans at the 2%/2mm γ criterion. Unlike prostate plans, the variance in the interplan averages for head and neck plans compared to the intraday and interday variances was much larger, indicating that the majority of the uncertainty in the average pass rates is due to the differences between different head and neck plans and not due to changes in set up or delivery.

Figure 5.4 displays intraday and interday average dose difference results for 3DVH® reconstructions compared to ECLIPSE. For prostate plans, the interday and intraday dose difference averages have similar standard deviations, which are about half of the standard deviations seen for interplan averages. The exception to this is the ion chamber versus ECLIPSE isocentre dose which shows almost no variation for the intraday average and similar standard deviations for the interday and interplan averages. The increase in standard deviations seen for interplan averages is greater for the dose difference metrics than was seen for the 3DVH® pass rates, as seen in figure 5.3. For head and neck plans, excluding the ion chamber versus ECLIPSE results, the interday standard deviations were about twice those seen in the intraday results; this effect can also be seen in the 3DVH® pass rates results in figure 5.3. For the mean dose difference metrics there is no significant change in standard deviations when comparing interday and interplan results; for the 3DVH® versus ECLIPSE isocentre dose difference the standard deviation is more than 3 times larger for the interplan average.

Overall for both diode measurements and in 3DVH®, the variation in intraday and interday measurements was less than the variation seen over different plans for the same site. The small variation in intraday and interday measurements indicates

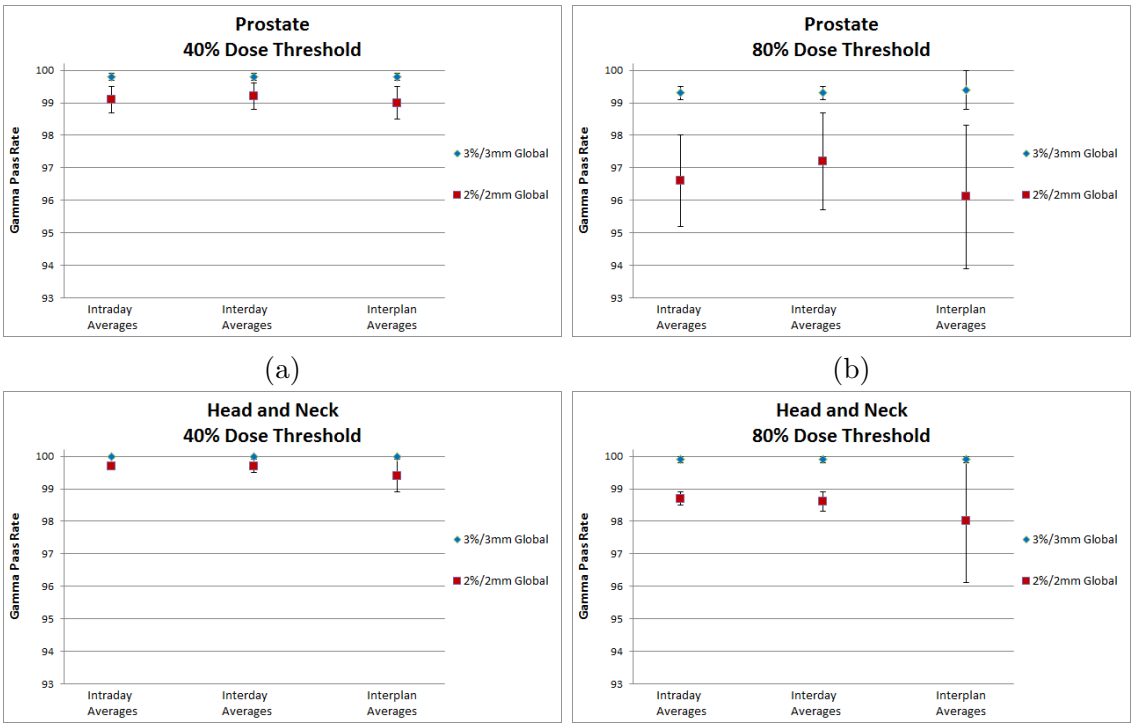

Figure 5.3: Intraday and interday γ-pass rate averages for a prostate and head and neck VMAT plans comparing 3DVH® to ECLIPSE using 40% and 80% dose thresholds. Also shown are the interplan average γ-pass rates for prostate and head and neck VMAT plans. Error bars represent standard deviation of the average γ-pass rates.

that the results for the ArcCHECK® phantom are reasonably stable over multiple measurements and multiple setups. For this reason the interplan variation was used to determine the confidence limits for γ-pass rates and dose difference metrics.

Table 5.4 summarizes the expected lower confidence limits for γ-pass rates for diode measurement and 3DVH® results. The confidence limits were calculated by multiplying 1.96 by the standard deviation for the interplan measurements, similar to the method used by Task Group 119 on IMRT commissioning [17]. The confidence limits determined for the ArcCHECK® diode measurements and 3DVH® reconstructions are tighter than the action level of 90% suggested by TG-119 and the confidence limit of 90% determined by Sanghangthum et al. [40]. The system based confidence limits established in table 5.4 are limited by the small sample of plans that were measured. The confidence limits determined by Sanghangthum et. al were established based on measurements of 50 different head and neck VMAT plans and

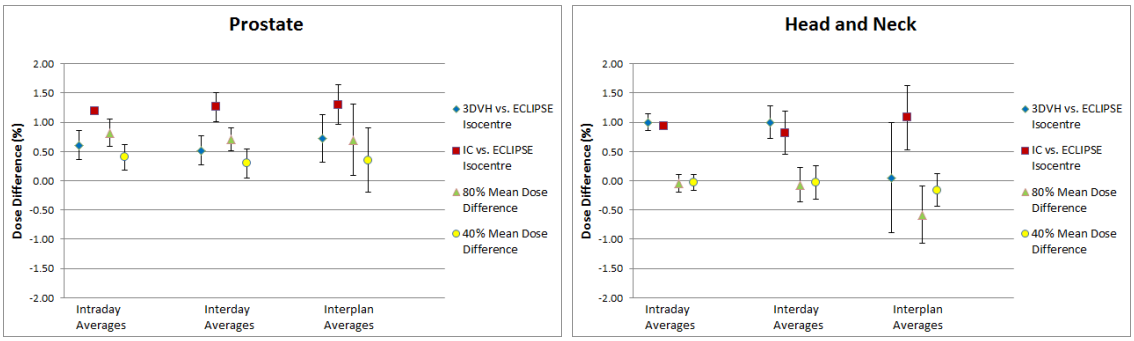

(a) (b)

Figure 5.4: Intraday and interday isocentre dose differences comparing 3DVH® to ECLIPSE and ion chamber measurements to ECLIPSE for a single prostate (a) and head and neck (b) plan. Also included is the mean dose difference between 3DVH® and ECLIPSE in the 80% isodose region. The interplan averages for these metrics are also shown. Error bars represent standard deviation of the average dose differences.

provide a wider sampling of results than used in this work.

Table 5.4: Summary of γ-pass rate lower limits based on results for interplan measurements of a 8 prostate and 8 head and neck VMAT plans.

	Prostate		**Head and Neck**	
γ criteria	2%/2mm Global	3%/3mm Global	2%/2mm Global	3%/3mm Global
Diode Measurements				
Average γ-pass rate	99.5%	100%	99.1%	100%
1.96σ	0.6	0.2	2.2	0.0
Lower Limit	**98.9%**	**99.8%**	**96.9%**	**100%**
3DVH 40% Threshold				
Average γ-pass rate	99.0%	99.8%	99.4%	100%
1.96σ	1.1	0.3	1.0	0.1
Lower Limit	**97.9%**	**99.6%**	**98.4%**	**99.9%**
3DVH 80% Threshold				
Average γ-pass rate	96.1%	99.4%	98.0%	99.9%
1.96σ	4.4	1.1	3.6	0.3
Lower Limit	**91.7%**	**98.3%**	**94.4%**	**99.6%**

Table 5.5 summarizes the upper and lower confidence limits for the dose difference metrics shown in figure 5.4. As with the γ-pass rate, the upper and lower limits were calculated by multiplying 1.96 by the standard deviations of interplan measurements. In the case of dose difference metrics the confidence limit is determined by adding

1.96σ to the absolute value of the mean to centre the upper and lower limit around zero. The confidence limits for isocentre dose differences determined from 3DVH® reconstructions are tighter than the 5% dose difference action level recommended by TG-119 for ion chamber point dose measurements [17], and the 3% action level used at BCCA-VIC for reference point dose measurements. The confidence limits for mean dose differences are tighter than the 2% action level used at BCCA-VIC for mean dose differences in the high and intermediate dose regions.

Table 5.5: Summary of dose difference lower and upper limits based on results for interplan measurements of a 8 prostate and 8 head and neck VMAT plans.

	Isocentre Dose Difference		**Mean Dose Difference**	
	3DVH versus ECLIPSE	Ion Chamber versus ECLIPSE	40% Isodose Region	80% Isodose Region
Prostate				
Average	+0.72%	+1.30%	+0.35%	+0.70%
1.96σ	0.80	0.66	1.07	1.19
Confidence Limit	**1.52%**	**1.96%**	**1.42%**	**1.89%**
Head and Neck				
Average	+0.05%	+1.08%	-0.16%	-0.58%
1.96σ	1.84	1.08	0.54	0.96
Confidence Limit	**+1.89%**	**+2.15%**	**+0.70%**	**1.53%**

5.3 Sensitivity of VMAT Plans to Errors

5.3.1 Monitor Unit Normalization

Figure 5.5 displays the effect that errors of up to 5% in dose normalization had on γ-pass rates when comparing diode measurements to ECLIPSE. For both prostate and head and neck plans, the diode measurements were biased towards positive normalization errors, as the pass rate curves were centred around a 0.995 normalization for the prostate plan and a 0.990 normalization for the head and neck plan. These normalization shifts correspond to the respective 3DVH® versus ECLIPSE dose differences at isocentre for the interday and intraday averages in figure 5.4 for the prostate and head and neck plan. For the prostate plan, pass rates dropped below the system based confidence limits established in section 5.2 at normalizations of +2% and -3%; adjusting for the bias, the prostate plan was sensitive to normalization errors of

greater than 2.5%. For the head and neck plan pass rates dropped below the system based confidence limits at +2% and -4%, so the head and neck plan was sensitive to normalization errors greater than approximately 3% when the bias is removed. Note that the system based tolerances are very tight compared to the conventional 90% pass rate action level for a 3%/3mm γ criterion. Using this 90% action level, neither the prostate or head and neck plan were sensitive to normalization errors up to 5%. For the ArcCHECK® diode measurements the 90% action level may be too low and the tighter, system based constraints are more useful metrics.

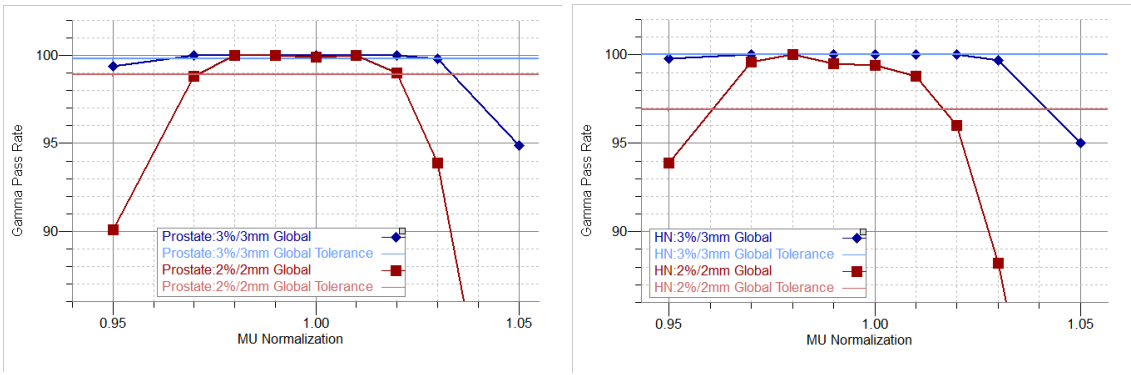

(a) (b)

Figure 5.5: γ-pass rates for a prostate (a) and head and neck (b) VMAT plan comparing diode measurements to ECLIPSE as a function of errors in MU normalization.

Figure 5.6 displays the effect that errors in dose normalization had on γ-pass rates in the 80% dose region when comparing 3DVH® reconstructions to ECLIPSE. The γ-pass rates for a +5% normalization is not included for the head and neck data because the 3DVH® software was unable to complete a reconstruction. The reconstruction failed due to the large number of diodes measurements with dose much higher than what was calculated in ECLIPSE. As with the diode measurements the prostate pass rate curve was centred around a normalization of 0.995. The head and neck pass rate curve, however, was centred around a normalization of 1.005, which was in the opposite direction of the bias for diode measurements. For the prostate plan, pass rates dropped below the system based confidence limits for normalization errors greater than approximately 1% and below the conventional 90% action level for normalizations errors greater than 2%. For the head and neck plan, pass rates dropped below the system based confidence limits for normalization errors greater than approximately 0.5% and below the conventional 90% action level for normalizations errors greater than 2%. Overall when using 3DVH®, the ArcCHECK® system

was extremely sensitive to normalization errors in VMAT plans and had greater sensitivity when compared to diode measurements only. Unlike the diode measurements results, 3DVH® was too sensitive to errors when the system based constrains were used, and the more relaxed 90% action level may be more appropriate.

Figure 5.7 displays the change in dose differences as errors dose normalization were introduced. As with the γ-pass rates the dose difference metrics are biased with respect to normalization errors. For prostate plans, both the 3DVH® dose at isocentre and mean dose within the 80% isodose region sit about 0.5% higher than ECLIPSE at a normalization of 1.00. For head and neck plans, the 3DVH® isocentre dose is about 1% higher than ECLIPSE at a normalization of 1.00 and the mean dose within the 80% isodose region shows almost no bias. For both prostate and head and neck plans the slopes of all three dose difference metrics are fairly consistent; a 1% change in normalization produces close to a 1% change in dose difference. Using the system based tolerance limits and adjusting for bias, the dose difference metrics are sensitive to normalization errors greater than approximately 2% for both prostate and head and neck plans. Overall, the dose difference metrics were less sensitive to normalization errors than the 3DVH® γ-pass rates.

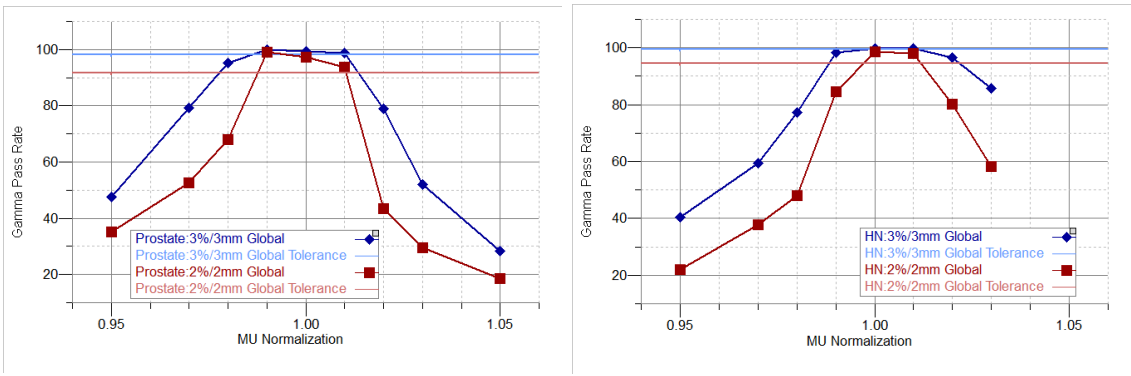

(a) (b)

Figure 5.6: γ-pass rates using an 80% dose threshold for a prostate (a) and head and neck (b) VMAT plan comparing 3DVH® reconstructions to ECLIPSE as a function of errors in MU normalization.

Figure 5.8 displays the γ-pass rate for a prostate and head and neck VMAT plan when the 3DVH® reconstructions analysed in figure 5.6 were compared to ECLIPSE plans with the changes in normalizations included in the calculation. These results serve as a test of the accuracy with which 3DVH® can reconstruct dose when given an error-free ECLIPSE plan to guide the reconstruction of an error-filled delivery.

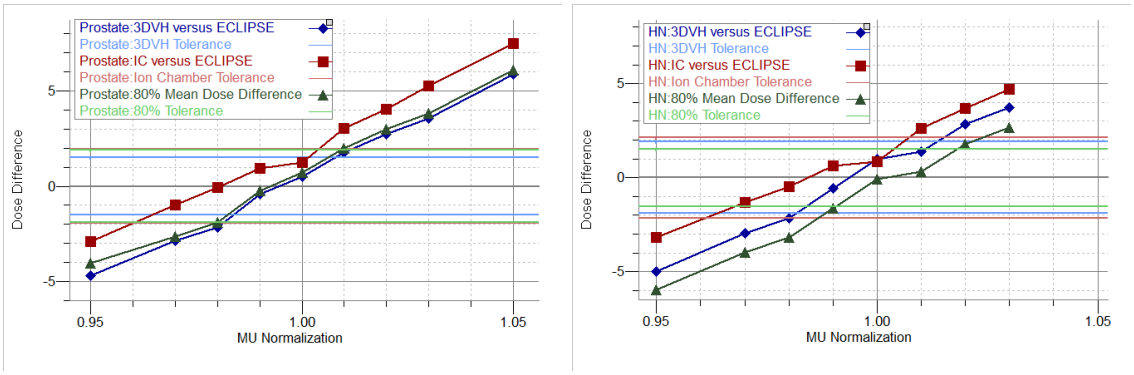

(a) (b)

Figure 5.7: Dose differences at isocentre and within the 80% isodose region for a prostate (a) and head and neck (b) VMAT plan comparing 3DVH® and ion chamber measurements to ECLIPSE as a function of errors in MU normalization.

For both the prostate and head and neck plan there was good agreement between the 3DVH® reconstructions and the error-filled ECLIPSE plans. This indicates that the 3DVH® reconstruction was not forced into agreement with the ECLIPSE plan that was used to guide it. The only significant drop in the γ-pass rate occurred when the normalization error was greater than -3%, again no result was available +5% normalization for the head and neck plan. Overall, when the the ECLIPSE plans used to guide 3DVH® differed in normalization from delivery by up to 3%, 3DVH® was able to provide an accurate reconstruction of the dose that was actually delivered.

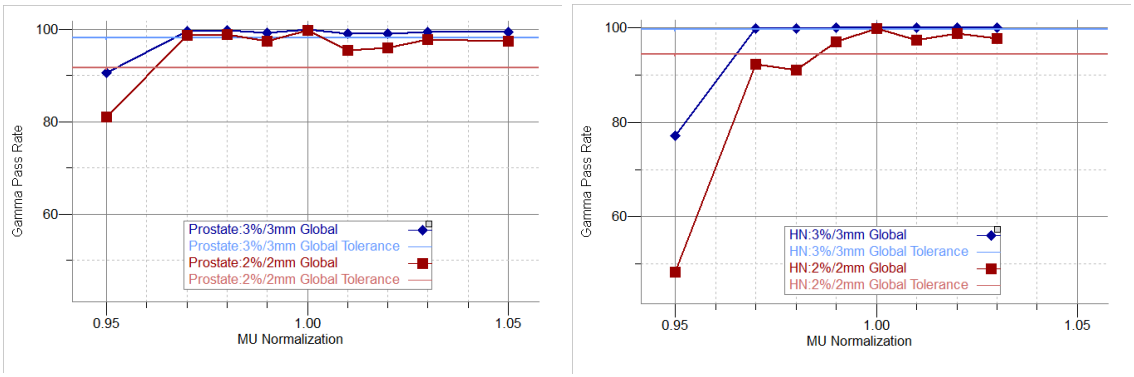

(a) (b)

Figure 5.8: Comparison of 3DVH® reconstructions guided by error-free ECLIPSE plans and error-filled delivery measurements to error-filled ECLIPSE plans for prostate (a) and head and neck (b) VMAT plans.

5.3.2 MLC position Errors

Systematic MLC Errors

Figure 5.9 displays the effect that systematic errors in MLC positions had on γ-pass rates when comparing diode measurements to ECLIPSE. The drop in γ-pass rates for systematic MLC errors is more drastic than for normalization errors, indicating that a systematic change of 1 mm to all MLC gaps had a more severe effect than a 1% change in normalization. As with normalization errors, the diode measurements were biased, with both prostate and head and neck plans biased towards positive, or open, systematic MLC errors. The pass rate curves were centred around a -0.5 mm MLC error for the prostate plan and a -1.0 mm error for the head and neck plan. Adjusting for biases the prostate plan was sensitive to systematic open or closed MLC errors greater than 0.5 mm when using the system based confidence limits; the head and neck plan was sensitive to errors greater than 1 mm. When a 90% action level was considered for the 3%/3mm γ criterion, the prostate and head and neck plans were sensitive to errors of greater than 2 mm and 3 mm, respectively.

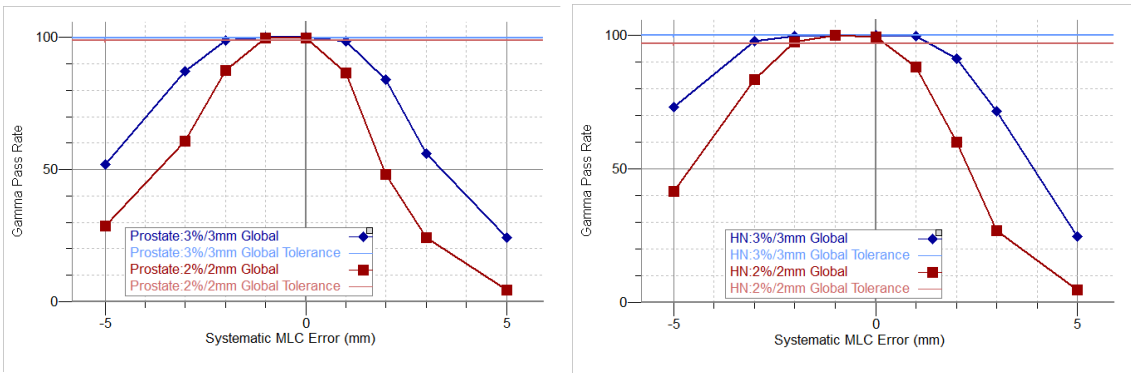

(a) (b)

Figure 5.9: γ-pass rates for a prostate (a) and head and neck (b) VMAT plan comparing diode measurements to ECLIPSE as a function of systematic errors in MLC leaf positions.

Figure 5.10 displays the effect that systematic errors in MLC positions had on γ-pass rates when comparing 3DVH® reconstructions to ECLIPSE. The γ-pass rates for MLC errors greater than 3 mm are not included because, as with the more extreme normalization errors, the 3DVH® software was unable to complete a reconstruction. For both prostate and head and neck plans, the pass rates decreased significantly when any systematic MLC error was introduced to the delivery, and all deliveries

with errors caused the pass rates to fall below the system based tolerance limits. Pass rates fell to near or below 50% when the MLC errors reached 2 mm. When a 90% action level was considered for the 3%/3mm γ criterion, the prostate and head and neck plans were sensitive to errors of greater than 0.5 mm and 1 mm, respectively. As with normalization errors, 3DVH® was more sensitive to systematic MLC errors than diode measurements alone and very sensitive to systematic MLC errors in general. High sensitivity to these types of errors is desirable as even small systematic changes to MLC leaf gaps can have a significant dosimetric impact on VMAT plans [67, 68].

Based on the diode measurement and 3DVH® results, the prostate plan appeared to be more sensitive to systematic MLC errors than the head and neck plan. One reason for the difference in sensitivity may be related to the difference in the mean MLC leaf gaps of the head and neck (33.4 mm) and prostate (23.6 mm) plan used for these tests. Oliver et. al [68] showed that dose sensitivity to systematic MLC errors decreases as the mean MLC leaf gap increases for prostate VMAT plans.

Figure 5.11 displays the change in dose differences as systematic MLC errors were introduced. For prostate plans, both the dose difference between 3DVH® and ECLIPSE at isocentre and the mean dose difference in the 80% isodose region had a sensitivity of 2.8%/mm. The dose difference at isocentre between ion chamber measurements and ECLIPSE had a sensitivity of 1.5%/mm. This suggests that the 3DVH® reconstruction was hypersensitive to systematic MLC errors compared to ion chamber measurements. For head and neck plans, the dose difference sensitivities for 3DVH® and ion chamber doses compared to ECLIPSE were 2.2%/mm and 1.6%/mm, respectively. For the head and neck plan, the increased sensitivity to systematic MLC errors in 3DVH® was smaller than for the prostate plan. Overall, relative to the confidence limits established in table 5.5, the 3DVH® dose difference metrics observed in figure 5.11 were sensitive to systematic MLC errors as small as 1 mm for both the prostate and head and neck plan.

Figure 5.12 displays the γ-pass rate for a prostate and head and neck plan when the 3DVH® reconstructions analysed in figure 5.10 were compared to ECLIPSE plans with the MLC errors included in the calculation. For smaller MLC errors, there was good agreement between the 3DVH® reconstruction and the error-filled ECLIPSE plans. However, when plans with MLC errors greater than 1 mm were delivered, the γ-pass rates decreased significantly. This shows the limit of using TPS data to guide a 3D dose reconstruction; when disagreements between measurement and prediction

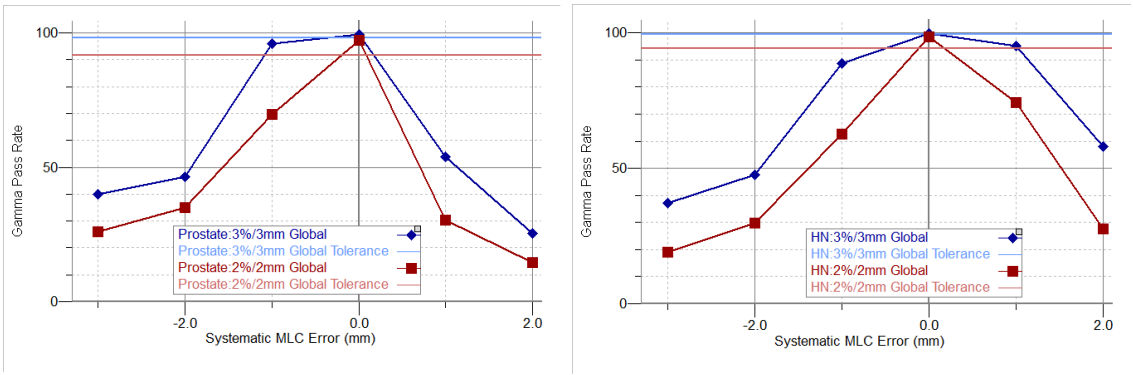

(a) (b)

Figure 5.10: γ-pass rates using an 80% dose threshold for a prostate (a) and head and neck (b) VMAT plan comparing 3DVH® reconstructions to ECLIPSE as a function of systematic errors in MLC leaf positions.

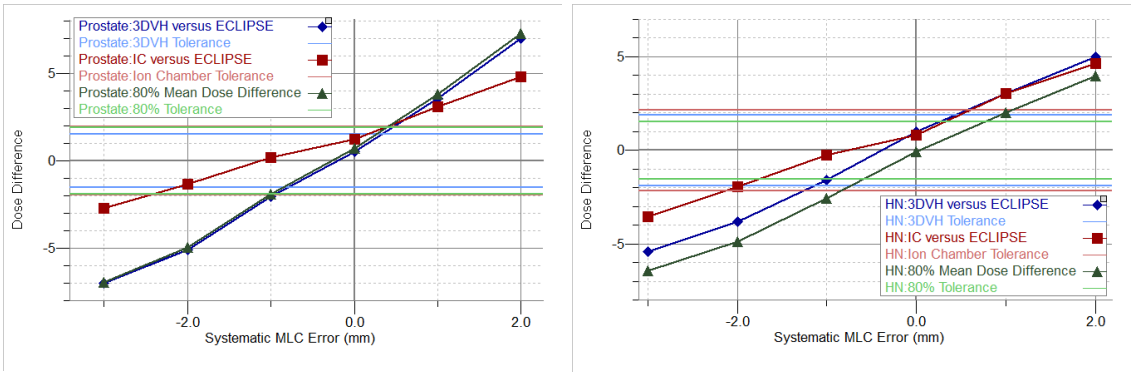

(a) (b)

Figure 5.11: Dose differences at isocentre and within the 80% isodose region for a prostate (a) and head and neck (b) VMAT plan comparing 3DVH® and ion chamber measurements to ECLIPSE as a function of systematic errors in MLC positions.

are large (approximately 5%), the reconstruction has difficulty producing an accurate 3D dose map.

Random MLC Errors

Figure 5.13 displays the effect that random errors in MLC positions had on γ-pass rates when comparing diode measurements to ECLIPSE. Unlike the systematic MLC errors, random errors had little effect on pass rates at the diode level. Only when the random MLC error is increased to 5 mm did the change in γ-pass rates drop below the system based confidence limits; at no point did the pass rates drop below 90%.

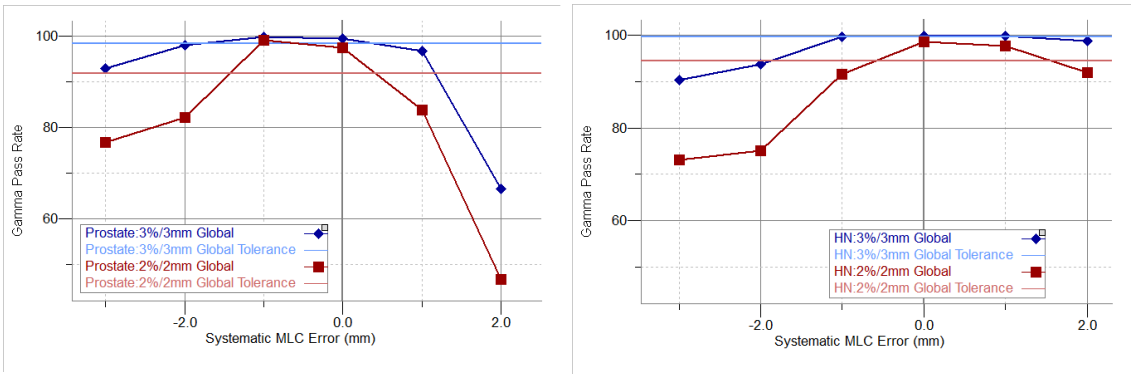

(a) (b)

Figure 5.12: Comparison of 3DVH® reconstructions guided by error-free ECLIPSE plans and error-filled delivery measurements to error-filled ECLIPSE plans for prostate (a) and head and neck (b) VMAT plans.

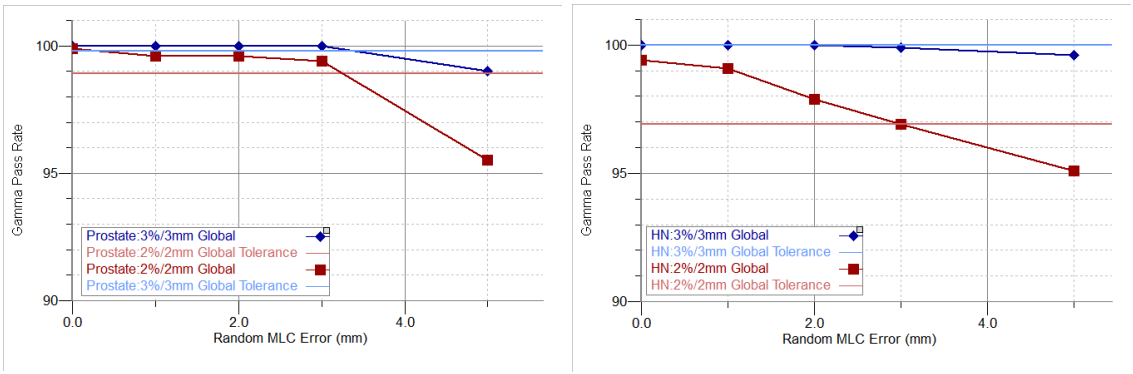

(a) (b)

Figure 5.13: γ-pass rates for a prostate (a) and head and neck (b) VMAT plan comparing diode measurements to ECLIPSE as a function of random errors in MLC leaf positions.

Figure 5.14 displays the effect that random errors in MLC positions had on γ-pass rates when comparing 3DVH® reconstructions to ECLIPSE. As with the diode measurements there was little to no change in pass rates due to the random MLC errors.

Figure 5.15 displays the change in dose differences between 3DVH® and ECLIPSE as random MLC errors were introduced. Both the isocentre dose differences and the dose difference within the 80% isodose region showed little change and remained within the system based limits for all random MLC errors induced.

Overall when using diode measurements alone or 3DVH®, the ArcCHECK®

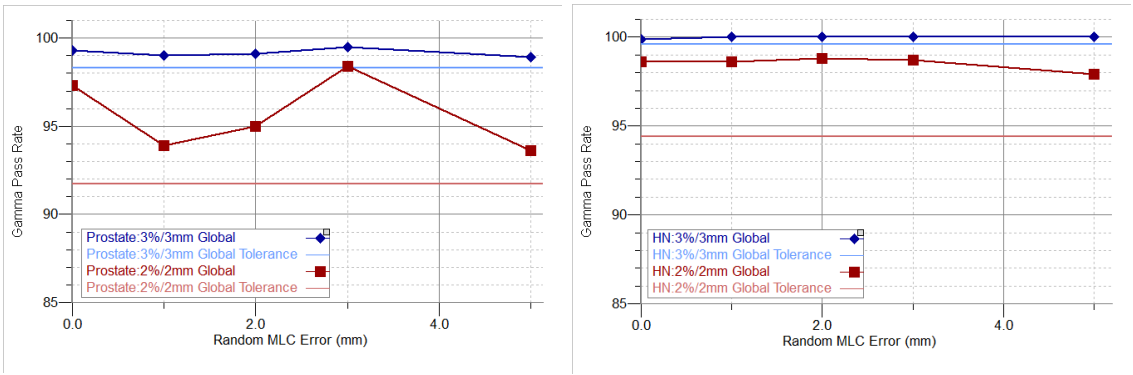

(a) (b)

Figure 5.14: γ-pass rates using an 80% dose threshold for a prostate (a) and head and neck (b) VMAT plan comparing 3DVH® reconstructions to ECLIPSE as a function of random errors in MLC leaf positions.

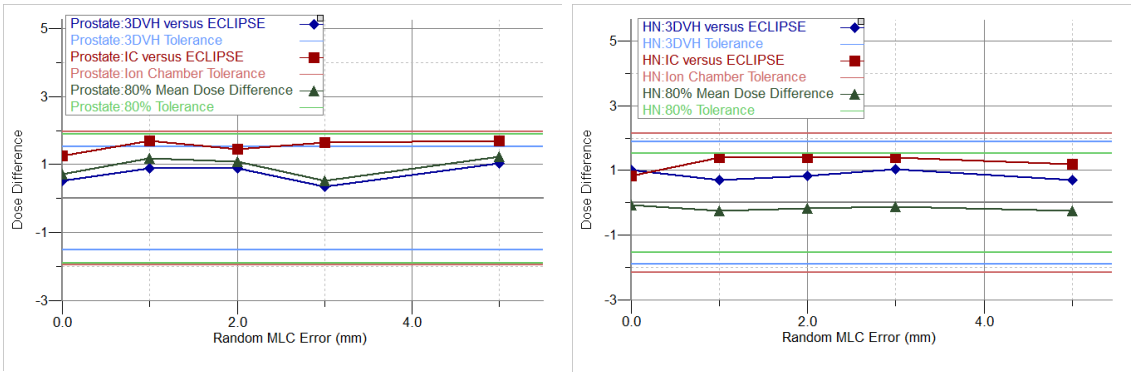

(a) (b)

Figure 5.15: Dose differences at isocentre and within the 80% isodose region for a prostate (a) and head and neck (b) VMAT plan comparing 3DVH® and ion chamber measurements to ECLIPSE as a function of random errors in MLC positions.

system showed almost no change in results when random MLC errors up to 5 mm were introduced in plan delivery. In this case the lack of sensitivity to these types of errors is acceptable, as random MLC errors up to 2 mm have been shown to have little or no significant dosimetric impact on VMAT plans [67, 68]. Results for random MLC errors greater than 2 mm are not available.

5.3.3 Gantry Position Errors

Systematic Gantry Errors

Figure 5.16 displays the effect that systematic errors in gantry position had on γ-pass rates when comparing diode measurements to ECLIPSE. For both the prostate and head and neck plan, γ-pass rates dropped as the gantry error increased, with pass rates falling below system based tolerance for 2° errors. At no point did the pass rates at the 3%/3mm γ criterion drop below the conventional 90% action level.

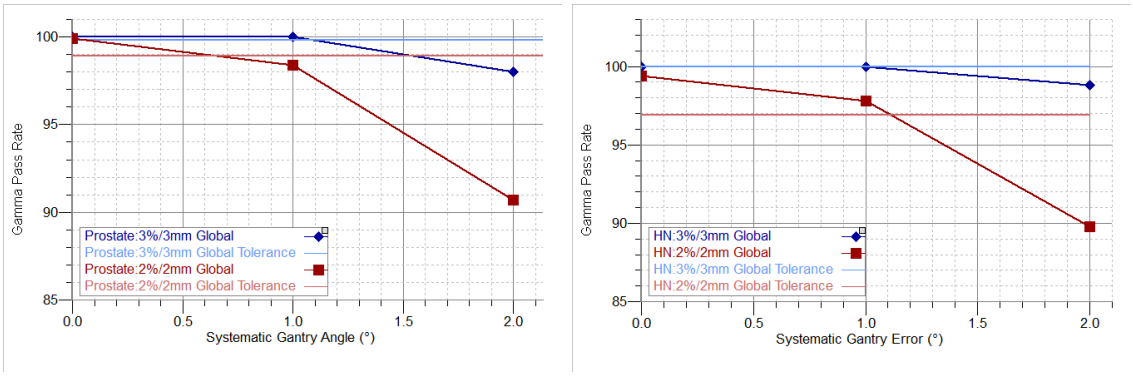

(a) (b)

Figure 5.16: γ-pass rates for a prostate (a) and head and neck (b) VMAT plan comparing diode measurements to ECLIPSE as a function of systematic errors in gantry position.

Figure 5.17 displays the effect that systematic errors in gantry positions had on γ-pass rates when comparing 3DVH® reconstructions to ECLIPSE. There was no significant change in γ-pass rates seen for systematic errors in gantry position. Figure 5.18 displays the change in dose differences as systematic gantry position errors were introduced. Both the isocentre dose differences and the dose difference within the 80% isodose region were unaffected by the errors.

Overall, diode measurements showed some sensitivity to systematic gantry errors, but γ-pass rates and dose difference metrics in 3DVH® showed almost no sensitivity to these errors. The low sensitivity to these types of errors can be considered acceptable as systematic gantry errors up to 1° have been found to have little effect on clinically relevant dosimetric factors [68].

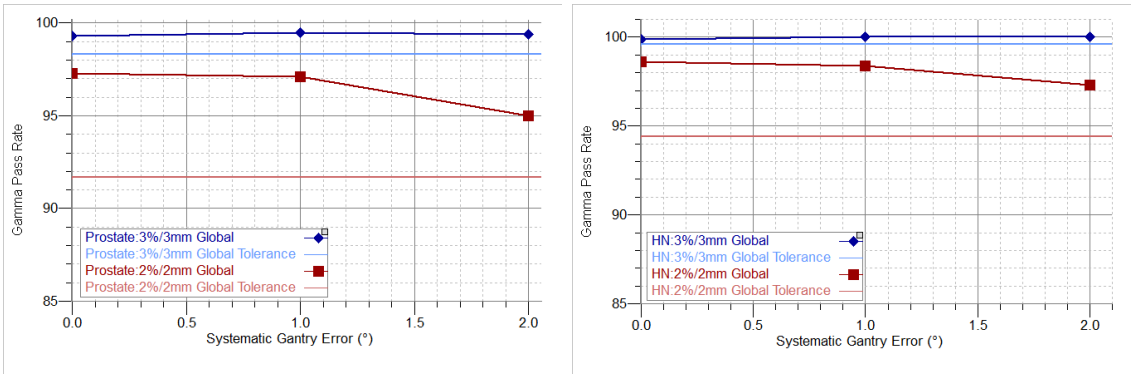

(a) (b)

Figure 5.17: γ-pass rates using an 80% dose threshold for a prostate (a) and head and neck (b) VMAT plan comparing 3DVH® reconstructions to ECLIPSE as a function of systematic errors in gantry position.

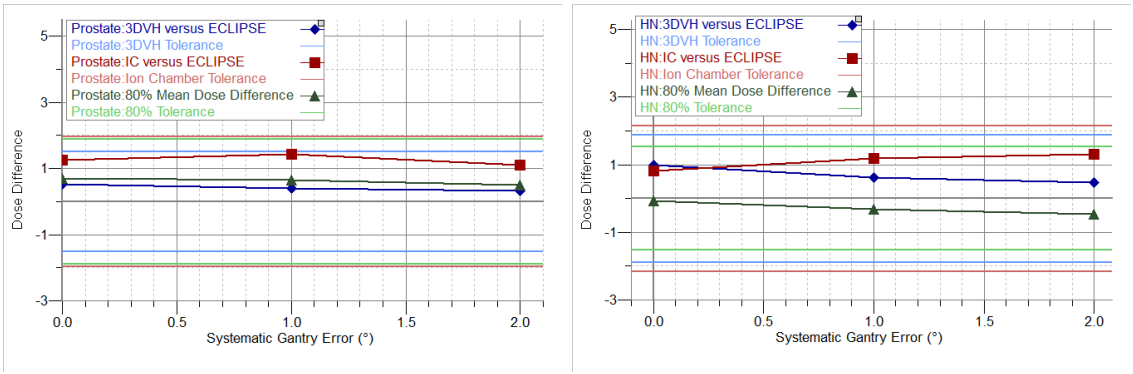

(a) (b)

Figure 5.18: Dose differences at isocentre and within the 80% isodose region for a prostate (a) and head and neck (b) VMAT plan comparing 3DVH® and ion chamber measurements to ECLIPSE as a function of systematic errors in gantry position.

Random Gantry Errors

Figure 5.19 displays the effect that random errors in gantry position up to 1° had on γ-pass rates when comparing diode measurements to ECLIPSE. For random errors the γ-pass rates of both the prostate and head and neck plan were almost unaffected for errors up to 1°.

Figure 5.20 displays the effect that random errors in gantry positions had on γ-pass rates when comparing 3DVH® reconstructions to ECLIPSE. As with systematic errors, no significant change in γ-pass rates was seen for random errors in gantry position for either the prostate or head and neck plan. Figure 5.21 displays the change

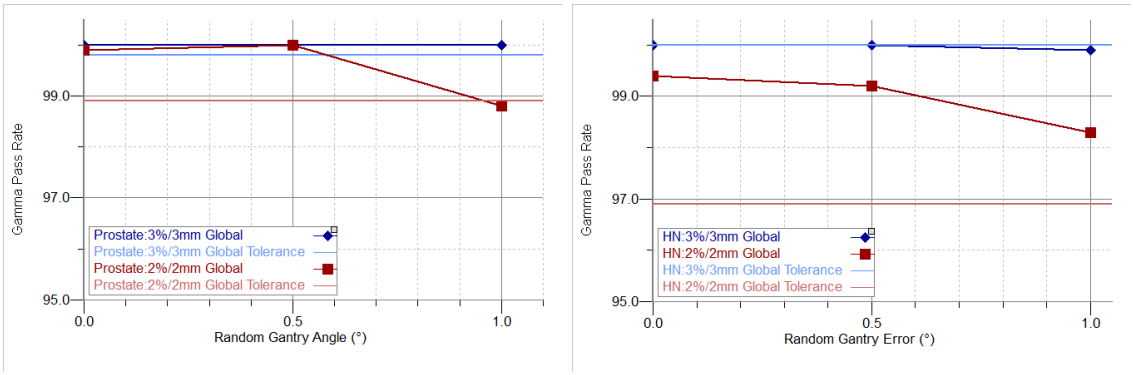

(a) (b)

Figure 5.19: γ-pass rates for a prostate (a) and head and neck (b) VMAT plan comparing diode measurements to ECLIPSE as a function of random errors in gantry position.

in dose differences between 3DVH® and ECLIPSE as random gantry position errors were introduced. As with systematic errors no significant change was produced by random gantry errors.

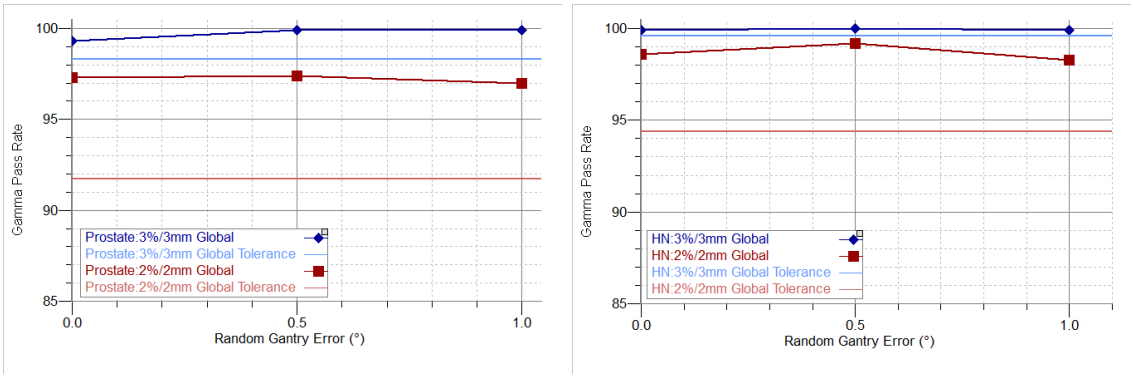

(a) (b)

Figure 5.20: γ-pass rates using an 80% dose threshold for a prostate (a) and head and neck (b) VMAT plan comparing 3DVH® reconstructions to ECLIPSE as a function of random errors in gantry position.

Overall when looking at diode measurements or 3DVH® reconstructions, the ArcCHECK® system showed no sensitivity to random errors in gantry position. Like systematic gantry errors, random errors of up to 1° in gantry position have been shown to have little effect on clinically relevant dosimetric factors [68].

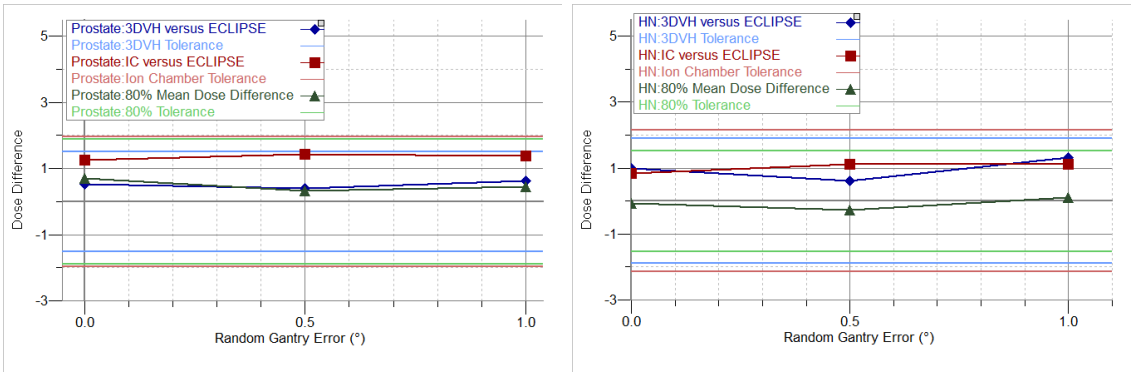

(a) (b)

Figure 5.21: Dose differences at isocentre and within the 80% isodose region for a prostate (a) and head and neck (b) VMAT plan comparing 3DVH® and ion chamber measurements to ECLIPSE as a function of random errors in gantry position.

5.3.4 Partial Delivery

Figure 5.22 displays the effect that partial deliveries had on γ-pass rates when comparing diode measurements to ECLIPSE. For both the prostate and head and neck plan, γ-pass rates fell below the system based confidence limits for all partial deliveries. When a 90% limit for the 3%/3mm γ criterion was considered all partial deliveries for the prostate plan passed; for the head and neck plan only the 95% partial delivery passed.

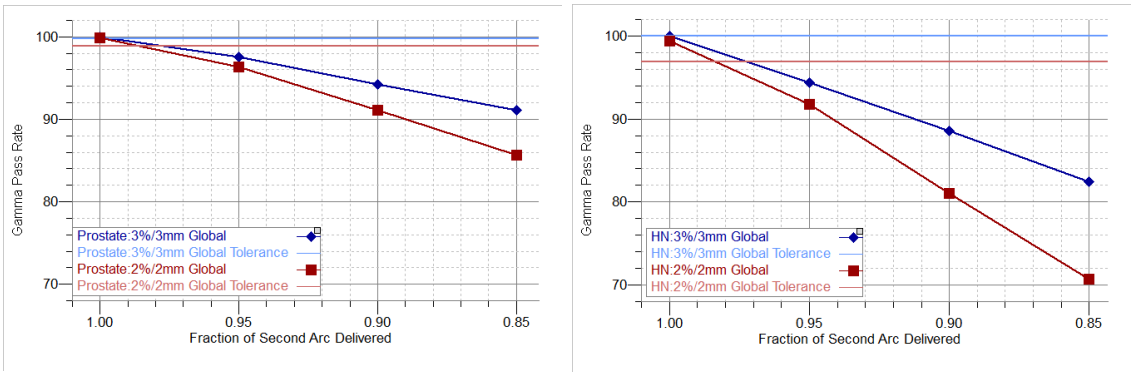

(a) (b)

Figure 5.22: γ-pass rates for a prostate (a) and head and neck (b) VMAT plan comparing diode measurements to ECLIPSE as a function of the fraction of the second arc delivered.

Figure 5.23 displays the effect that partial deliveries had on γ-pass rates when comparing 3DVH® reconstructions to ECLIPSE. For the prostate plan pass rates

only fell below the system based confidence limits when 85% of the arc was delivered. In fact, when 95% of the arc was delivered, pass rates in 3DVH® increased. The head and neck plan was more sensitive to partial deliveries, with pass rates dropping below the confidence limits for all fractions of the delivered arc. No partial delivery caused pass rates drop below the 90% limit at 3%/3mm γ criterion for the prostate plan, whereas the pass rates for the head and neck plan failed the 90% limit for all fractions of the arc that were delivered. Overall, the head and neck plan was much more sensitive to partial deliveries of the VMAT arc; this is seen in both diode measurements and 3DVH® reconstructions.

Figure 5.24 displays the change in dose differences between 3DVH® and ECLIPSE as a function of the fraction of the arc delivered. For the prostate plan, the 3DVH® isocentre dose difference and mean dose difference within the 80% isodose region decreased by 0.12% and 0.11%, respectively, for every 1% removed from the second arc of the plan; for head and neck plans these values were 0.54% and 0.60%. Overall, relative to the confidence limits established in table 5.5, the 3DVH® dose difference metrics observed in figure 5.24 were not sensitive to deliveries with as much as 15% of the second arc removed for the prostate plan, but sensitive to deliveries with as little as 5% of the second arc removed for the head and neck plan.

The difference in sensitivity between the prostate and head and neck plan may simply be a result of differences in the sizes of MLC apertures for the final portion of the second arc. If the prostate plan had very small apertures during the portion of the arc that was removed, it would not have a large effect on the dose. Conversely if the head and neck plan had very wide apertures near the end of the arc, removal of this portion of the beam could have had a significant impact on the dose delivered.

5.3.5 Dosimetric Leaf Gap Errors

As discussed in section 2.1.2, the dosimetric leaf gap (DLG) that is used in ECLIPSE calculations affects the dose calculated for plans using MLC modulation. VMAT plans were recalculated with different DLG values and compared to measurements. The original DLG was 1.4 mm and was also the value used to calculate all other VMAT plans in this work.

Figure 5.25 displays the effect that changes in the DLG had on γ-pass rates when comparing diode measurements to ECLIPSE. For both head and neck and prostate plans, γ-pass rates remained above system based confidence limits for all DLG values

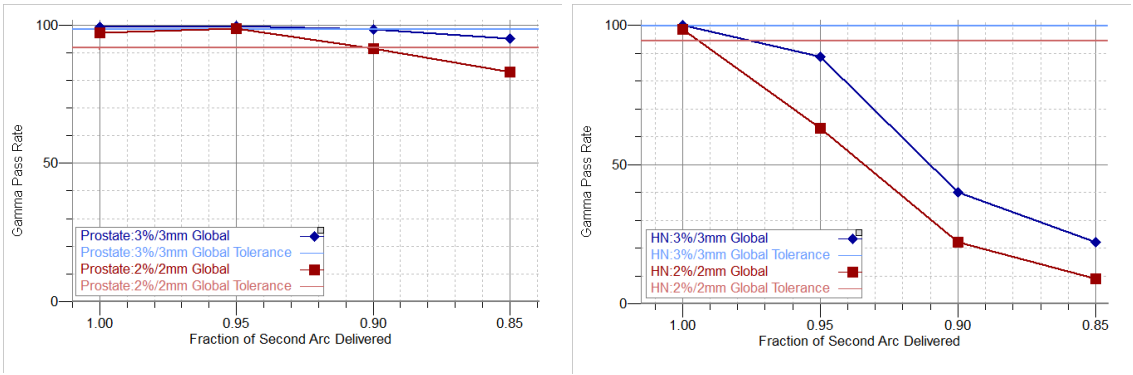

(a) (b)

Figure 5.23: γ-pass rates using an 80% dose threshold for a prostate (a) and head and neck (b) VMAT plan comparing 3DVH® reconstructions to ECLIPSE as a function of the fraction of the second arc delivered.

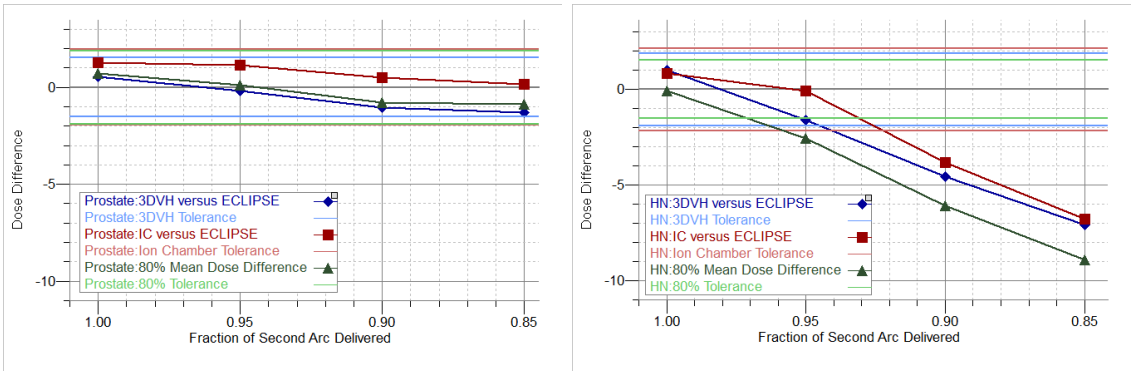

(a) (b)

Figure 5.24: Dose differences at isocentre and within the 80% isodose region for a prostate (a) and head and neck (b) VMAT plan comparing 3DVH® and ion chamber measurements to ECLIPSE as a function of the fraction of the second arc delivered.

tested. Using the 3%/3mm γ criterion, the changes made in the DLG had no effect on pass rates.

It should be noted that when using the 2%/2mm γ criterion both the prostate and head and neck plan achieved the highest pass rates when a dosimetric leaf gap of 1.8 mm was used. Shortly after the completion of this work, the dosimetric leaf gap for the treatment machine used was increased to 1.6 mm and may be further increased to 1.8 mm. This indicates that when using more stringent γ criteria the ArcCHECK® has value as a diagnostic tool for dosimetric leaf gap calibration.

Figure 5.26 displays the effect that changes in the DLG had on γ-pass rates when

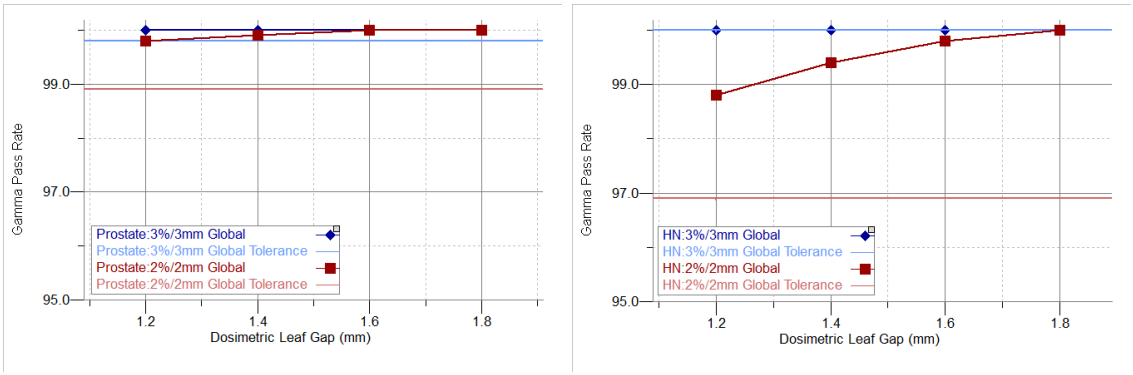

(a) (b)

Figure 5.25: γ-pass rates for a prostate (a) and head and neck (b) VMAT plan comparing diode measurements to ECLIPSE as a function of the dosimetric leaf gap used in the ECLIPSE calculation.

comparing 3DVH® reconstructions to ECLIPSE. As with diode measurements, there were no significant changes in 3DVH® γ-pass rates as the DLG was changed. For the prostate plan, the highest passing rates are seen at a DLG of 1.6 mm. At the original DLG of 1.4 mm the prostate plan had a high mean dose in 3DVH® when compared to ECLIPSE; increasing the DLG to 1.6 mm increased the dose calculated by ECLIPSE, producing better agreement. A similar effect was seen for the head and neck plan but the 3DVH® dose was originally lower than ECLIPSE, so decreasing the DLG improved results. Overall, the γ-pass rates for diode measurements and 3DVH® results were not sensitive to changes in the DLG.

For both prostate and head and neck plans the ion chamber dose at isocentre is moves closer to the ECLIPSE isocentre dose as the dosimetric leaf gap increases. This agrees with the results seen for the diode measurements as the dosimetric leaf gap was changed.

Figure 5.27 displays the change in dose differences as a function of the DLG. As with the γ-pass rate all dose difference metrics fell within the system based confidence limits for changes in DLG. For the prostate plan, the 3DVH® isocentre dose difference and mean dose difference within the 80% isodose region had dose sensitivities of -1.8%/mm and -2.8%/mm, respectively; for head and neck plans these values were -1.6%/mm and -1.7%/mm. The magnitude of these sensitivities are similar to those seen for systematic MLC errors, but with the opposite sign. This is an expected outcome, as adjusting the dosimetric leaf gap has the same effect as inducing a systematic error to all the leaf positions. The signs are reversed as in this case

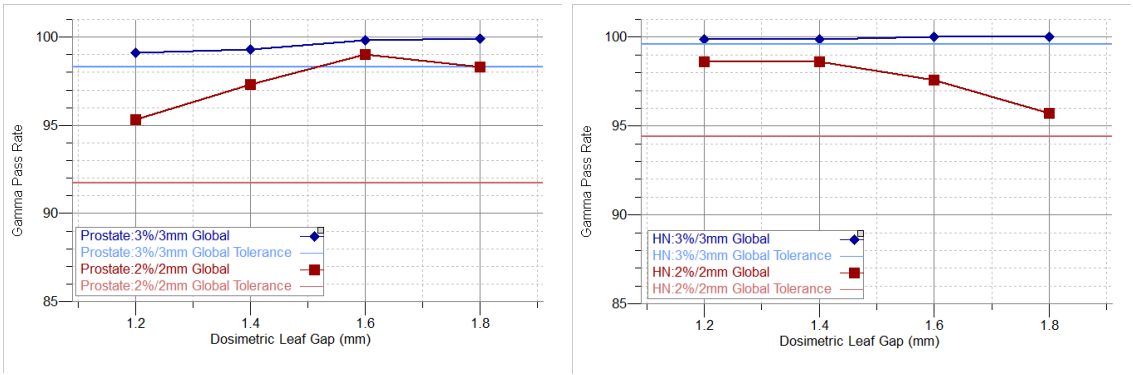

(a) (b)

Figure 5.26: γ-pass rates using an 80% dose threshold for a prostate (a) and head and neck (b) VMAT plan comparing 3DVH® reconstructions to ECLIPSE as a function of the dosimetric leaf gap used in the ECLIPSE calculation.

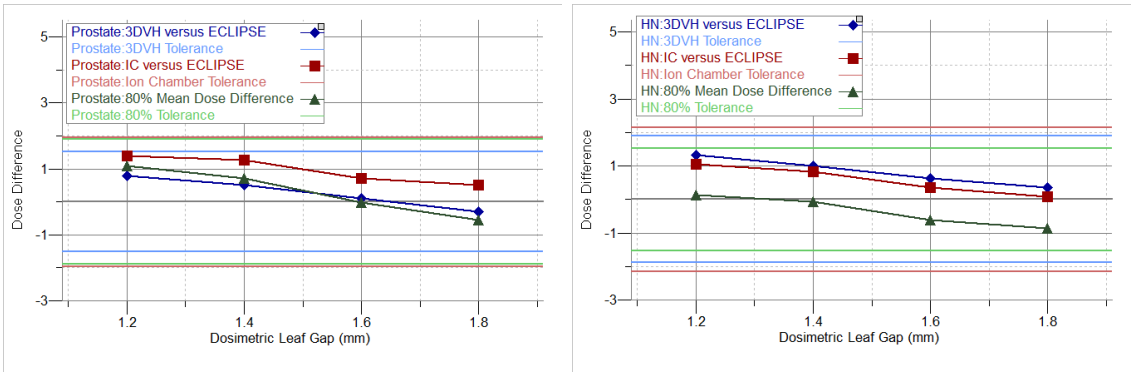

(a) (b)

Figure 5.27: Dose differences at isocentre and within the 80% isodose region for a prostate (a) and head and neck (b) VMAT plan comparing 3DVH® and ion chamber measurements to ECLIPSE as a function of the dosimetric leaf gap used in the ECLIPSE calculation.

the adjustment is made to the calculation in ECLIPSE, whereas for the MLC errors, the changes occur in the delivery and will appear in the diode measurements and 3DVH® reconstruction.

5.3.6 Summary of VMAT Errors

The sensitivity of the ArcCHECK® system was analysed using both diode measurements and the 3DVH® reconstruction software. When using the system based confidence limits established in section 5.2, the ArcCHECK® diode measurements

were sensitive to MU normalization errors, systematic MLC errors and partial delivery errors. There was some sensitivity to the most extreme random MLC errors and systematic gantry errors and no sensitivity to random gantry errors or DLG errors. When the often clinically used 90% action level at the 3%/3mm γ criterion was considered, the diode measurements showed almost no sensitivity to any of the errors investigated. Only for the most extreme errors in partial delivery and systematic MLC errors, did this 90% action level suggest failure in delivery. This suggests that a tighter action level is necessary for diode measurements using the ArcCHECK®, otherwise systematic errors as large as 5% in normalization or 3 mm in MLC positions could go unchecked.

It should also be noted that when using a 2%/2mm, global dose difference, γ criterion, ArcCHECK® diode measurements provided useful diagnostic information in the calibration of the dosimetric leaf gap.

In 3DVH®, the dose reconstructions were more sensitive than the diode measurements to errors in MU normalization and systematic MLC errors. 3DVH® was not sensitive to any random MLC errors, systematic or random gantry errors, or DLG errors. For partial deliveries, 3DVH® was sensitive to errors but not as sensitive as diode measurements alone. When the 90% action level at the 3%/3mm γ criterion was considered, 3DVH® was less sensitive to normalization and systematic MLC errors, but plans with larger dosimetric errors still failed. When using the system based confidence limits, plans with normalization errors as small as 0.5% fell outside of tolerance, suggesting that these limits were too tight. In the case of 3DVH® reconstructed dose distributions, the 90% action level may be a more reasonable limit.

Chapter 6

Conclusions

In this thesis, a novel diode detector array, ArcCHECK®, and accompanying 3D dose reconstruction software, 3DVH®, were evaluated for pretreatment verification of complex radiation therapy treatment.

For open fields, the agreement between ECLIPSE and both ArcCHECK® diode measurements and 3DVH® dose reconstructions was excellent. Ion chamber measurements provided further validation of the dose reconstructed by 3DVH®. When compared to Monte Carlo calculations, similarly good agreement was found.

For IMRT plans, the ArcCHECK® results were in excellent agreement with ECLIPSE and Monte Carlo. Both γ analysis and dose difference metrics showed that the ArcCHECK® diode measurements and 3DVH® reconstructions were well within commonly accepted and clinically used tolerances. The only discrepancy, was for head and neck IMRT plans delivered on the 21-EX. Both γ-pass rates and several dose difference metrics fell outside of tolerance when comparing ArcCHECK® results to ECLIPSE calculations. However, based on ion chamber measurements, Monte Carlo calculations and results from the Truebeam, it was determined that a contributing factor in the failure of head and neck IMRT plans was a suboptimal modelling of the MLC effects for 21-EX ECLIPSE calculations in combination with changes in linac MLC performance since commissioning.

VMAT plans showed better agreement than IMRT plans for both prostate and head and neck. The γ-pass rates and dose difference metrics were in excellent agreement with ECLIPSE and the system based confidence limits established using these measurements were much tighter than those typically used for pretreatment verification.

The ArcCHECK® and 3DVH® system was found to be sensitive to clinically

relevant errors such as MU normalization and systematic MLC shifts, and not sensitive to errors which have minimal dosimetric impact such as random MLC errors and gantry position errors. It was also determined that for ArcCHECK® diode measurements, tolerances for γ-pass rates need to be tighter than the 90% action level at a 3%/3mm γ criterion suggested by TG-119 [17]. For 3DVH® dose reconstructions, the 90% action level used in the intermediate and high dose region at BCCA-VIC may be an appropriate limit. For both diode measurements and 3DVH® doses, a wider study of VMAT patient plans would be necessary to determine the appropriate action levels for γ-pass rates and dose difference metrics.

In conclusion the ArcCHECK® detector combined with 3DVH® software has shown the potential be a useful tool for VMAT pretreatment verification. A wider study of more varied patient plans would provide a stronger case for the clinical use of this dosimeter than the limit sample of plans studied in this work.

The high quality of the 3DVH® results in this work also suggest that an investigation of the 3DVH® software reconstruction of dose into patient CT data may be warranted. The excellent results for the 3DVH® software in reconstructing dose into a homogeneous phantom provides a strong foundation for the next step in the use of this software as a dosimetric tool.

Bibliography

[1] J. Kozelka, J. Robinson, B. Nelms, G. Zhang, D. Savitskij, and V. Feygelman, "Optimizing the accuracy of a helical diode array dosimeter: a comprehensive calibration methodology coupled with a novel virtual inclinometer.," *Med. Phys.*, vol. 38, no. 9, pp. 5021–32, 2011.

[2] G. Li, Y. Zhang, X. Jiang, S. Bai, G. Peng, K. Wu, and Q. Jiang, "Evaluation of the ArcCHECK QA system for IMRT and VMAT verification.," *Physica medica*, pp. 1–9, 2012.

[3] F. García-Vicente, V. Fernández, R. Bermúdez, A. Gómez, L. Pérez, A. Zapatero, and J. J. Torres, "Sensitivity of a helical diode array device to delivery errors in IMRT treatment and establishment of tolerance level for pretreatment QA.," *J. Appl. Clin. Med. Phys.*, vol. 13, no. 1, p. 3660, 2012.

[4] Canadian Cancer Society's Steering Committee On Cancer Statistics, "Candian Cancer Statistics 2012," tech. rep., Canadian Cancer Society, Toronto, ON, 2012.

[5] A. V. D. Kogel and M. Joiner, *Basic Clinical Radiobiology*. Hodder Arnold, 2009.

[6] H. E. Johns and J. R. Cunningham, *The Physics of Radiology*. Charles C Thomas, 1983.

[7] S. Webb, "The physical basis of IMRT and inverse planning," *British Journal of Radiology*, vol. 76, no. 910, pp. 678–689, 2003.

[8] J. Staffurth, "A review of the clinical evidence for intensity-modulated radiotherapy.," *Clin. Oncol. (R. Coll. of Radiol.)*, vol. 22, no. 8, pp. 643–57, 2010.

[9] K. Otto, "Volumetric modulated arc therapy: IMRT in a single gantry arc," *Med. Phys.*, vol. 35, no. 1, p. 310, 2008.

[10] C. C. Popescu, I. a. Olivotto, W. a. Beckham, W. Ansbacher, S. Zavgorodni, R. Shaffer, E. S. Wai, and K. Otto, "Volumetric modulated arc therapy improves dosimetry and reduces treatment time compared to conventional intensity-modulated radiotherapy for locoregional radiotherapy of left-sided breast cancer and internal mammary nodes.," *Int. J. Radiat. Oncol.*, vol. 76, no. 1, pp. 287–95, 2010.

[11] D. Palma, E. Vollans, K. James, S. Nakano, V. Moiseenko, R. Shaffer, M. McKenzie, J. Morris, and K. Otto, "Volumetric modulated arc therapy for delivery of prostate radiotherapy: comparison with intensity-modulated radiotherapy and three-dimensional conformal radiotherapy.," *Int. J. Radiat. Oncol.*, vol. 72, no. 4, pp. 996–1001, 2008.

[12] L. Van Benthuysen, L. Hales, and M. B. Podgorsak, "Volumetric modulated arc therapy vs. IMRT for the treatment of distal esophageal cancer.," *Med. Dosim.*, vol. 36, no. 4, pp. 404–9, 2011.

[13] E. J. Hall, "Intensity-modulated radiation therapy , protons , and the risk of second cancers," *Int. J. Radiat. Oncol.*, vol. 65, no. 1, pp. 1–7, 2006.

[14] C. Ling, P. Zhang, T. Etmektzoglou, J. Star-Lack, M. Sun, E. Shapiro, and M. Hunt, "Acquisition of MV-scatter-free kilovoltage CBCT images during RapidArc or VMAT.," *Radiotherapy Oncol.*, vol. 100, no. 1, pp. 145–9, 2011.

[15] M. M. Matuszak, D. Yan, I. Grills, and A. Martinez, "Clinical applications of volumetric modulated arc therapy.," *Int. J. Radiat. Oncol.*, vol. 77, no. 2, pp. 608–16, 2010.

[16] G. a. Ezzell, J. M. Galvin, D. Low, J. R. Palta, I. Rosen, M. B. Sharpe, P. Xia, Y. Xiao, L. Xing, and C. X. Yu, "Guidance document on delivery, treatment planning, and clinical implementation of IMRT: Report of the IMRT subcommittee of the AAPM radiation therapy committee," *Med. Phys.*, vol. 30, no. 8, p. 2089, 2003.

[17] G. a. Ezzell, J. W. Burmeister, N. Dogan, T. J. LoSasso, J. G. Mechalakos, D. Mihailidis, A. Molineu, J. R. Palta, C. R. Ramsey, B. J. Salter, J. Shi, P. Xia, N. J. Yue, and Y. Xiao, "IMRT commissioning: Multiple institution planning and dosimetry comparisons, a report from AAPM Task Group 119," *Med. Phys.*, vol. 36, no. 11, p. 5359, 2009.

[18] Intensity Modulated Radiation Therapy Collaborative Working Group, "Intensity-Modulated Radiotherapy : Current status and issues of interest," *Int. J. Radiat. Oncol.*, vol. 51, no. 4, pp. 880–914, 2001.

[19] B. Poppe, A. Djouguela, A. Blechschmidt, K. Willborn, A. Rühmann, and D. Harder, "Spatial resolution of 2D ionization chamber arrays for IMRT dose verification: single-detector size and sampling step width.," *Phys. Med. Biol.*, vol. 52, no. 10, pp. 2921–35, 2007.

[20] V. Feygelman, B. E. Nelms, A. Rosenfeld, T. Kron, F. DErrico, and M. Moscovitch, "Dose Verification in IMRT and VMAT," *AIP. Conf. Proc.*, vol. 145, no. 1, pp. 145–164, 2011.

[21] A. S. Saini and T. C. Zhu, "Energy dependence of commercially available diode detectors for in-vivo dosimetry," *Med. Phys.*, vol. 34, no. 5, p. 1704, 2007.

[22] P. a. Jursinic, "Angular dependence of dose sensitivity of surface diodes," *Med. Phys.*, vol. 36, no. 6, p. 2165, 2009.

[23] P. a. Jursinic and B. E. Nelms, "A 2-D diode array and analysis software for verification of intensity modulated radiation therapy delivery," *Med. Phys.*, vol. 30, no. 5, p. 870, 2003.

[24] W. U. Laub and T. Wong, "The volume effect of detectors in the dosimetry of small fields used in IMRT," *Med. Phys.*, vol. 30, no. 3, p. 341, 2003.

[25] J. Herzen, M. Todorovic, F. Cremers, V. Platz, D. Albers, a. Bartels, and R. Schmidt, "Dosimetric evaluation of a 2D pixel ionization chamber for implementation in clinical routine.," *Phys. Med. Biol.*, vol. 52, no. 4, pp. 1197–208, 2007.

[26] A. Van Esch, C. Clermont, M. Devillers, M. Iori, and D. P. Huyskens, "On-line quality assurance of rotational radiotherapy treatment delivery by means of a 2D ion chamber array and the Octavius phantom," *Med. Phys.*, vol. 34, no. 10, p. 3825, 2007.

[27] W. van Elmpt, L. McDermott, S. Nijsten, M. Wendling, P. Lambin, and B. Mijnheer, "A literature review of electronic portal imaging for radiotherapy dosimetry.," *Radiotherapy Oncol.*, vol. 88, no. 3, pp. 289–309, 2008.

[28] B. E. Nelms, H. Zhen, and W. a. Tome, "Per-beam, planar IMRT QA passing rates do not predict clinically relevant patient dose errors," *Med. Phys.*, vol. 38, no. 2, p. 1037, 2011.

[29] J. J. Kruse, "On the insensitivity of single field planar dosimetry to IMRT inaccuracies," *Med. Phys.*, vol. 37, no. 6, p. 2516, 2010.

[30] G. Yan, C. Liu, T. a. Simon, L.-C. Peng, C. Fox, and J. G. Li, "On the sensitivity of patient-specific IMRT QA to MLC positioning errors.," *J. Appl. Clin. Med. Phys.*, vol. 10, no. 1, p. 2915, 2009.

[31] D. Letourneau, J. Publicover, J. Kozelka, D. J. Moseley, and D. a. Jaffray, "Novel dosimetric phantom for quality assurance of volumetric modulated arc therapy," *Med. Phys.*, vol. 36, no. 5, p. 1813, 2009.

[32] V. Feygelman, G. Zhang, C. Stevens, and B. E. Nelms, "Evaluation of a new VMAT QA device, or the "X" and "O" array geometries.," *J. Appl. Clin. Med. Phys.*, vol. 12, no. 2, p. 3346, 2011.

[33] G. Yan, B. Lu, J. Kozelka, C. Liu, and J. G. Li, "Calibration of a novel four-dimensional diode array," *Med. Phys.*, vol. 37, no. 1, p. 108, 2010.

[34] J. L. Bedford, Y. K. Lee, P. Wai, C. P. South, and A. P. Warrington, "Evaluation of the Delta4 phantom for IMRT and VMAT verification.," *Phys. Med. Biol.*, vol. 54, no. 9, pp. N167–76, 2009.

[35] R. Sadagopan, J. A. Bencomo, R. L. Martin, G. Nilsson, T. Matzen, and P. A. Balter, "Characterization and clinical evaluation of a novel IMRT quality assurance system," *J. Appl. Clin. Med. Phys.*, vol. 10, no. 2, pp. 104–119, 2009.

[36] L. Masi, F. Casamassima, R. Doro, and P. Francescon, "Quality assurance of volumetric modulated arc therapy: Evaluation and comparison of different dosimetric systems," *Med. Phys.*, vol. 38, no. 2, p. 612, 2011.

[37] V. Feygelman, K. Forster, D. Opp, and G. Nilsson, "Evaluation of a biplanar diode array dosimeter for quality assurance of step-and-shoot IMRT," *J. Appl. Clin. Med. Phys.*, vol. 10, no. 4, pp. 64–78, 2009.

[38] S. Korreman, J. Medin, and F. Kjaer-Kristoffersen, "Dosimetric verification of RapidArc treatment delivery.," *Acta oncologica*, vol. 48, no. 2, pp. 185–91, 2009.

[39] M.-H. Lin, S. Koren, I. Veltchev, J. Li, L. Wang, R. a. Price, and C.-M. Ma, "Measurement comparison and Monte Carlo analysis for volumetric-modulated arc therapy (VMAT) delivery verification using the ArcCHECK dosimetry system.," *J. Appl. Clin. Med. Phys.*, vol. 14, no. 2, p. 3929, 2013.

[40] T. Sanghangthum, S. Suriyapee, S. Srisatit, and T. Pawlicki, "Statistical process control analysis for patient-specific IMRT and VMAT QA.," *Journal of radiation research*, vol. 54, no. 3, pp. 546–52, 2013.

[41] T. Teke, A. M. Bergman, W. Kwa, B. Gill, C. Duzenli, and I. A. Popescu, "Monte Carlo based, patient-specific RapidArc QA using Linac log files," *Med. Phys.*, vol. 37, no. 1, p. 116, 2010.

[42] W. Luo, J. Li, R. a. Price, L. Chen, J. Yang, J. Fan, Z. Chen, S. McNeeley, X. Xu, and C.-M. Ma, "Monte Carlo based IMRT dose verification using MLC log files and R/V outputs," *Med. Phys.*, vol. 33, no. 7, p. 2557, 2006.

[43] E. Schreibmann, A. Dhabaan, E. Elder, and T. Fox, "Patient-specific quality assurance method for VMAT treatment delivery," *Med. Phys.*, vol. 36, no. 10, p. 4530, 2009.

[44] W. Ansbacher, "Three-dimensional portal image-based dose reconstruction in a virtual phantom for rapid evaluation of IMRT plans," *Med. Phys.*, vol. 33, no. 9, p. 3369, 2006.

[45] A. J. Olch, "Evaluation of the accuracy of 3DVH software estimates of dose to virtual ion chamber and film in composite IMRT QA.," *Med. Phys.*, vol. 39, no. 1, pp. 81–6, 2012.

[46] B. E. Nelms, D. Opp, J. Robinson, T. K. Wolf, G. Zhang, E. Moros, and V. Feygelman, "VMAT QA: measurement-guided 4D dose reconstruction on a patient.," *Med. Phys.*, vol. 39, no. 7, pp. 4228–38, 2012.

[47] H. Zhen, B. E. Nelms, and W. a. Tome, "Moving from gamma passing rates to patient DVH-based QA metrics in pretreatment dose QA.," *Med. Phys.*, vol. 38, no. 10, pp. 5477–89, 2011.

[48] F. M. Kahn, *The Physics of Radiation Therapy.* Lippincott Williams and Wilkins, 2003.

[49] T. LoSasso, C. S. Chui, and C. C. Ling, "Physical and dosimetric aspects of a multileaf collimation system used in the dynamic mode for implementing intensity modulated radiotherapy.," *Med. Phys.*, vol. 25, no. 10, pp. 1919–27, 1998.

[50] J. Sievinen, W. Ulmer, and W. Kaissl, "AAA Photon Dose Calculation Model in Eclipse," tech. rep., Varian Medical Systems, Palo Alto, CA, 2005.

[51] P. Andreo, "Monte Carlo techniques in medical radiation physics," *Phys. Med. Biol.*

[52] D. W. O. Rogers, B. A. Faddegon, G. X. Ding, C.-M. Ma, J. We, and T. R. Mackie, "BEAM: A Monte Carlo code to simulate radiotherapy treatment units," *Med. Phys.*, vol. 22, no. 5, pp. 503–524, 1995.

[53] D. W. O. Rogers, B. R. Walters, and I. Kawrakow, "BEAMnrc Users Manual," *NRC Report*, 2006.

[54] B. R. Walters, I. Kawrakow, and D. W. O. Rogers, "DOSXYZnrc Users Manual," *NRC Report*, 2006.

[55] I. a. Popescu, C. P. Shaw, S. F. Zavgorodni, and W. a. Beckham, "Absolute dose calculations for Monte Carlo simulations of radiotherapy beams.," *Phys. Med. Biol.*, vol. 50, no. 14, pp. 3375–92, 2005.

[56] K. Bush, R. Townson, and S. Zavgorodni, "Monte Carlo simulation of RapidArc radiotherapy delivery.," *Phys. Med. Biol.*, vol. 53, no. 19, pp. N359–70, 2008.

[57] K. Bush, S. Zavgorodni, I. Gagne, R. Townson, W. Ansbacher, and W. Beckham, "Monte Carlo evaluation of RapidArc oropharynx treatment planning strategies for sparing of midline structures.," *Phys. Med. Biol.*, vol. 55, no. 16, pp. 4465–79, 2010.

[58] D. Létourneau, M. Gulam, D. Yan, M. Oldham, and J. W. Wong, "Evaluation of a 2D diode array for IMRT quality assurance.," *Radiotherapy Oncol.*, vol. 70, no. 2, pp. 199–206, 2004.

[59] D. a. Low, W. B. Harms, S. Mutic, and J. a. Purdy, "A technique for the quantitative evaluation of dose distributions.," *Med. Phys.*, vol. 25, no. 5, pp. 656–61, 1998.

[60] P. S. Basran and M. K. Woo, "An analysis of tolerance levels in IMRT quality assurance procedures," *Med. Phys.*, vol. 35, no. 6, p. 2300, 2008.

[61] A. Bakai, M. Alber, and N. Fridtjof, "A revision of the γ -evaluation concept for the comparison of dose distributions," *Phys. Med. Biol.*, vol. 45, pp. 3543–3553, 2003.

[62] E. Vanetti, G. Nicolini, A. Clivio, A. Fogliata, and L. Cozzi, "The impact of treatment couch modelling on RapidArc.," *Phys. Med. Biol.*, vol. 54, no. 9, pp. N157–66, 2009.

[63] R. a. Popple, J. B. Fiveash, I. a. Brezovich, and J. a. Bonner, "RapidArc radiation therapy: first year experience at the University of Alabama at Birmingham.," *Int. J. Radiat. Oncol.*, vol. 77, no. 3, pp. 932–41, 2010.

[64] M. Van Prooijen, T. Kanesalingam, M. K. Islam, and R. K. Heaton, "Assessment and management of radiotherapy beam intersections with the treatment couch.," *J. Appl. Clin. Med. Phys.*, vol. 11, no. 2, p. 3171, 2010.

[65] T. Teke, B. Gill, C. Duzenli, and I. a. Popescu, "A Monte Carlo model of the Varian IGRT couch top for RapidArc QA.," *Phys. Med. Biol.*, vol. 56, no. 24, pp. N295–305, 2011.

[66] H. Li, A. K. Lee, J. L. Johnson, R. X. Zhu, and R. J. Kudchadker, "Characterization of dose impact on IMRT and VMAT from couch attenuation for two Varian couches.," *J. Appl. Clin. Med. Phys.*, vol. 12, no. 3, p. 3471, 2011.

[67] M. Oliver, I. Gagne, K. Bush, S. Zavgorodni, W. Ansbacher, and W. Beckham, "Clinical significance of multi-leaf collimator positional errors for volumetric modulated arc therapy.," *Radiotherapy Oncol.*, vol. 97, no. 3, pp. 554–60, 2010.

[68] M. Oliver, K. Bush, S. Zavgorodni, W. Ansbacher, and W. a. Beckham, "Understanding the impact of RapidArc therapy delivery errors for prostate cancer.," *J. Appl. Clin. Med. Phys.*, vol. 12, no. 3, p. 3409, 2011.